Masters Theses

Graduate School

5-2012

A GPS-based Mobility Power Model for Military Vehicle Applications

George William Bozdech
gbozdech@gmail.com

To the Graduate Council:

I am submitting herewith a thesis written by George William Bozdech entitled "A GPS-based Mobility Power Model for Military Vehicle Applications." I have examined the final electronic copy of this thesis for form and content and recommend that it be accepted in partial fulfillment of the requirements for the degree of Master of Science, with a major in Biosystems Engineering.

Paul D. Ayers, Major Professor

We have read this thesis and recommend its acceptance:

David K. Irick, John B. Wilkerson

Accepted for the Council:
Dixie L. Thompson

Vice Provost and Dean of the Graduate School

(Original signatures are on file with official student records.)

A GPS-BASED MOBILITY POWER MODEL FOR MILITARY VEHICLE APPLICATIONS

A Thesis
Presented for the
Master of Science
Degree
The University of Tennessee, Knoxville

George William Bozdech
May 2011

Abstract

In recent years, military vehicles have been equipped with hybrid, diesel-electric drives to improve fuel efficiency and stealth capabilities. These vehicles require an accurate estimate of the power duty cycles during distinct operating conditions. To meet this demand, a GPS-based mobility power and duty cycle analysis is one approach to predict the power requirements of on-road and off-road vehicles. The dynamic vehicle parameters needed to estimate the forces developed during locomotion are determined from the GPS tracking data, and these forces include the following: the motion resistance, gravitational, linear inertia, rotational inertia, and aerodynamic drag. The motion resistance force generated at the wheel and soil interface is quantified via the U.S. military's Vehicle Terrain Interaction (VTI) model.

On-road controlled tests were performed to validate the motion resistance, grade, and inertia components of the model. Uncontrolled tests were performed to validate the model in a scenario that simulated a U.S. military reconnaissance mission. GPS data was collected from Trimble 132 and Garmin 18 GPS receivers. The predicted mobility power values from the GPS data were compared to the measured drivewheel power estimated from engine data transmitted on the vehicle's Controller Area Network (CAN). The results from the validation tests indicated that the model accurately predicted the average power requirements of the vehicle while the model had a moderate level of variability when estimating the power requirements at discrete points in time during testing. The motion resistance tests conducted at slow speeds provided for reasonable estimates of the required mobility power. The absolute average percent error of the average positive power requirements during the grade and inertia tests was 6 and 21% respectively from the Trimble 132 GPS receiver. The absolute average percent error during the

ii

uncontrolled test was 20% from the Trimble 132 GPS receiver. The model was applied to GPS

tracking data collected for the U.S. Army's 8-wheeled Stryker vehicle conducting reconnaissance

missions at Fort Lewis, Washington and Pohakuloa Training Area (PTA), Hawaii. The mission-

specific power duty cycle characteristics were quantified, and the average positive power

requirement at Fort Lewis and PTA was 65.4 and 43.6 kW respectively.

Acknowledgements

I would like to thank Paul Ayers, my adviser, for his steadfast guidance and support during this project. I would like to recognize committee members, John Wilkerson and David Irick, for their assistance during the completion of my thesis. Furthermore, the completion of this research was possible because David Irick facilitated in the use of the Mechanical Engineering department's test vehicle for validation of the model.

I want to thank Heidi Howard and Niels Svendsen from the U.S. Army Corps of Engineers' Construction Engineering Research Laboratory (CERL) for putting me in contact with Paul Ayers. Otherwise, this research opportunity would not have been possible for me. I want to also express my gratitude for the guidance and encouragement I received during my studies at the University of Illinois from Alan Hansen and Prasanta Kalita. I would like to acknowledge fellow graduate students Brett Connell and Kenneth Swinson for their assistance during my project

Finally, I would like to recognize my family for their tireless guidance and support during my academic career. My mother, father, and sister, Karen, Stephen, and Audrey Bozdech, have provided me with encouragement, love, and support in all of life's endeavors. I want to also acknowledge my grandparents, Bill Bozdech & family, close relatives, and friends for their continued support and motivation during my studies. My experiences at the Bozdech Family Farm significantly influenced the research and career path I have chosen.

Table of Contents

List of Tables

List of Figures

Chapter 1: Introduction

In general, the military's requirement for a tactical vehicle's continuous gross traction ratio is 60% (Taylor, 2011). The capacity of such vehicles to maintain such a high load on the power source and drivetrain for a continuous period results in the careful consideration that must be made in selecting the appropriate engine size, cooling system, and drivetrain components (Taylor, 2011). According to Rutherford (2004), the delivery of fuel to military vehicles is the single greatest logistical challenge during a military operation. The costs associated with the delivery of fuel easily exceed $50 per a gallon of fuel. The use of hybrid-electric military vehicles has the potential to substantially reduce the fuel costs required to operate military vehicles while the improved fuel efficiency may justify any additional cost associated with a hybrid-electric drivetrain. A hybrid military vehicle that is capable of operating in a "pure electric" mode where only the electric motors power the vehicle allows the vehicle to be "stealth mode" capable is advantageous for today's military personnel. This feature extends the silent watch capability of the vehicle while reducing the heat signature of the vehicle during the stationary or low speed maneuvers. Furthermore, a hybrid-electric drivetrain allows for the vehicle to be a source of mobile power generation (Rutherford, 2004).

The control systems for the complex drivetrains of hybrid electric vehicles must efficiently and precisely supply, harvest, and manage the power required for locomotion. Such systems demand accurate estimates of the power requirements of the vehicle during all types of combat operations. According to Brudnak (2008), previous efforts to estimate the power requirements during certain vehicle operations utilized a virtual vehicle-terrain interface to develop the simulated, mission-specific power requirements. Currently, there is not an in-field method for

quantifying a vehicle's power requirements from a "comprehensive combat vehicle usage profile, or 'duty cycle' " for a given vehicle type (Brudnak et al., 2008).

Recent research by Taylor (2011) at the U.S. Army Aberdeen Test Center has investigated the effect of varying a given vehicle's drivetrain (conventional, series hybrid, parallel hybrid, etc.) on the fuel consumption requirements of the vehicles during typical military vehicle duty cycles. Possible fuel efficiency improvement for a given vehicle platform is important when evaluating various drivetrain configurations. The power/fuel duty cycle requirement of military vehicles "is ever changing, unknown, and is certainly not defined by an agreed upon duty schedule available for all platforms and weight classe   s of wheeled and tracked vehicles" (Taylor, 2011).

Current methods for assessing vehicle performance occur in a chassis dynamometer laboratory where such fuel efficiency and emissions testing occur according to the Urban Dynamometer Driving Schedule (UDDS), the Highway Fuel Economy Test (HFET), and the US06 (Gonder et al., 2007). These chassis dynamometer tests rely upon coastdown testing to provide estimates of the load that must be applied to a vehicle at a given point in a driving schedule. Coastdown testing is accepted by the U.S. Environmental protection agency (EPA) as a means of determining the dynamic load to apply to a vehicle during chassis dynamometer testing (Yasin, 1978).

However, these tests may not be indicative of the actual vehicle performance and operating characteristics during a given real-world duty cycle (Gonder et al., 2007). The electrical energy generation, consumption, and harvesting characteristics of a hybrid vehicle are substantially

effected by the power duty cycle requirements for a given vehicle operation. Gonder et al. (2007) identified the on-road driving characteristics of 227 operators of standard passenger vehicles operating in an urban environment via GPS tracking of the vehicles. The results indicated that the laboratory duty cycles did not accurately represent the significantly greater acceleration/decelerations that occurred in the observed urban maneuvers. As a result, the Environmental Protection Agency (EPA) has adjusted the methods for determining the fuel economy ratings of light-duty cars and trucks. This indicates that the laboratory tests may underestimate the power requirement and the potential regenerative braking energy for vehicles operating in this urban environment. In-field estimation of the power and energy requirements of military vehicles during specific maneuvers is necessary to characterize the vehicle's mobility power duty cycles. A GPS-based method for estimating the power duty cycle requirements of military vehicles would provide a cost-effective procedure for determining the duty cycle characteristics of a large fleet of vehicles. The duty cycles could be developed from current or historical GPS tracking data of military vehicles where sophisticated data acquisition equipment for each vehicle may not be practical.

Chapter 2: Objectives

The principle objective of this study was to develop, validate, and apply a GPS-based mobility power model to characterize the power requirements of vehicles. Identifying all of the forces that effect vehicle locomotion was a critical task during model development. Model validation occurred by performing on-road, controlled and uncontrolled vehicle tests while tracking the vehicle with GPS and logging the vehicle's Controller Area Network (CAN) signals which provided for engine and vehicle parameters. The specific objectives were to:

1. perform controlled tests to validate the motion resistance, grade, and inertia components of the model,

2. validate and conduct an accuracy assessment of the model during the motion resistance, grade, and inertia controlled tests,

3. conduct an uncontrolled test that simulated the maneuvers of military vehicles during reconnaissance mission executed by the U.S. Army,

4. validate and conduct an accuracy assessment of the model during the uncontrolled test,

5. apply the mobility power model to historical GPS tracking of the U.S. Army's Stryker vehicle conducting reconnaissance missions at Fort Lewis, Washington and the Pohakuloa Training Area (PTA), Hawaii, and

6. develop, compare, and contrast the power duty cycle characteristics of the Stryker vehicles operating at Fort Lewis and PTA.

Chapter 3: Literature Review

3.1 Global Positioning System (GPS)

A Global Positioning System (GPS) is a form of a Global Navigation Satellite System (GNSS) developed by the United States Department of Defense initially for maritime navigation. A GNSS system typically requires approximately 20 to 30 satellites to cover the entire Earth, and these satellites may or may not be in the geosynchronous orbit. Three to six orbital planes are typically used in a GNSS system. A GPS system functions by accurately measuring the time it takes for a GPS receiver to receive a signal transmitted from at least four satellites. The distance from the GPS receiver to each satellite is computed by multiplying each associated time value by the speed of light (ie the speed at which the signals are transmitted), and this distance is called the pseudorange. Advanced algorithms are used to compute the precise position of the GPS receiver from the pseudorange values and the precise position of each satellite, and this method is called trilateration. Four satellites are needed to solve for the 3-dimensional position of the receiver because the error of the receiver's internal clock must also be calculated. Differential correction of GPS relies upon a master control system that monitors the precise orbit and clock drift corrections for all of the satellites of a constellation. The pseudorange correction data is transmitted to the receiver from each satellite to update the receiver on the corrected distance between the receiver and the satellites. This correction data allows for a differentially corrected GPS position (Bevly, 2010).

According to the National Marine Electronics Association (NMEA) 0183 Standard (1995), the

GPS signals can be serially transmitted at a 4800 baud rate. The critical GPS data for vehicle

tracking are available on the $GPGGA and the $GPRMC NMEA strings. The date, time,

position, elevation, speed, and heading are transmitted on these NMEA strings (NMEA Standard,

1995). All of these parameters are important in the assessment of the mobility characteristics of

a vehicle. A description of the information transmitted on the $GPGGA and $GPRMC strings

are given in Figures 1 and 2 respectively.

```
GGA - Global Positioning System Fix Data
Time, position and fix related data for a GPS receiver.

                            Differential reference station ID, 0000-1023 ┐ see
                                          Age of Differential GPS data ┐  Notes
                            Units of Geoidal separation, meters ┐       │  2&3
                                         Geoidal separation ┐   │       │
                       Units of antenna altitude, meters ┐  │   │       │
          Antenna altitude re: mean-sea-level (geoid) ┐  │  │   │       │
                    Horizontal dilution of precision ┐ │  │  │   │       │

$--GGA,hhmmss.ss,llll.ll,a,yyyyy.yy,a,x,xx,x.x,x.x,M,x.x,M,x.x,xxxx
                                                        *hh<CR><LF>
                                                └ Number of satellites in use,
                                                  00-12, may be different from
                                                  the number in view
                                              └ GPS Quality indicator¹
                                            └ Longitude - E/W
                                  └ Latitude - N/S
               └ UTC of position
Notes:
```
1) GPS Quality Indicator: 0 = Fix not available or invalid
                          1 = GPS SPS Mode, fix valid
                          2 = Differential GPS, SPS Mode, fix valid
                          3 = GPS PPS Mode, fix valid
2) Time in seconds since last SC104 Type 1 or 9 update, null field when DGPS is not used
3) Geoidal Separation: the difference between the WGS-84 earth ellipsoid and mean-sea-level
   (geoid), "-" = mean-sea-level below ellipsoid.

Figure 1: A description of the $GPGGA string (Source: NMEA Standard, 1995)

```
RMC - Recommended Minimum Specific GPS/TRANSIT Data
Time, date, position, course and speed data provided by a GPS or TRANSIT navigation receiver. This
sentence is transmitted at intervals not exceeding 2-seconds and is always accompanied by RMB when
a destination waypoint is active.  RMC and RMB are the recommended minimum data to be provided
by a GPS or TRANSIT receiver.  All data fields must be provided, null fields used only when data is
temporarily unavailable.

                                    Magnetic variation, degrees E/W ┬────  see Note 1
                                        Date: dd|mm|yy ┐             │
                    Course Over Ground, degrees True ┐ │             │
$--RMC,hhmmss.ss,A,llll.ll,a,yyyyy.yy,a,x.x,x.x,xxxxxx,x.x,a*hh<CR><LF>
                                              └ Speed over ground, knots
                                               └ Longitude, E/W
                                    └ Latitude, N/S
                          └ Status: A = Data valid
                                    V = Navigation receiver warning
              └ UTC of position fix

Notes:
1) Easterly variation (E) subtracts from True course
   Westerly variation (W) adds to True course
```
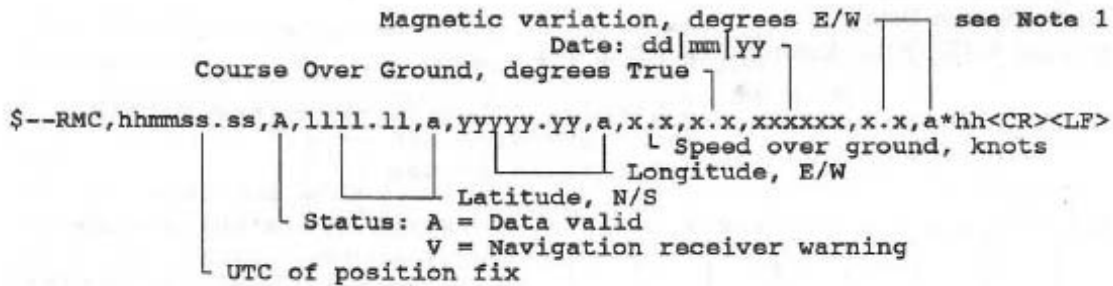
Figure 2: A description of the $GPRMC string (Source: NMEA Standard, 1995)

The GPS speed data can be estimated using several different approaches. The methods used by

the manufacturers of the GPS receivers to estimate speed are typically proprietary. The simplest

approach is to determine the speed of the receiver from the estimated displacement between the

GPS points' position. However, only a limited degree of accuracy can be attained using this

approach, especially if there is significant error in the estimates of the receivers' position.

Previous efforts by How et. al (2002) indicated that the measurement of each satellites Doppler

frequency allowed for very accurate estimates of a test vehicle's travel speed. The changes in the

frequencies of the signals that are transmitted from the satellite to the receiver allow for the

speed of the receiver to be estimated. A principle advantage of this method is that the bias or

error from the receiver's internal clock does not affect the estimate of speed (How et al., 2002).

It is thought that the proprietary approach each GPS manufacturer has for estimating vehicle

speed relies upon a combination of these two methods along with some filtering technique.

7

3.2 Controller Area Network (CAN)

3.2.1 CAN Background

The Controller Area Network (CAN) was developed by Robert Bosch in the 1980's to decrease the complexity of the wiring in automotives. At the time, dedicated wiring was required between each component or device while vehicles began to be equipped with engine controller modules (ECM), traction control systems, and anti-lock brake systems (ABS). The control system of the vehicles began to exceed the physical limitations of a system with dedicated wiring to each component. As a result, the CAN network was developed where multiple devices can communicate across a single pair of wires. The complexity of the wiring of the vehicle is dramatically reduced with a CAN network. The messages transmitted through a CAN network have a unique 11 bit identifier that provides the message's information and priority. Each 11 bit CAN signal transmitted contains multiple vehicle or engine parameters. A node in a CAN network is any device that receives or transmits a message in the CAN network. The CAN controller formats the messages sent by the nodes. Only one node can transmit across the network at a given time, and all other nodes become receivers. Other advantages of the CAN network include the following: low cost, efficient data transmission, error detection, and the ability to transmit messages to multiple nodes. The CAN network has been used for the control of agricultural and construction equipment along with controlling complex devices found in the manufacturing and transportation industries (Farsi, 1999).

The CAN data from a vehicle can be used to estimate the engine power of the engine. However, this estimated power is not the required mobility power or power delivered to the tractive

elements of the vehicle since drivetrain losses occur between the engine and the driven wheels or sprockets. According to SAE Standard J1939-71 (1998), CAN bus diagnostics provide for several hundred vehicle and engine parameters. A few of the vehicle and engine parameters typically embedded in the 11 bit CAN signals include the following: vehicle speed, engine speed, fuel consumption, throttle position, temperature, and pressure. The temperature and pressure of fluids within the following components are typically measured in a CAN bus system: air intake manifold, turbocharger, exhaust, oil pump, and water pump (SAE Standard, 1998). Engine diagnostic values are transmitted through the CAN network approximately every 0.01 s (10 ms). An engine torque diagnostic value is available in certain CAN bus signals. This diagnostic value is determined from several "lookup tables" stored in the engine control module (ECM). Lookup tables allow the ECM to estimate and control certain functions of the engine and vehicle based on the output from the various sensors on the vehicle and engine. For example, a lookup table that determines the fuel injection advancement may be estimated from the measured mass air flow rate and engine speed sensors. The volumetric efficiency of an engine is stored in a lookup table in the ECM, and it is a function of the intake air's density and the engine speed. An engine torque CAN message is estimated for a diesel engine from a lookup table that was developed from engine maps where engine torque is known at the given levels of engine speed and fuel consumption. The engine maps are generated from testing the engine on a dynamometer. Previous research with on-road trucks indicated that the estimated engine torque from the ECM's lookup tables can predict the actual engine torque within 5% while the vehicle is under load (David Irick, University of Tennessee, personal communication, 31 January 2012). The validity of messages such as engine speed, engine torque, and wheel speed are typically transmitted in the same CAN signal that the vehicle or engine parameters are transmitted. This

allows for the validity of any messages being logged from the CAN network to be checked. The brake power of the engine must be used to power such engine components as the fan, alternator, water pump, oil pump, fuel pump, and compressor. Brake power from the engine is also absorbed or dissipated in such drivetrain components as the transmission, differential, and PTO shaft (Rakha et al., 2001; Rakha et al., 2004). Transmission efficiencies usually range from approximately 0.89 to 0.94 but can vary due to type and complexity. All of these factors contribute to the deviation between the estimated engine brake power value and a vehicle's required mobility power. In a CAN bus based estimate of power, an indirect estimation of power is done where the power loss due to the drivetrain's mechanical efficiency losses and engine accessories must be considered to estimate the vehicle's mobility power.

3.2.2 Engine Speed

Engine speed is a critical engine parameter that is transmitted in various CAN signals, and it is an input to numerous engine functions controlled by the ECM. Engine speed is typically measured by inductive or Hall-effect sensors. Inductive sensors are typically positioned near the teeth of a gear on the flywheel or crankshaft. The teeth of the rotating gear produce a voltage across a coil in the sensor, and the frequency and amplitude of the sinusoidal voltage is directly proportional to the speed of the rotating shaft. Hall-effect sensors are semiconductor sensors that consist of several magnets, a magnetic rotor, and a microchip that processes the voltage signal. The hall-effect occurs when a voltage difference is produced perpendicular to the applied voltage, current, and magnetic field, and the perpendicular voltage produced is proportional to the rotating speed of the shaft (Bosch, 1993).

3.2.3 Engine Torque

According to Irick, engine torque values found in certain CAN signals come from a lookup table stored on the engine control module's (ECM) memory. For a diesel engine, inputs to the lookup table are the fueling rate to the engine, engine speed, and/or several other engine parameters. The fueling rate is estimated from lookup tables while the inputs to the lookup tables are the duration each diesel fuel injector is spraying fuel into the cylinders and the pressure at each injector. Previous laboratory testing for the given fuel injector allows for the flow rate through the injectors to be characterized. The ECM of a gasoline engine requires similar inputs to estimate engine torque except the intake manifold pressure or mass airflow rate is typically an input to the lookup table instead of the engine fueling rate since most gasoline engines operate at the stoichiometric air to fuel ratio. A torque value is interpolated by the ECM from the engine torque lookup table according to the values of the inputs to the lookup table. The lookup tables are generated from proprietary engine maps that were generated from measured data while the engine was loaded via an engine dynamometer. Numerous engine parameters are measured while a known torque load is applied by the dynamometer at a certain engine speed. The proprietary software used by the ECM is typically kept internal to the manufacturer, and there is not publicly available literature that describes each manufacturer's proprietary methods for estimating engine parameters from lookup tables (David Irick, University of Tennessee, personal communication, 31 January 2012).

Any negative torque value in an engine torque lookup table comes from the measured negative torque from the engine dynamometer at a given positive fueling rate and one of the following: positive engine speed, intake pressure (absolute), and/or another engine sensor(ex. absolute boost

11

pressure) or possibly from another lookup table's outputted engine parameter value. Negative

torque can be attained on a dynamometer when, instead of the engine driving the dynamometer,

the dynamometer's inertia is driving the engine. For example, when the dynamometer goes from

applying a high engine load to suddenly zero load at the rated engine speed, the result is that the

fueling rate is low and the dynamometer is actually applying a negative torque to the engine.

3.2.4 Wheel Speed

The wheel speed of each wheel on a vehicle is transmitted through the CAN network. Each

wheel speed is directly measured at each wheel. The output from the wheel speed sensors is sent

through the CAN network to be possibly used as inputs to other functions controlled by the ECM

such as the vehicle's traction control system or anti-lock brake system (ABS). The same types of

sensors used to measure engine speed are also used to measure the vehicle's wheel speeds.

Inductive or Hall-effect sensors are positioned near the rotating teeth of a gear on the half-shafts

of each driven axle (Bosch, 1993).

3.3 Longitudinal Vehicle Model

There are numerous forces that must be overcome in order for vehicle locomotion to occur while

the gravitational force may aid or resist vehicle motion. The summation of these forces in the

longitudinal direction results in the net tractive effort or thrust force required for the given

operating conditions (Rakha, 2001; Rakha, Rutherford, 2004; Standford, 2001; Wong, 2008;

Wong, 2010). The following equation represents the longitudinal vehicle model:

$$F_{Thrust} = F_{MR} \pm F_{Gravity} + F_{Lin.Inertia.} + F_{Drag} + F_{Drawbar} \qquad (1)$$

Where

F_{Thrust} is the thrust force from the powered wheels,

F_{MR} is the motion resistance force generated at the tire-terrain interface,

$F_{Gravity}$ is the gravitational force exerted on the vehicle,

$F_{Lin.Inertia}$ is the force associated with any increase or decrease of the vehicle's linear

inertia,

F_{Drag} is the aerodynamic drag force exerted by the air flowing over the surface of the

vehicle,

$F_{Drawbar}$ is the drawbar load applied at the hitchpoint of the vehicle.

Equation (1) provides the basis for estimating the energy and power required to propel a vehicle

at a given speed, degree of acceleration, grade of the terrain, and applied drawbar load. Research

by Rakha et al. (2001) and Rakha et al. (2004) utilized the longitudinal vehicle model to estimate

the peak acceleration characteristics of on-road trucks. An important constraint of the model was

that the thrust force associated with the peak acceleration did not exceed the static frictional

force between the tires and pavement. The vehicle dynamics-based approach accounted for the

external motion resistance, aerodynamic drag, and elevation grade forces along with the

frictional mechanical losses in the drivetrain to predict peak accelerations. Such models attempt

to imitate the actual speed and acceleration characteristics of vehicles while a GPS-based

mobility power model uses the actual operating characteristics to estimate vehicle power. The

longitudinal vehicle model was able to accurately estimate the acceleration characteristics of on-

highway trucks at different power to weight ratios. The predicted acceleration characteristics

from the model were compared to 1 Hz GPS data collected during testing to validate the model,

and the results indicated that the longitudinal model can be used to estimate the acceleration

profiles for 13 cars, Sport Utility Vehicles (SUV), and light-duty trucks along with heavy-duty

trucks at 10 different power to weight ratios (Rakha et al., 2001; Rakha et al., 2004).

Previous efforts by Suvinen et al. (2006) utilized GPS and CAN bus data to characterize the site

specific forces that effect the locomotion of 8-wheeled forwarders (forestry vehicle). A data

acquisition unit was used to log such CAN bus data as the following at a sampling rate of 4 Hz:

event time, torque of the drive axle, rotational speed of hydraulic motors/pumps, working

pressure of hydraulic circuit, and the gross power on the driveline. The net resistive force was

quantified by dividing the gross power on the driveline by the GPS determined vehicle travel

speed as it maneuvered on a tarmac and a firm soil road. In the analysis, the aerodynamic drag

force and inertia force required to accelerate/decelerate the vehicle were considered to be

negligible at the low travel speeds and accelerations that occurred during the tests (< 0.50 m/s

average travel speed), and these terms were omitted from the model's governing longitudinal

vehicle model equation. The frictional losses in the driveline contributed to the net motion

resistance, but these losses were also assumed to be negligible.

The three forces that resisted vehicle maneuvers were quantified from the tests conducted, and

they included the following: the motion resistance force at the tire soil interface, the resistance

force due to the vehicle's elevation change, and the winding resistance or force generated during

turning that occurs due to the vehicle's direct driveline (Suvinen et al., 2006). The direct

driveline resulted in all of the wheels having the same rotational speed but different levels of wheel slip (positive and negative) during turning. This caused an increase in the vehicle's motion resistance force, and the increase was defined as the winding force. The researchers validated the GPS and CAN bus data-based model for predicting the resistive forces encountered by a forwarder while applying a modified form of the longitudinal vehicle model. The 3-point turning radius calculations performed by Suvinen et al. (2006) were smoothed by using a 5 s moving average of the GPS position data.

Suvinen et al. (2006) concluded that the GPS elevation data could detect grades as small as 0.5%. It was noted that a lag existed between the predicted and measured percent grade traversed by the vehicle because the GPS antenna was located 3 m in front of the vehicle's center of gravity. The straight-line motion resistance ratio of the forwarder on the smooth tarmac surface was determined to be 0.055, and this value increased as soil strength decreased in the off-road terrain (Suvinen et al., 2006). The power transmitted through the vehicle's driveline increased up to approximately 300% during sharp turning maneuvers due to the winding force developed by the direct driveline.

3.4 Motion Resistance Power

Empirical methods for evaluating the performance of wheeled vehicles are useful because the complicated tractive element-terrain interaction is difficult to characterize. Empirical models are developed by measuring certain performance criteria at the measured terrain and vehicle conditions and fitting equations through the measured data.

3.4.1 Vehicle Terrain Interaction (VTI) Model

The motion resistance characteristics of tractive elements are oftentimes evaluated via homogenous soil bins in laboratory setting. These controlled conditions do not reflect the heterogeneous nature of off-road terrains where soil strength and condition along with the terrain's topography and roughness can vary dramatically. The effect of turning on the motion resistance force generated by the wheels is difficult to quantify in a lab setting. To determine the motion resistance (MR) of the tractive elements during operation, the vehicle terrain interaction (VTI) model developed by the U.S. Army Corps of Engineers at the Waterways Experiment Station (WES) facility in Vicksburg, Mississippi was utilized in the analysis (Jones et al., 2007). For wheeled vehicles, the dimensionless wheel numeric, N_c, is determined for the non-steered wheels of the vehicle while operating in a fine-grained soil, and the equation is given by the following:

$$N_c = \frac{CI \cdot bd}{W\left(1 - \dfrac{\delta}{h}\right)^{3/2}\left(1 + \dfrac{b}{d}\right)^{3/4}} \tag{2}$$

Where

CI is the measured cone index (CI) of the 0 to 0.152 m layer of the soil determined for on-road and off-road conditions,

b is the tire section width,

d is the nominal wheel diameter,

h is the tire section height,

δ is the tire deflection,

W is the normal load per a tire.

A geometrical representation of the tire parameters found in Equation (2) is given in Figure 3 (Brixius, 1987).
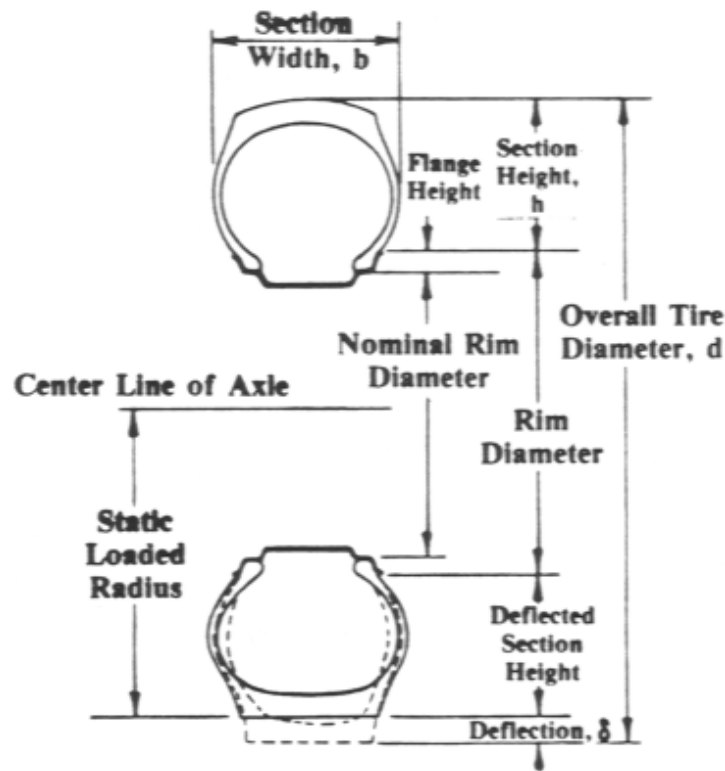
Figure 3: Tire parameters used to calculate dimensionless wheel numeric (Source: Brixius, 1987)

A cone penetrometer is often used to measure *CI* which is a combined indicator of the soil's shear and compressive strength properties. The cone penetrometer consists of a 30° steel cone with a base area of 3.22 cm^2 along with a sensor for measuring the force required to press the cone perpendicular into the soil at a constant rate (30 mm/s). The force required to press the cone into the soil divided by the base area of the cone represents the CI value (ASAE Standard, 2004). *CI* is a required input to the VTI model for estimating the motion resistance force generated by the tractive elements during the vehicle maneuvers.

The steered-wheel numeric ($N_{c\alpha}$) for vehicles operating in fine-grained soils is determined from the following equation:

$$N_{c\alpha} = N_c\left(1 - 2.26\alpha^{3/2}\right) \tag{3}$$

Where α is the tire steering angle (radians) for each wheel determined from the GPS data (Jones et al., 2007). The motion resistance force, R, generated as the vehicle traverses in a fine-grained soil is calculated by the following:

$$R = W\left(\frac{12}{N_c^2} + .007\right) \tag{4}$$

R for steered wheels utilizes the same equation; except, $N_{c\alpha}$ is substituted for N_c (Jones et al., 2007). To estimate the power that is required to overcome the motion resistance of the vehicle's tractive elements, the following equation determines the equivalent motion resistance power:

$$P_{MR} = \sum_{i=1}^{n}\left(V_{Vehicle} \cdot R_i\right) \tag{5}$$

Where

P_{MR} is the motion resistance power,

n is the number of wheels,

$V_{Vehicle}$ is the travel speed,

R_i is the motion resistance force for the ith wheel.

The equations presented from the VTI model allow for the motion resistance force of a vehicle operating in a fine-grained soil to be predicted, but numerous other equations are available for estimating such mobility parameters as the following: rut depth, wheel slip, and drawbar pull for wheeled and tracked vehicles. Equations are provided for vehicles operating in both fine and coarse-grained soils (Jones et al., 2007). It is thought that the fine-grained equations provide a better representation of the interaction between the tractive element and the terrain compared to the coarse-grained equations.

3.4.2 Agricultural Semi-Empirical Model

Research by Wismer and Luth (1973) and Brixius (1987) investigated the tractive performance of agricultural type tires. The modeling approach taken was similar to the VTI model because a dimensionless wheel numeric was developed from test data, and a least-squares regression analysis was used to estimate the coefficients of the semi-empirical relationships. The tractive performance models developed were for pneumatic tires with common agricultural tread geometry while utilizing the tire manufacturer's specifications and a soil strength index as input parameters to the model. The nominal inflation pressure at the rated normal load of these tires typically results in a deflection that is approximately 20% of tire's section height. The estimated rolling resistance from models developed by Wismer and Luth (1973) and Brixius (1987) differ from the VTI model because the tire geometry, deflection, tread type, and inflation pressure of agricultural and military can differ substantially. These models were developed to predict motion resistance, net traction, and input torque as a function of wheel slip and normal load

19

while the VTI model is focused on defining the motion resistance of the tractive elements and the resultant rut depth produced by the vehicle.

3.4.3 Rolling Resistance Coefficients

Bosch (2003) provides guidelines for estimating the rolling resistance coefficients (Analogous to motion resistance ratio) for primarily cars and on-road heavy trucks, and these values are found in Table 1. The resultant coefficient of motion resistance (R/W) from the VTI model approaches the coefficient of rolling resistances values for concrete and asphalt found in Table 1 as the measured CI of the soil approaches infinity.

Table 1: Rolling resistance coefficients for different vehicles operating on different surfaces (Source: Bosch, 1993)

Road Surface	Coefficient of rolling resistance
Car tires	
Concrete, asphalt	0.013
Rolled gravel	0.02
Tarmacadam	0.025
Unpaved road	0.05
Field	0.1 - 0.35
Truck tires	
Concrete, asphalt	0.006 - 0.01
Track-type tractor in field	0.07 - 0.12
Wheel on rail	0.001 - 0.002

Bosch (2004) indicates that the rolling resistance coefficient (ie motion resistance ratio) is directly proportional to the deflection of the tire and inversely proportional to the radius of the tire.

3.4.4 Existing U.S. Army Models

A popular method for evaluating the performance of vehicles is the U.S. Army Corps of
Engineers' vehicle cone index (VCI) model (Wong, 2010). Model development consisted of
evaluating the performance of military vehicles at various soil-strength conditions in fine and
coarse-grained soils. The output of the model are two VCI values (VCI_1, VCI_{50}); they represent
the minimum Cone Index (CI) values needed in the critical layer of the soil for the vehicle to
make 1 and 50 passes respectively over the terrain. To calculate VCI_1 and VCI_{50} for a given
vehicle, the Mobility Index (MI) must be estimated, and it is given by the following:

$$MI = \left(\frac{contact\_pressure\_factor \times weight\_factor}{track\_factor \times grouser\_factor} + bogie\_factor - clearance\_factor \right) \times$$
$$engine\_factor \times transmission\_factor \tag{6}$$

Where

contact_pressure_factor is the mean contact pressure of the vehicle (psi),

weight_factor is a weighting factor that ranges between 1.0 and 1.8, depending on vehicle
weight,

track_factor is the track width divided by 100.0 (in),

grouser_factor is 1.0 for grousers less than 1.5 in and 1.1 for grousers greater than 1.5 in,

bogie_factor is the gross weight divided by the product of the number of bogies in
contact with the ground and area of the track shoe (in^2),

clearance_factor is the ground clearance divided by 10 (in),

engine_factor is 1.0 if the power density is greater than or equal to 8.2 kW/tonne and 1.1
if it less than 8.2 kW/tonne,

transmission_factor is 1.0 and 1.05 for automatic and manual transmissions respectively.

The equations for calculating VCI_1 and VCI_2 are given by the following equations:

$$VCI_1 = 7.0 + 0.2MI - \frac{39.2}{MI + 5.6} \tag{7}$$

$$VCI_{50} = 19.27 + 0.43MI - \frac{125.79}{MI + 7.08} \tag{8}$$

If VCI_1 is greater than the measured CI value, the vehicle can effectively make a single pass across the terrain while the vehicle can make 50 consecutive passes over a given terrain if VCI_{50} is greater than the CI of the soil. The difference between the VCI and CI terms is an indicator of the excess soil strength. The VCI model for fine-grained soils is utilized in predicting the output of the NATO Reference Mobility Model (NRMM) model. Figure 4 details the effect of the excess soil strength on the motion resistance (MR) coefficient for wheeled vehicles.
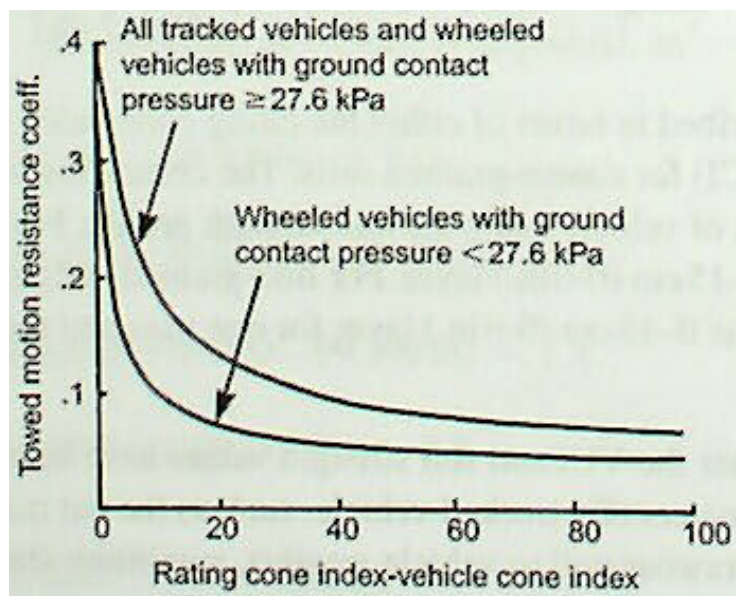
Figure 4: Motion resistance coefficient as a function of the excess soil strength (Source: Wong, 2010)

The predecessor of the NRMM was the U.S. Army Mobility Model (AMM-75). The NRMM attempts to estimate the mean travel speed between two points based on the interaction of system parameters such as the terrain conditions, vehicle specifications, and the operator (Wong, 2010). The NRMM model relies on the VCI model for estimating the maximum travel speed of a vehicle. In the model, the terrain is divided into discrete terrain units where the mean travel speed in each unit is assumed to be constant. Factors that may limit the travel speed of a vehicle are maximum drivewheel power, soil strength, operator discomfort, limited visibility, maneuverability concerns, and obstacle avoidance. The factor with the lowest predicted mean travel speed is the limiting factor for mobility of the military vehicle. Mobility maps such as Figure 5 for a truck weighing 22.24 kN can be developed for a given vehicle which allows for the optimal travel route to be predicted.
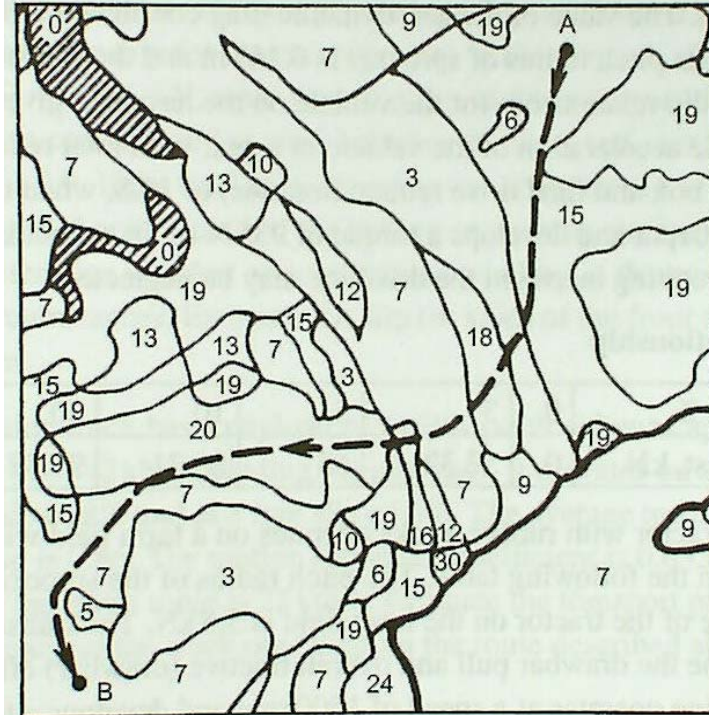
Figure 5: A mobility map for a 22.24 kN truck shows the maximum travel speed (mph) and ideal travel path in a given offroad-terrain (Source: Wong, 2010)

There is the potential that similar maps could be developed that estimate the power required to traverse a given region from GPS tracking data of military vehicles. The fuel required to travel along the optimum travel path could be predicted from power maps by making assumptions about the energy dissipated between the fuel to the drivewheels. Providing accurate estimates of the fuel requirements for a fleet of military vehicles is of critical interest for military personnel. The use of power maps along with the NRMM may allow for decreased fuel delivery cost while improving delivery efficiency.

3.5 Grade Power

By determining the rate at which the elevation of the terrain changes as a function of time, the required power to displace the vehicle vertically is defined by the following:

$$P_{Grade} = (mg) \cdot \frac{\partial_h}{\partial_t} \tag{9}$$

Where

P_{Grade} is the grade power,

m is the mass of the vehicle,

g is the acceleration due to gravity,

$\frac{\partial_h}{\partial_t}$ is the rate of elevation change acquired from the GPS data.

Determining the road grade is of particular interest for commercial heavy-duty vehicles (Semi-trailers) with a low power-to-weight ratio because the towed force can vary significantly, making road grades greater than 4% difficult to travel at high speeds. Researchers at Stanford University (2001) detailed two processes for determining the road grade of a ground vehicle via global positioning system (GPS) units. The first method required two GPS antennas mounted on the vehicle to measure the angle of the vehicle in the pitch plane. The road grade was predicted from the GPS elevation data from the two GPS receivers and the known distance between the receivers (Stanford University, 2001). The second method compared the horizontal speed and change in elevation data from a single GPS unit to predict road grade of the vehicle. The researchers conducted an accuracy assessment on the test data available for the Mercedes-Benz

E320 test vehicle, and the results indicated that low frequency GPS data (1 Hz) can be used with both methods for providing reasonable estimates of road grade. The results indicated both methods could predict the road grade traversed by a vehicle, but the more complex method that relied on two GPS antennas was much more sensitive to acceleration changes by the vehicle because any acceleration produced vehicle pitch. The change in vehicle pitch introduced additional variability in the estimates of grade from the two GPS receivers (Stanford University, 2001).

3.6 Inertia Power

3.6.1 Linear Inertia Power

The linear inertia power necessary to increase or decrease the vehicle's speed along the path traversed is calculated by the following equation:

$$P_{Lin.Inertia} = F_{Lin.Inertia.} \cdot V_{Vehicle} = (m \cdot a) \cdot V_{Vehicle} \qquad (10)$$

Where

$P_{Lin.Accel.}$ is the linear inertia power,

$F_{Lin.Accel.}$ is the force required to accelerate the vehicle,

a is the acceleration of the vehicle.

The acceleration of the vehicle has a significant impact on the estimated mobility power of a vehicle. Jun et al. (2006) addressed the effects of the various methods for calculating acceleration from discrete velocity data when accelerometers are not available. The three approaches for calculating acceleration from velocity as function of time data are the forward, backward, and central difference methods. Previous research with large on-road vehicles indicated that the central difference method for calculating acceleration provided for the most accurate indicator of the required engine power (Jun et al., 2006).

The GPS points stored during tracking maneuvers have a Coordinated Universal Time (UTC) and a speed value associated with each point. The acceleration ($a(t_o)$) of the vehicle is calculated from the GPS speed data ($v(t_o)$) using the three-point central difference acceleration equation given by the following:

$$a(t_o) = \frac{v(t_o + h) - v(t_o - h)}{2h} \tag{11}$$

Where h is the absolute difference between the UTC times ($h = 1$ s assuming 1 Hz GPS data). Equation (11) is an average of the forward and backward difference methods for calculating acceleration, and it removes some of the variability associated with using GPS data to calculate acceleration of a vehicle (Jun et al., 2006).

Jun et al. (2006) investigated the effect of the different acceleration calculation methods on a vehicle engine power model for estimating emission rates. The model's governing equation is based on the longitudinal vehicle model and is similar to the proposed models's governing

27

equation.   The results from the study indicate that each method for calculating acceleration provided a statistically different engine power distribution when the vehicle travel speed was less than 27 m/s (Jun et al., 2006).

3.6.2 Rotational Inertia Power

The increase in the linear inertia of a vehicle by a power source such as an engine must be accompanied by an increase in the rotational inertia of the vehicle's engine, transmission, differential, and drivewheels. Millo (2011) and Irick (2012) indicated that the vehicle equivalent mass value (γ) for a given vehicle relates the power required to vary the rotational inertia of the engine and drivetrain components and linear inertia of the vehicle. γ represents the ratio of an equivalent mass of the rotating components to the actual mass of the entire vehicle. γ effectively allows for the power required to vary the rotational inertia of the drivetrain components to be estimated from the known mass (m), velocity, and wheel speed of the vehicle. γ is maximum in the lowest gear of the transmission, and decreases substantially as the transmission is shifted into higher gears (Millo, 2011; David Irick, University of Tennessee, personal communication, 31 January 2012).   The vehicle equivalent mass (m_{eq}) is introduced to account for the power that is required to vary the inertia of the engine and drivetrain components, and it is given by the following expression:

$$m_{eq} = m \cdot (1 + \gamma) \tag{12}$$

Equation (10) is modified to include the effects of any increase or decrease of the vehicle's

rotational inertia, and the expression is represented by the following:

$$P_{Inertia} = \left(m_{eq} \cdot A\right) \cdot V \qquad (13)$$

Equation (13) predicts the power requirement to vary both the linear inertia of the vehicle and

rotational inertia drivetrain and engine. γ is a maximum in the transmission's lowest gear

because the engine speed associated with any level of acceleration in the lowest gear is the

greatest compared to any higher gears. Also, rotational kinetic energy is a function of the square

of the rotational speed of the rotating component. This indicates that the total rotational kinetic

energy of all rotating engine component's increases by 1600% when engine speed is increased

from 1000 RPM to 4000 RPM. γ is a minimum while the transmission's highest gear is engaged

because most of any rotational inertia change occurs from the drivetrain components instead of

the engine's rotating components (David Irick, University of Tennessee, personal

communication, 31 January 2012).

3.7 Aerodynamic Drag Power

As the viscous fluid (air) flows over the surface of the vehicle during locomotion, a drag force

that resists forward motion is exerted on the vehicle (Gillsepie, 1992; Wong, 2008; Wong, 2010).

The drag force exerted on a body is given by the following equation:

$$F_{Drag} = \frac{\rho}{2} C_D A_f V_r^2 \qquad (14)$$

Where

F_{Drag} is the drag force exerted on the vehicle that opposed forward movement,

ρ is the density of the air,

C_D is the drag coefficient of the vehicle,

A_f is the frontal area of the vehicle,

V_r is the speed of the air, relative to the vehicle.

The density of air, ρ (kg/m^3), is given by the following expression:

$$\rho = 1.225 \left(\frac{P_r}{101.325} \right) \left(\frac{288.16}{273.16 + T_r} \right) \tag{15}$$

Where

P_r is average atmospheric pressure (kPa) at the given elevation,

T_r is the mean air temperature (ºC) (Gillsepie, 1992).

The drag power (P_{Drag}) is determined from the following equation:

$$P_{Drag} = F_{Drag} \cdot V_{Vehicle} = \left(\frac{\rho}{2} C_D A_f V_r^2 \right) \cdot V_{Vehicle} \tag{16}$$

If V_r is assumed to be equal to the vehicle speed because the relative air speed is not measured, the expression for P_{Drag} reduces to the following:

$$P_{Drag} = \left(\frac{\rho}{2} C_D A_f \right) \cdot V_{Vehicle}^3 \qquad (17)$$

An aerodynamic drag force is exerted on any vehicle during locomotion, assuming a non-zero relative air speed. To calibrate a model due to the effect of the aerodynamic drag force exerted on a vehicle, a coastdown test may be performed to estimate the vehicle's drag coefficient (C_D). A coastdown test can be performed by disengaging the drivetrain of the vehicle after reaching a certain speed and measuring the change in the vehicle's speed as a function of time until the vehicle becomes stationary (Gillsepie, 1992). C_D values for various vehicle geometries and types are given in Table 2.

Table 2: Drag coefficients (C_D) for various vehicle types

(Source: Bosch, 2003)

	Drag coefficient c_w	Drag power in kW, average values for $A = 2\,m^2$ at various speeds[1]			
		40 km/h	80 km/h	120 km/h	160 km/h
Open convertible	0.5 ... 0.7	1	7.9	27	63
Station wagon (2-box)	0.5 ... 0.6	0.91	7.2	24	58
Conventional form (3-box)	0.4 ... 0.55	0.78	6.3	21	50
Wedge shape, headlights & bumbers integrated in body, wheels covered, underbody covered, optimized flow of cooling flow.	0.3 ... 0.4	0.58	4.6	16	37
Headlights and all wheels enclosed within body, underbody cover	0.2 ... 0.25	0.37	3.0	10	24
K-shape (minimal cross section at tail)	0.23	0.38	3.0	10	24
Optimum streamlining	0.15 ... 0.20	0.29	2.3	7.8	18
Trucks, combinations	0.8 ... 1.5	—	—	—	—
Motorcycles	0.6 ... 0.7	—	—	—	—
Buses	0.6 ... 0.7	—	—	—	—
Streamlined buses	0.3 ... 0.4	—	—	—	—

Yasin (1978) detailed the methodology for conducting on-road coastdown tests for estimating the aerodynamic drag force exerted on a vehicle. A total of 157 coastdown tests were conducted on 22 different small passenger cars and light-duty trucks on flat, paved surfaces. The resistive forces generated during coastdown tests were averaged for two tests conducted in opposite directions to minimize the effect of a head or tailwind. It was concluded that a wind correction factor was not accurate in predicting the variation of the drag force due to crosswinds. Coastdown tests should be conducted only during low crosswinds (< 4.5 m/s) to obtain accurate estimates of a vehicle's drag coefficient (C_D). The drag coefficient can be estimated for the vehicle by conducting a least-squares regression analysis of the measured coastdown test data. This least-squares regression analysis requires some estimate of the motion resistance forces generated by the tires to estimate in C_D Equation (14). The drag force and the motion resistance forces estimated from coastdown testing are at approximately the same level of precision that can be obtained from wind tunnel and chassis dynamometer testing for a vehicle (Yasin, 1978).

Previous research indicates that the effect of F_{Drag} on off-road vehicle performance is minimal when the vehicles do not exceed 48 km/hr (30 mph) (Wong, 2010). Military vehicles oftentimes exceed 48 km/hr during certain operations, thus the effect of F_{Drag} must be considered. Testing of heavy-duty vehicles such as tanks or armored personnel carriers with frontal areas in the range of 6 – 8 m^2 indicated such vehicles have a C_D value of approximately 1.0. A 50 ton tank with a C_D value of 1.17 has a drag force of 0.828 kN exerted on it by the air flowing over the tank's surface which amounts to about 11 kW of net power that must be delivered to the tractive elements (Wong, 2010).

3.8 Drawbar Power

A towed implement or trailer exerts a force upon the hitch of a vehicle at some angle to the longitudinal axis (Θ) which opposes the forward motion of the vehicle during locomotion. This force is termed the drawbar load ($F_{Drawbar}$) on a vehicle, and the subsequent drawbar power ($P_{Drawbar}$) required to tow the implement is given by the following equation:

$$P_{Drawbar} = \left(F_{Drawbar} \bullet Cos(\Theta)\right) \cdot V_{Vehicle} \tag{18}$$

3.9 Net Mobility Power

The power required to overcome the forces in Equation (1) along with rotational inertia of the wheels represents a wheeled vehicles mobility power. Mobility power is the power dissipated by the wheels of the vehicle in order to develop the tractive or thrust force along the vehicle's travel path. The total mobility power, $P_{Mobility}$, required for the vehicle to maneuver across the terrain at the measured velocity, turning radius, and loading conditions, while taking into account the vehicle's tire characteristics, is determined from the following equation:

$$P_{Mobility} = P_{MR} + P_{Grade} + P_{Inertia} + P_{Drag} + P_{Drawbar} \tag{19}$$

The calculated mobility power can be equated with the required engine power for the vehicle by completing a drivetrain analysis that calculates the overall drivetrain efficiency losses between the engine and the tractive elements. Equation (19) could also be applied to tracked vehicles by utilizing the Vehicle Terrain Interaction (VTI) model's motion resistance equations for tracked

vehicles operating in fine and coarse-grained soils. Estimating a tracked vehicle's equivalent mass for the rotational inertia component of the model would be an important parameter to consider since sophisticated tracked vehicle systems tend to have a greater magnitude of rotational and linear inertia compared to wheeled vehicles.

3.10 Mobility Energy

The mobility power can be estimated from discrete GPS tracking data for a given vehicle using Equation (19), and integration of the mobility power function yields the energy required during a given time span. The net energy (E) required for mobility power in a given time period ($t_2 - t_1$) is defined by the following equation:

$$E = \int_{t_1}^{t_2} \left(P_{Mobility} \cdot dt \right) \qquad (20)$$

The power and torque requirements for a given military vehicle on various on and off-road test courses would provide engineers the critical information necessary to properly determine the power and energy needed from a parallel hybrid's two power sources (Taylor, 2011). Instrumenting a fleet of military vehicles to characterize the power requirements during specific on-road and off-road operations is oftentimes very costly. The mobility power model that uses the dynamic vehicle parameters from GPS tracking data and the soil's measured or estimated cone index (*CI*) may represent an affordable method of estimating the mission-specific power and energy requirements.

If a vehicle is equipped with a hybrid powertrain, the positive specific energy consumption value can be estimated for the vehicle which represents the mobility energy required by the electric power source during specific operations. The potential specific energy production estimated from the model for the vehicle can provide an estimate of the theoretical energy available for harvesting via regenerative braking from a hybrid powertrain. Estimating the specific energy consumption and potential specific energy production may allow for the duration that a hybrid military vehicle can operate during "silent watch" operations (electric power only) to be predicted for the given terrain conditions. The silent watch capabiliy of current military vehicles is of principle importance when evaluating the in-field performance of hybrid vehicles.

3.11 Summary

The use of hybrid-electric military vehicles is of particular interest in recent years for the U.S. military because such vehicles may substantially reduce fuel costs to operate the vehicle. The hybrid-electric drivetrain increases a military vehicle's silent watch capability by allowing the vehicle to operate for longer periods where only the relatively quiet electric motors propel the vehicle. The precise power requirement for locomotion must be known when designing a hybrid-electric military vehicle's complex drivetrain. At this time, there are not standardized power duty cycles for a given type of military vehicle because the duty cycle characteristics can vary substantially depending on the terrain type and the mission being performed. As a result, there is a need to determine the terrain and mission-specific power duty cycles of military vehicles.

Costly methods of data acquisition can be used to quantify the power duty cycles for military vehicles. Instrumenting the driven wheels of a vehicle to obtain a direct measurement of drivewheel power represents the most expensive solution. The complexity and costs associated with directly measuring drivewheel power limits the use of this method across vehicle platforms. Estimating drivewheel power from a military vehicle's Controller Area Network (CAN) is another option. However, it may be difficult to log the CAN signals necessary to estimate drivewheel power. Furthermore, the data acquisition equipment required to estimate drivewheel power from CAN data may be considered an invasive approach where data acquisition equipment may hinder the military personnel operating the vehicle and performing the training mission or the necessary CAN signals that transmit engine power values may be proprietary.

GPS tracking data of military vehicle provides for several critical dynamic vehicle parameters such as position, speed, acceleration, elevation (height above ellipsoid), and heading. The GPS data can be used to estimate the power required for the vehicle to overcome the motion resistance, grade, inertia, and aerodynamic forces that occurred during locomotion. These important vehicle parameters allow for the power duty cycle requirements for the given mission and terrain conditions to be characterized from a GPS-based mobility power model. Developing a vehicle's power duty cycles from GPS data is a non-invasive and cost-effective alternative compared to logging signals from a vehicle's CAN network. The effect of varying soil strength, elevation grade, and vehicle turning radius can be quantified from the GPS-based mobility power concept.

A GPS-based mobility power model may provide a cost-effective solution for characterizing the power requirements of military vehicles, but currently a GPS model that predicts vehicle power for military vehicle applications has not been validated. Validation of such a model is necessary to determine the accuracy of the predicted vehicle power duty cycles. The model can be applied to current and historical GPS tracking data of military vehicles after the model has been validated to estimate the mission and terrain-specific power duty cycles.

Chapter 4: Validation

4.1 Model Development

The development of the model began by defining all of the components of the model that sum to a vehicle's required mobility power. The longitudinal vehicle model given by Equation (1) provided the basis for the resistive forces generated during locomotion. Equations (2 – 5) and (9 – 18) were used to quantify the motion resistance, grade, inertia, and aerodynamic drag power components of the model. The model validated does not include any drawbar loads because the test vehicle did not have an applied drawbar load during the tests; thus $P_{Drawbar}$ was assumed to be zero. Equation (19) was slightly modified so that the governing equation of the mobility power model validated is given by the following:

$$P_{Mobility} = P_{MR} + P_{Grade} + P_{Inertia} + P_{Drag} \qquad (21)$$

The input parameters to the model such as the vehicle's position, speed, acceleration, rate of elevation change, and time are all determined from the GPS data acquired during the vehicle maneuvers. The vehicle, tire, and drivetrain specifications are the other necessary input parameters to the model that are not obtained from the GPS data.

4.2 Materials

4.2.1 Validation Testing Sites

The location where validation occurred was at certain test sites in the Knoxville, Tennessee area. The controlled motion resistance and inertia tests occurred at a test site with minimal grade. The grade tests were conducted along a travel path with a continuously positive grade and an elevation gain of approximately 50 m. Figure 6 provides an aerial map of the test location where the motion resistance and inertia tests were conducted. The latitude and longitude of the motion resistance and inertia test site was approximately the following: N 35.9497°, W 83.9371°. Figure 7 details the test site where the grade tests were performed. The latitude and longitude of the grade test site was approximately the following: N 35.9935°, W 83.8470°. Figure 8 provides a representation of the travel path taken by the test vehicle during the uncontrolled validation test that simulated a U.S. Army reconnaissance mission. The latitude and longitude of the uncontrolled test start location was N 35.9449°, W 83.9093°. The controlled and uncontrolled validation tests were performed on the 16$^{\text{th}}$ and 20$^{\text{th}}$ of December 2011 respectively. There was not a significant amount of wind at the locations where validation testing occurred so it was acceptable to apply the assumption implied in Equation (17) from Section 3.7 for estimating the aerodynamic drag power of the test vehicle.
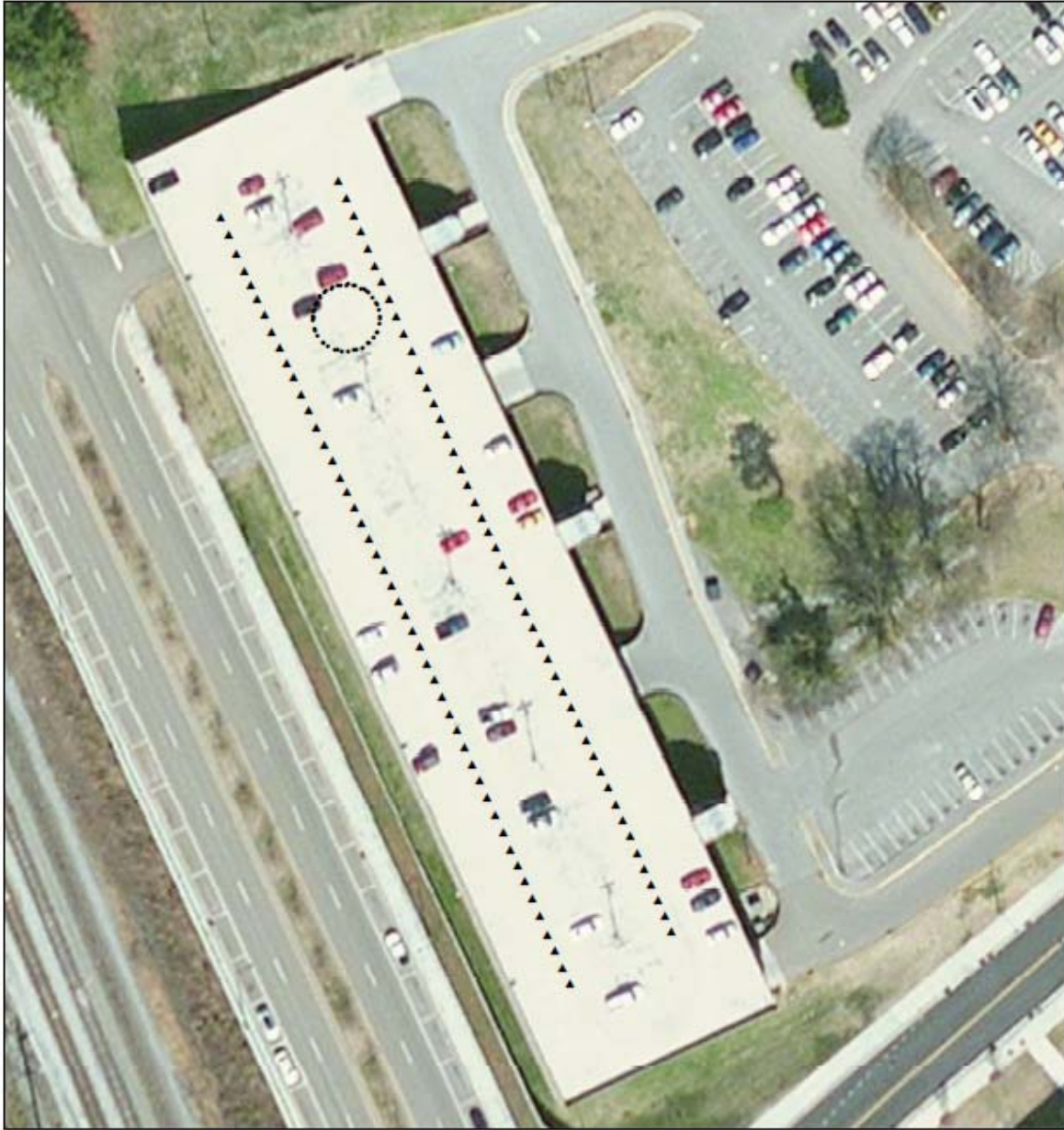
Legend
▲ M.R. and inertia test travel paths
• 5 m constant turning radius circle test

Figure 6: The motion resistance and inertia test location
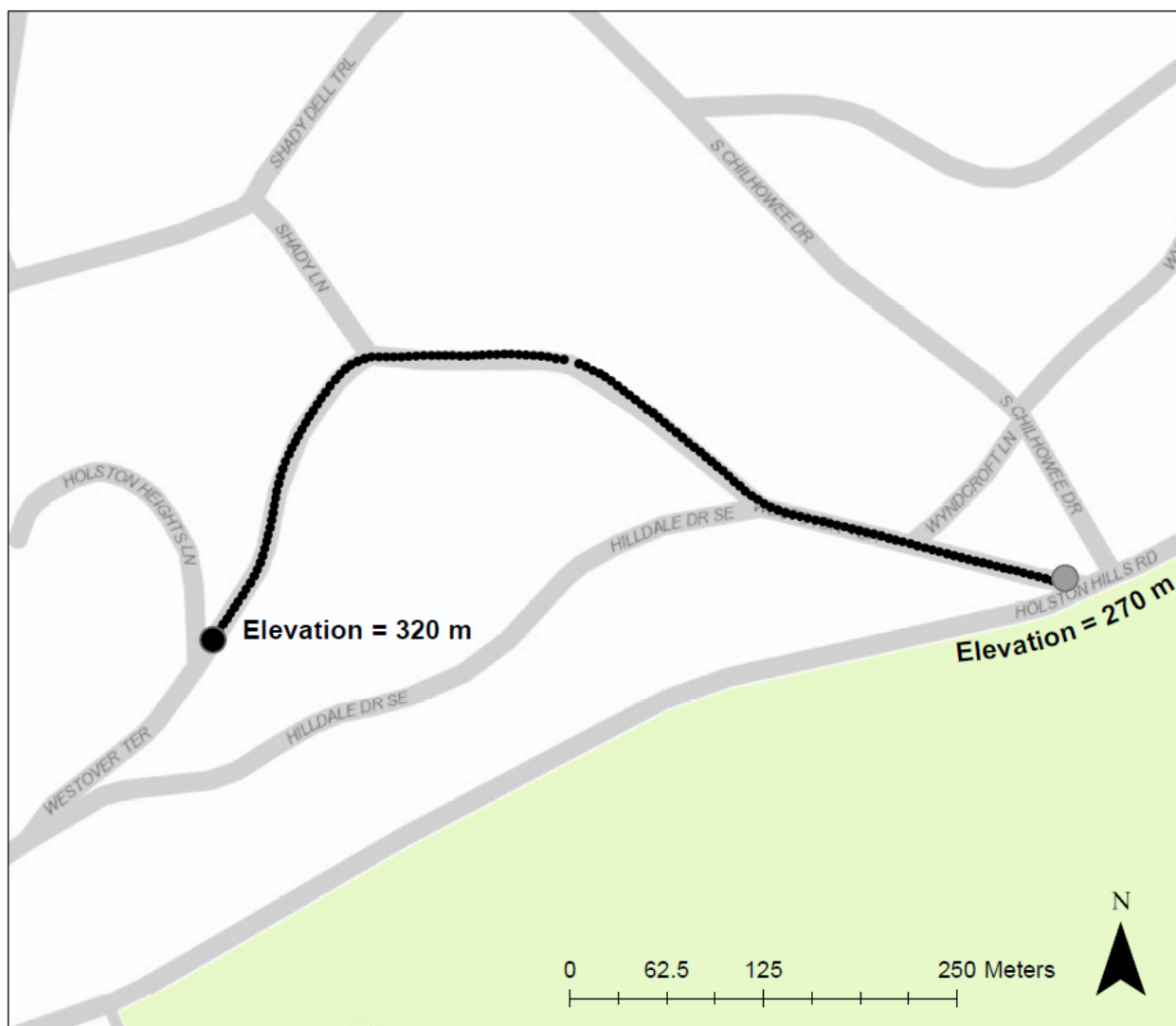
Figure 7: The travel path taken at the grade test site

Figure 8: The uncontrolled test travel path along with the discrete predicted mobility power values from the Trimble 132 GPS receiver for a section of the test

43

4.2.2 Vehicle Tracking System Components

Previously developed Vehicle Tracking System (VTS) units were used to gather the necessary

GPS data for the mobility power model. The VTS system is comprised of a serial data recorder

(SDR) that typically stores data from a Garmin 18 Wide Area Augmentation System (WAAS)

Differential Global Positioning System (DGPS) receiver while powered by 12 V batteries and

enclosed in a watertight case. The components of the VTS system can be seen in Figure 9. The

Garmin 18 GPS receiver is shown in Figure 9.

Figure 9: Vehicle Tracking System (VTS) components

The VTS units were designed to be compact and cost-effective devices that can be mounted to

any type of vehicle. No external power source is needed while approximately 10 days of GPS

data can be acquired from the stand-alone device. The GPS and SDR are supplied 12 V DC

power from two lead-acid batteries, and the components are self-contained in a watertight plastic case, except for the GPS receiver that is magnetically mounted to the exterior of the case or vehicle (Howard et al., 2011).

4.2.2.1 GPS Receivers – Garmin 18 and Trimble 132

The VTS units utilized a Garmin 18-PC WAAS DGPS receiver that was configured to output data at a sampling rate of 1 Hz. This Garmin receiver is typically used with the VTS unit because it weighs only 1.08 N, is small, and can be attached magnetically to the exterior of a vehicle or VTS case. Furthermore, the receiver can operate at ambient temperatures between -30°C and 85°C and at an unregulated DC input voltage range between 6 and 40 V (Garmin, 2008; Potteti, 2009). Power is supplied to the Garmin receiver via a single cable. The GPS data outputted by the Garmin GPS18 GPS receiver was recorded by the SDR on a compact flash card. The GPS data is in National Marine Electronics Association (NMEA) string format, and only the $GPGGA and $GPRMC are stored to the SDR during vehicle tracking (Potteti, 2009). The following parameters are transmitted on these two NMEA strings: Coordinated Universal Time (UTC), latitude (Coordinate system: WGS 1984), longitude (Coordinate system: WGS 1984), Speed Over Ground (SOG) (ie travel speed), Coarse Over Ground (COG) (ie heading), Height Above Ellipsoid (Elevation), and date (NMEA Standard, 1995). The critical data transmitted on the $GPGGA and $GPRMC strings represents the vehicle parameters necessary to apply the mobility power model to GPS data.

A separate VTS unit was used to log GPS data from a Trimble AgGPS132 receiver with Omnistar differential correction so that the vehicle was tracked simultaneously by two different

types of GPS receivers. The differential correction used by the Trimble GPS receiver tends to

result in more accurate and precise position, speed, and grade elevation data while tracking

vehicles. The manufacturer claims sub-meter static accuracy can be attained by the GPS

receiver. The GPS receiver's dynamic mode was configured to "land" (Trimble, 2003). Figure

10 shows the Garmin 18 and Trimble 132 GPS receivers mounted on the roof of the test vehicle.
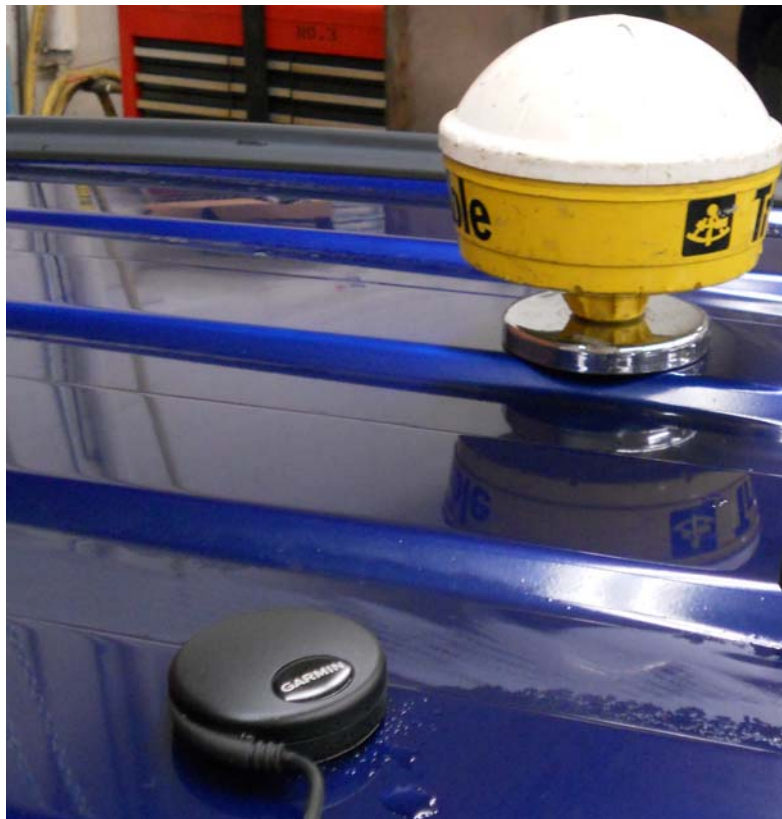
Figure 10: The Garmin 18 and Trimble 132 GPS receivers mounted on the test vehicle

4.2.2.2 Serial Data Recorder (SDR)

The GPS data is stored via Acumen's DataBridge SDR2-CF on a 256 MB compact flash card.

The device is compact (12.4 X 8.57 X 3.12 cm) and is enclosed in a durable aluminum

enclosure. The SDR device requires approximately 350 mW of electrical power while logging

data. The SDR can operate at ambient temperatures between -40°C and 85°C and at an input DC

voltage range between 5 V and 30 V. The SDR can collect 1 Hz GPS data for 20 days with a

256 MB flash card. The serial data was stored to a flash card in FAT32 format (Potteti, 2009).

4.2.2.3 Power Supply

Two Odyssey rechargeable drycell 12 V batteries (PC625) were used to power the GPS receiver

and the SDR. The lead-acid battery is a starved electrolyte dry cell battery that is explosion and

corrosion proof. The battery can be shipped via conventional methods since it is dry cell battery.

The battery can operate at ambient temperatures between -40°C and 60°C.

4.2.2.4 Protective Case

A small Pelican case contains the GPS receiver, SDR, and two batteries that comprise the VTS

system. The small case (36 X 27 x 15 cm) is rated as impact resistant and waterproof, and it can

easily be mounted externally or internally in a cargo storage area of the vehicle. A small piece of

sheet metal (ferrous) is fixed to the outside of the case where the GPS receiver can be

magnetically attached.

4.2.3 Vehicle, CAN Hardware, and CAN Software Components

A 2005 Chevrolet Equinox was the vehicle used during validation testing. The vehicle was

equipped with Intrepid Control Systems, Inc.'s NeoVI Pro hardware that receives and transmits

CAN signals in order to control the vehicle and engine. The NeoVI Pro executed a Vehicle Spy

3 file (*.vs3) that controlled the vehicle and engine while logging the desired CAN signals such as engine speed, engine torque, and wheel speed.

4.2.3.1 Test Vehicle

The 2005 Chevrolet Equinox had a 1.9 L Fiat turbocharged diesel engine that propelled the 19.3 kN vehicle. The engine's peak power and torque ratings are 109 kW (at 4000 RPM) and 326 Nm (at 2000 RPM) respectively. The vehicle is capable of being operated as a parallel through-the-road hybrid where rear drivewheel power is supplied by an electric motor, but the vehicle was operated during validation testing with a conventional drivetrain (ie diesel engine sole power source). The engine power was delivered via a six-speed Fiat manual transmission to the front axle of the vehicle. The Fiat engine's maximum torque and power as a function of engine speed are represented in Figures 64 and 65 respectively from Appendix A. The vehicle was equipped with Michelin's PAX runflat tires (Model: Challenge X235-710 R460A) with a rolling resistance coefficient of 0.00675. The drag coefficient (C_D) provided by General Motors was 0.42. The vehicle, engine, drivetrain efficiency ($\eta_{Drivetrain}$), and equivalent mass (γ) specifications provided by General Motors are given in Tables 23 and 24 in Appendix A. The vehicle mass in Table 23 from Appendix A includes the mass of a 70 kg operator and a 70 kg passenger. An image of the vehicle used during validation is given in Figure 11.

Figure 11: The 2005 Chevrolet Equinox vehicle used during validation testing

4.2.3.2 NeoVI Pro Hardware

The test vehicle's CAN network was controlled via Intrepid's NeoVI Pro device. The device executed a *.vs3 file generated in the Vehicle Spy 3 software. The *.vs3 file was stored on the flash card that was connected to the NeoVI hardware. The device's primary function was to receive and transmit CAN signals so that the engine and vehicle were controlled according to the program stored on the flash card and the input from the operator. The *.vs3 file used during validation testing allowed for logging of the necessary vehicle and engine parameters. The NeoVI Pro device used during testing is shown in Figure 12.
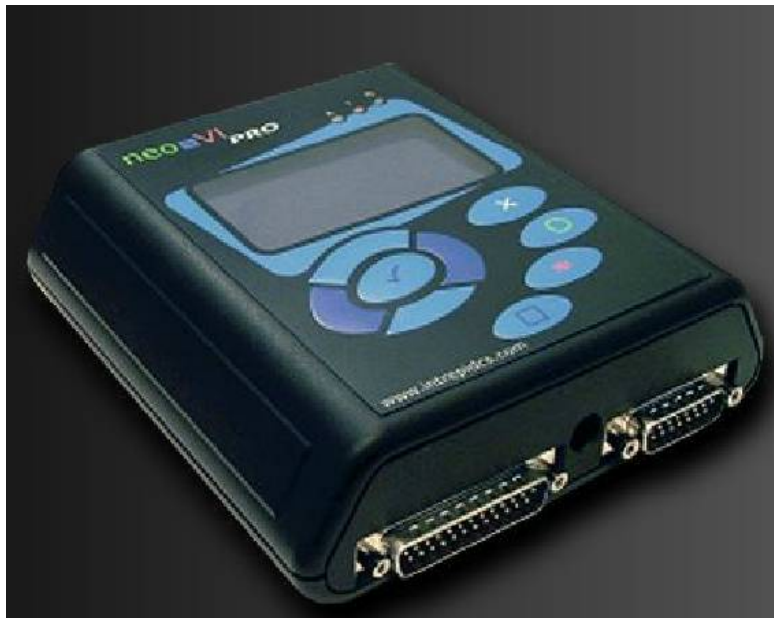
Figure 12: The NeoVI Pro device

4.2.3.3 Vehicle Spy 3 Software

Vehicle Spy 3 (Version 1.11) was the software used to create the *.vs3 file for controlling the

CAN network and logging the appropriate CAN signals. The *.vs3 file was transferred to the

NeoVI Pro's flash card after it was generated with the Vehicle Spy 3 software. The powerful

software allows for communication across multiple CAN networks while providing the user with

a helpful tool for testing and analysis of vehicles with a CAN network. The *.vs3 file used

during testing was created so that the engine speed, engine torque, and wheel speed data from the

CAN network were stored to the NeoVI Pro's flash card at a sampling rate of 25 Hz. As

discussed in Section 3.2, the engine torque values found in certain CAN signals were estimated

from a lookup table stored on the engine control module's (ECM) memory. Since the test vehicle

had a diesel engine, inputs to the lookup table were the fueling rate to the engine, engine speed,

and/or several other engine parameters. Engine and wheel speed values transmitted on two

separate CAN signals were measured from either hall-effect or induction type rotational speed

sensors. A screenshot of the logging window used to select and log the appropriate CAN signals

can be seen in Figure 13.
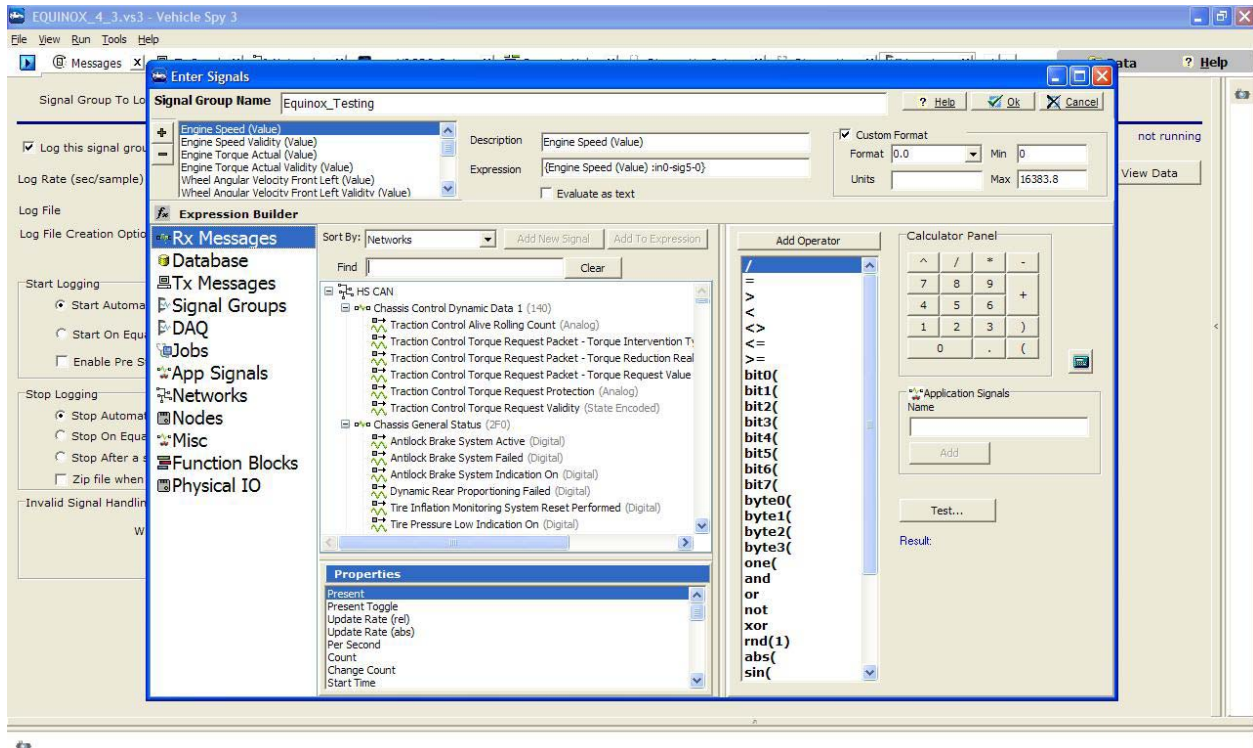
Figure 13: The Vehicle Spy 3 software's user interface

4.2.4 ArcGIS 10 Software

ArcGIS 10 was necessary to spatially map the GPS tracking data for the development of aerial

maps of the test sites and mobility power maps of the vehicles analyzed. The software was also

used to convert the GPS position data from a spherical coordinate system to the Universal

Transverse Mercator (UTM) projected coordinate system. Haugen (2002) indicated that the

conversion of the spatial GPS data to a projected coordinate system allows for the vehicle's

turning radius to be calculated from the GPS data via the three-point method (Haugen, 2002).

The three-point method was used to estimate the vehicle's turning radius during testing.

4.2.5 MATLAB 2010B Software

A MATLAB program was developed to convert the 25 Hz signals logged from the CAN network

to the 1 Hz sampling rate that the GPS data was collected at. A simple average was taken from

the 25 Hz data to estimate the associated 1 Hz value. The software was necessary due to the

data's tendency for having unequal sampling intervals between each data point.

4.3 Methods

4.3.1 Model Verification

Verifying the model was necessary to ensure that the calculations performed by the mathematical

model during validation met the model developer's intentions. The model's mathematical

operations, unit conversions, and logic were checked for accuracy during verification. A known,

discrete measured drivewheel power value was compared to the model's predicted discrete

mobility power value from GPS data collected during testing in order to verify the model. Data

collected during validation testing was used during verification of the model. The methodology

used in the model for calculating mobility power from GPS data was independent of the GPS

receiver used; thus calculations are only shown for a single receiver.

4.3.1.1 Measured Drivewheel Power Calculations

The measured drivewheel power value was determined from the CAN data's measured engine power, but the power dissipated through the drivetrain and by the accessory components of the engine had to be taken into account. The further use of the term "measured drivewheel power" refers to the calculated drivewheel power values estimated from the engine speed and engine torque messages transmitted on certain 11 bit CAN signals. The measured engine power was calculated from the engine speed and engine torque values which were 1894 RPM and 88.64 Nm respectively for the discrete dataset that was verified. The engine power was calculated from Equation (22) in Section 4.3.2 and is given by the following:

$$P_{Engine} = \frac{2\pi \cdot T_{Engine} \cdot n_{Engine}}{60000} = \frac{2\pi \cdot 88.64 Nm \cdot 1894 RPM}{60000} = 17.58 kW$$

It should be noted that equation numbers are not shown in Section 4.3.1 when illustrating the required calculations for model verification. The power transmitted to the accessory components of the engine was subtracted from the measured engine power since it was not delivered to the drivewheels of the test vehicle. Equation (23) from Section 4.3.4 was used to calculate the accessory power demand, and the calculations are represented by the following:

$$P_{Accessory} = 0.0013 \cdot n_{Engine} + 0.3317 = 0.0013 \cdot 1894 RPM + 0.3317 = 2.79 kW$$

The vehicle was operating in the 2nd gear of the transmission, and the associated net drivetrain efficiency value of 0.91 was used from Table 24 in Appendix A. The calculated engine and

accessory power along with the known drivetrain efficiency in 2nd gear allowed for the measured

drivewheel power to be computed from Equation (25) from Section 4.3.6, and the following

expression details the calculation:

$$P_{Drivewheel} = \left(P_{Engine} - P_{Accessory}\right) \cdot \eta_{Drivetrain} = (17.58 - 2.79) \cdot 0.91 = 13.46 kW$$

The measured drivewheel power value was 13.46 kW, and this value was used to compare the

predicted mobility power value during verification of the model.

4.3.1.2 Predicted Mobility Power Calculations

The GPS based mobility power model used during validation testing utilized Equations (2 – 20)

from Chapter 3 where the summation of each component of the model represented the mobility

power of the test vehicle. The critical parameters from the discrete GPS data that were used to

verify the model are given in Table 3. The values of the important test vehicle and terrain

parameters used during verification of the model are given in Table 4.

Table 3: The critical parameters from the GPS data used during model verification

Pertinent GPS Parameters	
Δ t (s):	1
Speed (m/s):	9.16
Acceleration (m/s^2):	-0.026
Elevation rate (m/s):	0.58
Turning radius (m):	>> 500

Table 4: The vehicle and terrain parameters used during model verification and validation

Model Parameters	
RCI[on-road] (kPa):	4137
W_{total} (kN):	20.88
$W_{per\ tire}$ (kN):	5.22
d (m):	0.71
b(m):	0.225
h(m):	0.125
δ (m):	0.017
Number Tires:	4
Frontal Area (m^2)	2.686
Drag Coefficient:	0.42
Air Density (kg/m^3):	1.21

Verification of the model required Equations (2 – 5) from Section 3.4.1 to compute the value of the motion resistance power of the model for the discrete GPS data point. The first step to calculate the motion resistance component of the model was to calculate the non-steered wheel numeric. The wheel numeric for each non-steered wheel was calculated according to the following expression:

$$N_c = \frac{CI \cdot bd}{W_{per-tire}\left(1-\dfrac{\delta}{h}\right)^{3/2}\left(1+\dfrac{b}{d}\right)^{3/4}} = \frac{4137\ kPa \cdot 0.225\ m \cdot 0.71 m}{5.22\ kN\left(1-\dfrac{0.017}{0.125}\right)^{3/2}\left(1+\dfrac{0.225}{0.71}\right)^{3/4}} = 127.7$$

For the purpose of model verification, the steered wheel numeric was assumed to be equal to the non-steered wheel numeric since the estimated vehicle turning radius exceeded 500 m. The motion resistance force for each tire was estimated from Equation (3) and is represented by the following:

$$R_{per-tire} = W_{per-tire}\left(\frac{12}{N_c^2} + .007\right) = 5.22kN\left(\frac{12}{127.7^2} + .007\right) = 0.040kN$$

Since R was assumed to equal for all tires, Equation (5) reduced to the following expression for calculating the motion resistance power:

$$P_{MR} = \sum_{i=1}^{n}\left(V_{Vehicle} \cdot R_i\right) = 4 \cdot \left(V_{Vehicle} \cdot R_i\right) = 4 \cdot \left(9.16m/s \cdot 0.040kN\right) = 1.48kW$$

The grade power value for the discrete GPS point was calculated from the GPS data's estimated rate of elevation increase and the known mass of the test vehicle. Equation (9) from Section 3.5 was used to compute to the grade power component of the model, and it is given by the following expression:

$$P_{Grade} = (mg) \cdot \frac{\partial_h}{\partial_t} = \left(W_{Total}\right) \cdot \frac{\partial_h}{\partial_t} = 20.88kN \cdot 0.58m/s = 12.11kW$$

The power required to vary the linear inertia of the vehicle and the rotational inertia of the engine and drivetrain was determined by applying Equations (12) and (13) from Section 3.6.2. The gamma value was 0.3 when the transmission was in 2nd gear as shown in Table 24 from Appendix A. Hence the equivalent mass of the vehicle was calculated as follows:

$$m_{eq} = m \cdot (1+\gamma) = \left(W_{Total}/g\right) \cdot (1+0.3) = \left(20.88\times10^3 N/9.81m/s^2\right) \cdot (1+0.3) = 2767kg$$

The acceleration and speed values found in Table 3 along with the calculated equivalent mass allowed for the inertia component of the model to be computed, and it is represented by the following expression:

$$P_{Inertia} = \left(m_{eq} \cdot A \right) \cdot V = \left(2767kg \cdot \left(-0.026m / s^2 \right) \right) \cdot 9.16m / s = -0.65kW$$

The aerodynamic drag power that was transmitted to the drivewheels to overcome the drag force exerted on the vehicle was calculated using Equation (15) from Section 3.7, and it is given by the following:

$$P_{Drag} = \left(\frac{\rho}{2} C_D A_f \right) \cdot V_{Vehicle}^3 = \left(\frac{1.206kg / m^3}{2} 0.42 \cdot 2.686m^2 \right) \cdot \left(9.16m / s \right)^3 = 0.52kW$$

There was not a drawbar load on the test vehicle so this component of the model was not used any further during verification and validation analyses (ie $P_{Drawbar} = 0$). Calculating the non-zero value for each component of the model allowed Equation (21) from Section 4.1 to be utilized to calculate the predicted mobility power of the vehicle. The net mobility of the test vehicle for the discrete GPS data point analyzed is expressed by the following:

$$P_{Mobility} = P_{MR} + P_{Grade} + P_{Inertia} + P_{Drag} = 1.48kW + 12.11kW + (-0.65kW) + 0.52kW = 13.46kW$$

The measured drivewheel power and predicted vehicle power both had a value of approximately 13.46 kW. This indicated that the model's calculated output was in agreement with the actual or

indicated power value delivered to the drivewheels of the test vehicle. It appeared that the mathematical model developed met the model developer's programming intentions while the calculations and unit conversions performed were checked. The approach for estimating the discrete mobility power value from the model and comparing these values to the measured drivewheel power values has been verified.

4.3.2 CAN Data Analysis and Conversion

The sole power source of the Chevrolet Equinox during testing was the 1.9 L Fiat diesel engine. The engine power determined from the data acquired from the vehicle's CAN network and the vehicle's drivetrain efficiency must be known to estimate the vehicle's mobility power requirements. For a rotating power source such as the Fiat engine, the net engine power (P_{Engine}) produced by the engine is given by the following equation:

$$P_{Engine} = \frac{2\pi \cdot T_{Engine} \cdot n_{Engine}}{60000} \tag{22}$$

Where P_{Engine} is engine power (kW),
T_{Engine} is the net torque or load on the engine (Nm),
n_{Engine} is the engine speed (RPM).

CAN network signals such as engine speed, engine torque, and wheel speeds were logged via the NeoVI Pro controller (CAN controller hardware) at a sampling rate of 25 Hz. The 25 Hz CAN data was converted to the 1 Hz sampling rate of the GPS data in order to validate the GPS-based mobility power model. For a given second of GPS UTC time, the given CAN signal's values that

were plus or minus one half second above or below the given UTC time were summed, and a simple average was taken for the given UTC time. In other words, integrating across all of the available data for a given second was chosen because the net power and associated energy supplied by the engine during an entire second has an equal effect on the resultant movement of the vehicle. In effect, this simple average integrates over all available data points for a given second to provide an averaged representative value from the 25 Hz data. A comparison of the 25 Hz and averaged 1 Hz engine speed and torque data acquired from CAN signals can be seen in Figures 14 and 15. A *.m MATLAB file was used to convert the raw 25 Hz CAN data stored as a *.CSV file into averaged 1 Hz data. The program used to average the CAN data is given in Appendix B.
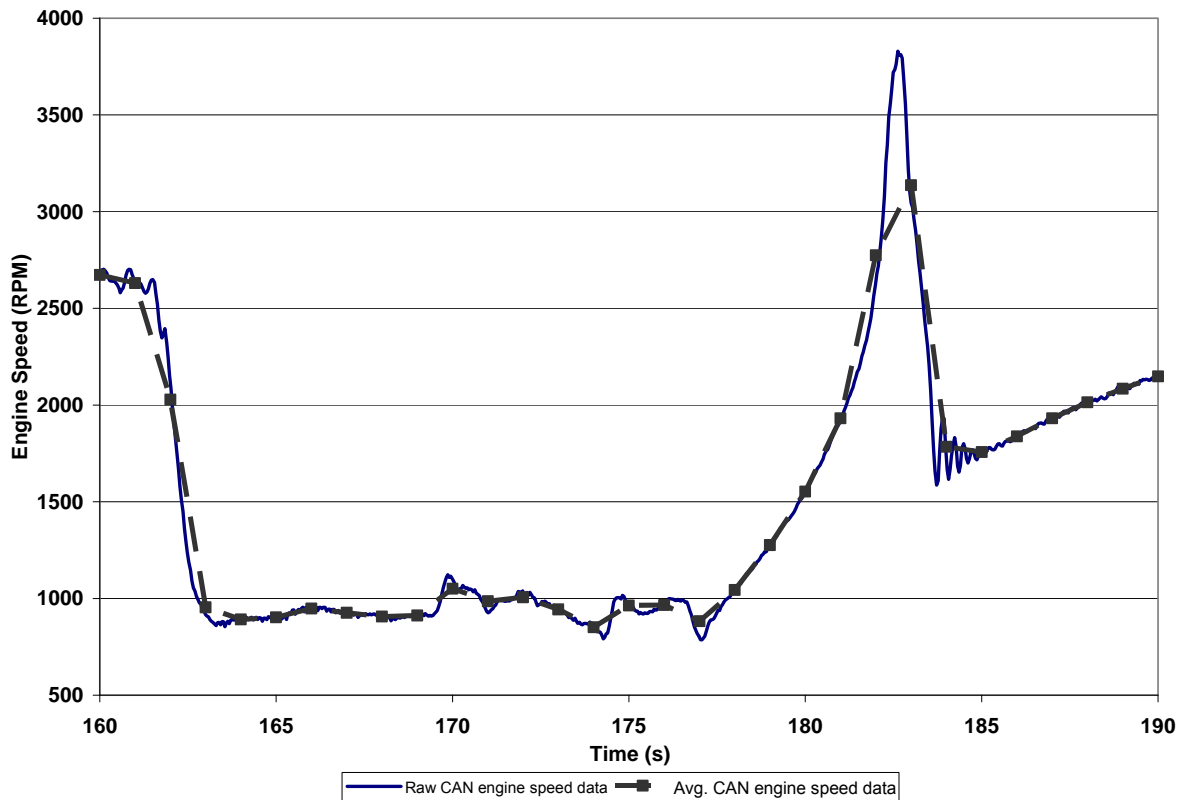
Figure 14: Raw 25 Hz CAN engine speed data and the averaged 1 Hz engine speed data
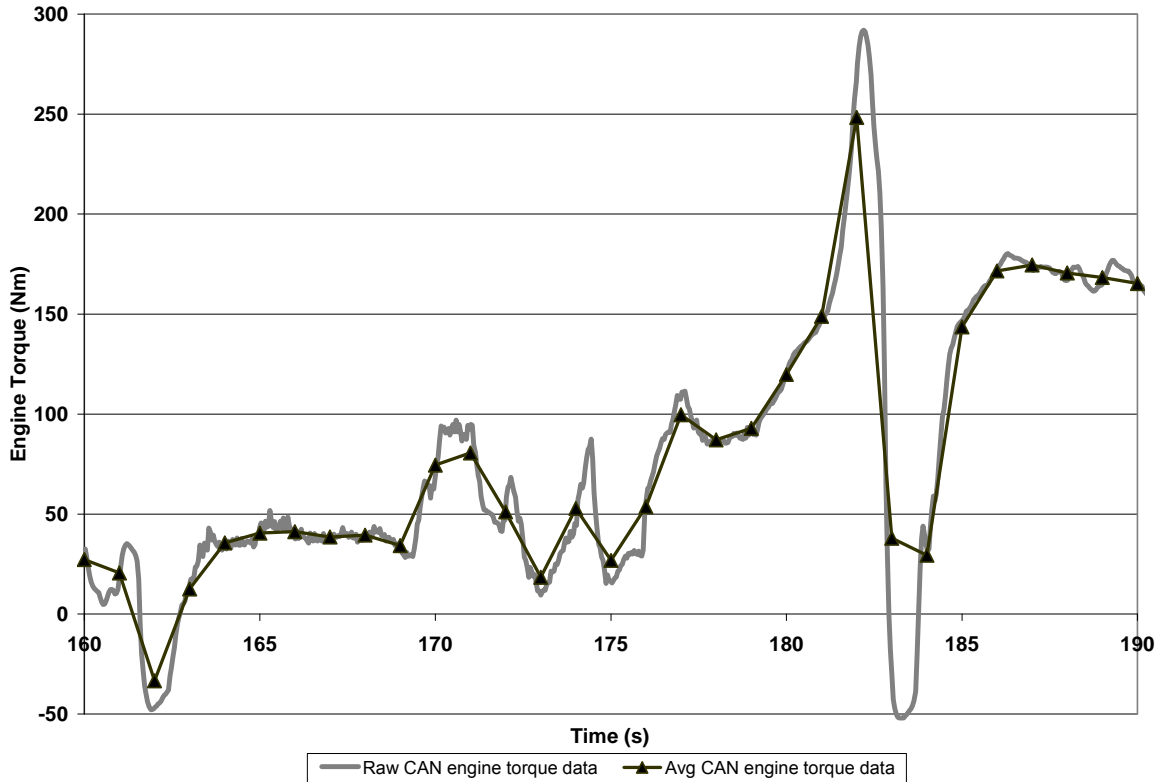
Figure 15: Raw 25 Hz CAN engine torque data and the averaged 1 Hz engine torque data

After comparing the GPS and CAN data, it was concluded that the absolute time (s) associated

with the CAN data logged with NeoVI Pro was slightly inaccurate. By looking into the data

further, it was determined that a one second period of GPS UTC time corresponded to

approximately 0.996994 s of the CAN data's absolute time. An approximate 11 second offset

occurred after one hour of testing. The conversion factor of time between the two sets of data

was necessary to align the data for validation of the model. Static time checks were performed

during testing so that the offset between the sets of data could be monitored. It was also

concluded that minimal offset or delay in time occurred between when the *.vs3 file was

manually executed by the NeoVI Pro (ie program selected by the operator via NeoVI Pro's user

interface) and when the NeoVI Pro device began logging the CAN signals. However, an

approximate 8 s offset or delay of logging the CAN signals occurred after the NeoVI Pro device was supplied electrical power and the device automatically executed the appropriate *.vs3 file.

4.3.3 Test Vehicle Equivalent Mass

Equation (13) allows for the power required to vary the rotational and linear inertia of a vehicle to be estimated from GPS data's estimated speed and acceleration values. The inertia power of the vehicle represented by Equation (13) requires that the test vehicle's equivalent mass (m_{eq}) be estimated. The equivalent mass of the test vehicle varied depending on what gear was engaged in the transmission. The gamma value (γ) for each gear of the transmission is given in Table 3 of Appendix A. The m_{eq} for the test vehicle was calculated from Equation (12) according to the given gear engaged in the transmission while the vehicle was operated.

4.3.4 Engine Accessory Power

The engine data acquired from the CAN network indicated that a non-zero, positive power requirement was required by the engine while the engine was under zero load. The power measured under no load was dissipated by the belt-driven accessory components such as the engine's fuel pump, water pump, oil pump, and alternator. The most significant parasitic load included in the accessory power demand was the engine's fuel pump because the diesel engine had a high pressure common rail fuel injection system. The summation of the power required to drive these components represented the accessory power required to overcome these parasitic loads on the engine. The accessory power measured from the CAN signal's engine data was proportional to the engine speed.

Some amount of accessory power must be subtracted from the engine power calculated from the

CAN engine data to determine the power delivered to the drivewheels of the Equinox. The

Equinox's engine was operated under no load (ie transmission in neutral) for 30 s at various

engine speeds to develop a relationship between accessory power and engine speed. The tests

began at an idle engine speed of approximately 900 RPM while the engine speed was increased

every 30 s until an engine speed of 4000 RPM was attained. Engine data from the CAN network

was logged via the NEOVi Pro controller to estimate the engine's accessory power under no

load.

A linear least-squares regression analysis was applied to the engine data acquired to develop a

relationship between the independent variable, engine speed, and the dependent variable,

accessory power. The measured accessory power data and the least-squares linear fit of the data

are given in Figure 16.   The linear relationship between accessory power and engine speed is

given by the following equation:

$$P_{Accessory} = 0.0013 \cdot n_{Engine} + 0.3317 \tag{23}$$

Where $P_{Accessory}$ is the engine accessory power demand (kW) and n_{engine} is the engine speed

(RPM). The least-squares linear fit of the engine data had a coefficient of determination (R^2)

value of 0.619.
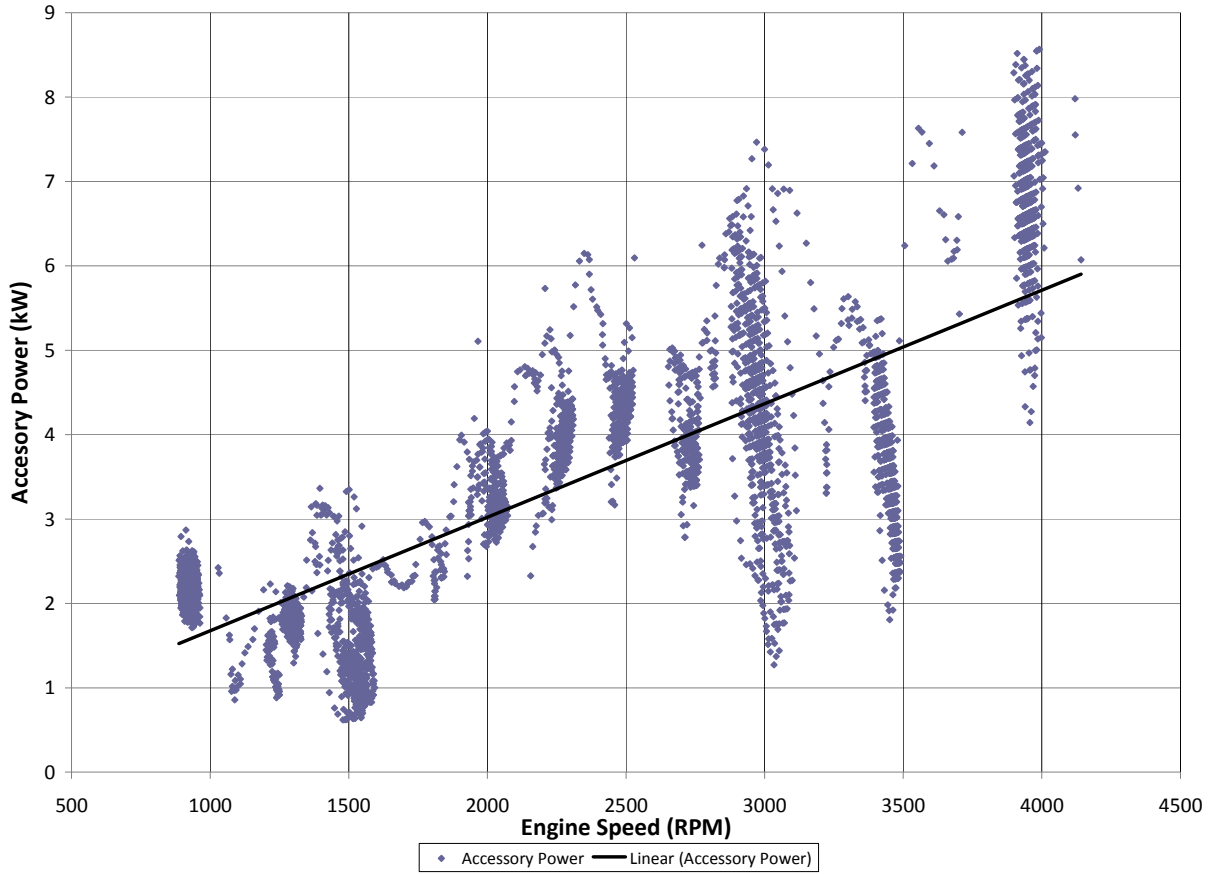
Figure 16: The Fiat engine's accessory power demand data as a function of engine speed and the least-squares linear fit of the accessory power

4.3.5 Test Vehicle Drivetrain Efficiency

The drivetrain efficiency ($\eta_{Drivetrain}$) must be considered when calculating drivewheel power. $\eta_{Drivetrain}$ represents the efficiency of transferring power through the drivetrain to the driven wheels, and it is given by the following:

$$\eta_{Drivetrain} = \frac{P_{Drivewheel}}{P_{Engine}} \qquad (24)$$

The drivetrain efficiency of the Equinox vehicle while operating in a given gear is provided in Table 24 in the Appendix A.

4.3.6 Drivewheel Power

The drivewheel power supplied by the engine for vehicle locomotion can be calculated by accounting for the accessory power ($P_{Accessory}$) of the engine and the vehicle's net drivetrain efficiency ($\eta_{Drivetrain}$). The equation used to estimate drivewheel power during testing for validation of the model is given by the following:

$$P_{Drivewheel} = \left(P_{Engine} - P_{Accessory}\right) \cdot \eta_{Drivetrain} \tag{25}$$

Equation (25) provided for discrete measured power values calculated from the CAN messages that were logged to the compact flash card, and they were compared to the discrete predicted power values during the tests performed. The flow of energy from the engine's fuel to the drivewheels is given in Figure 17, and it provides a qualitative representation of the relationship between engine and drivewheel power. The further use of the term "measured drivewheel power" refers to the calculated drivewheel power values estimated from the engine speed and engine torque messages transmitted on certain 11 bit CAN signals.
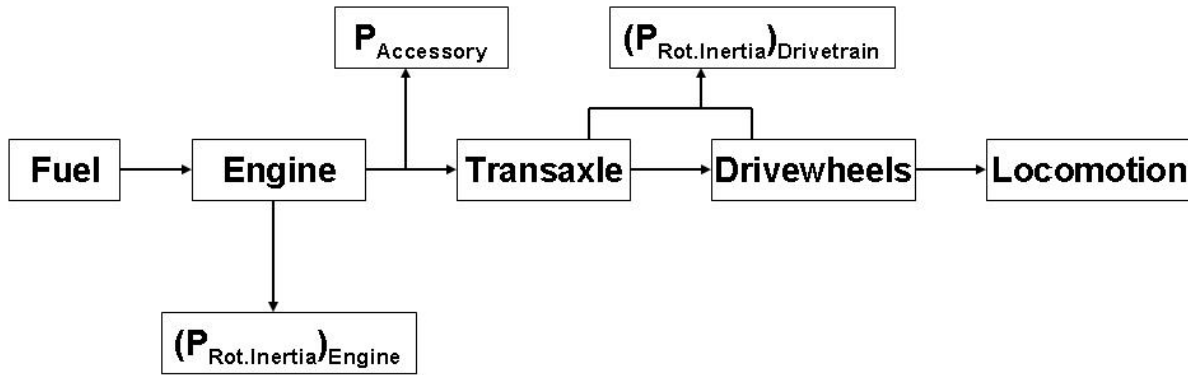
Figure 17: The flow of energy from the fuel to the movement of the vehicle

4.3.7 Controlled Tests

Validation of the mobility power model occurred while conducting controlled and uncontrolled

tests in an on-road environment in the Knoxville, TN area. The controlled tests were performed

at two on-road test locations on 16 December 2011. The vehicle was tested on firm pavement

during the controlled and uncontrolled tests. The controlled tests were performed to isolate each

component of the model. The motion resistance, grade, and inertia components of the model

were each validated by attempting to maintain constant levels of speed, elevation grade, and

acceleration respectively during each test. A group of tests for a each component of the model

had an accuracy assessment performed after the validation tests in order to identify the variability

associated with each component. Evaluation of each test occurred by comparing the discrete

values and the average predicted power values from the GPS-based mobility power model to the

measured drivewheel power values estimated from the vehicle's CAN data.

4.3.7.1 Motion Resistance Tests

The VTI model's fine-grained equations were utilized to estimate the motion resistance force generated at the soil/tire interface even though the surface that all tests were conducted on was a firm, concrete surface. The VTI model's fine-grained equations were used in the model to estimate the test vehicle's motion resistance force because the equations were thought21 to provide for a more accurate prediction of the resistive force generated compared to the motion resistance force estimates from the VTI model's coarse-grained equations. The motion resistance tests were performed on a flat, concrete surface, and the test site is represented in Figure 6. The *CI* value of the firm concrete surface could not be measured with a cone penetrometer so the *CI* value in Equation (2) from Section 3.4.1 was assigned to be 4137 kPa (600 psi) for all controlled tests because firm pavement is typically assigned this value for military vehicle mobility applications (Richmond, 2006). This *CI* value was also used for tests when the vehicle was operating on an asphalt surface. The motion resistance power tests were conducted on smooth, asphalt surfaces with minimal grade (i.e. flat ground) while attempting to maintain a constant travel speed. The length of each straight-line test was approximately 110 m.

Six straight-line, motion resistance tests were conducted at the following approximate average travel speeds: of 2.6, 4.8, and 6.7 m/s. Six tests each were conducted at the 6.7 m/s average travel speed while the transmission was in 1st and 2nd gear. This resulted in a total of 24 straight-line tests that were performed for validation of the motion resistance component of the model. After completing the straight-line maneuvers, five constant turning radius motion resistance tests were performed at travel speeds of approximately 2.3, 3.3, and 5.0 m/s to verify the assumption that the motion resistance increased as the vehicle's turning radius increases. The operator began

66

the maneuvers by initially turning the steering wheel to attain a constant turning radius at a certain speed while continuing to maintain the constant turning radius for five revolutions. The constant turning radius tests were performed at the turning radii of approximately 4.9 m and 9.5 m and at average travel speeds of 2.3 and 3.3 m/s. The tighter 4.9 m turning radius test could not be performed at the 5.0 m/s travel speed without being traction limited during the constant turning radius tests. Thus only the 9.5 m constant turning radius test was evaluated at the 5.0 m/s travel speed.

4.3.7.2 Grade Tests

The effect of the grade power component of the model was tested by maneuvering the vehicle at a constant travel speed on a firm asphalt surface. The grade test location is represented in Figure 7. The controlled grades tests were performed while the vehicle was increasing in elevation (ie positive grade) at a constant speed to determine the accuracy of the model at predicting the vehicle's positive mobility power requirement. Nine positive grade tests were performed at the single testing location. The elevation gain and average percent grade traversed during each grade test were 50 m and 7.5% respectively. Tests were conducted at average travel speeds of approximately 3.3, 4.8, 7.1, 9.3, and 11.4 m/s. Three grade tests were performed at the 3.3 m/s average travel speed while two grade tests each were conducted at average travel speeds of 7.1 and 11.4 m/s. The grade tests performed at slower travel speeds (7.1 m/s or less) had the 1st gear of the transmission engaged while the high travel speed grade tests were completed in 2nd gear. A positive grade was traversed by the test vehicle at a constant speed so that only discrete positive grade power estimates were analyzed during validation. The grade power component was the primary source of the vehicle's required mobility power during these tests.

4.3.7.3 Inertia Tests

Inertia tests were conducted at a location with a hard, concrete surface where the operator accelerated the vehicle along a straight-line path from the minimum vehicle travel speed for a given gear (ie 0 m/s for 1st gear, approximately 5 m/s for 2nd gear) to the maximum attainable travel speed in the given gear. The inertia tests were conducted at the same test site where the motion resistance tests were conducted, and the location is represented in Figure 6. The maximum attainable travel speed in a given gear could not always be attained because the tests were limited by the 150 m length of the test track. The test began when the transmission was shifted into the specified gear and the clutch was engaged so that power was transmitted from the engine through the drivetrain to the drivewheels. The end of each test occurred when the maximum possible speed was attained, and the clutch was disengaged by the operator. The tests were used for the combined validation of the linear and rotational inertia power components of the model. Three degrees of approximately constant acceleration were maintained during the inertia tests. The three levels of acceleration were classified as "slow", "medium", and "fast." The operator attempted to maintain a constant rate of increase in the engine speed; thus, an approximate constant level of acceleration (slow, medium, fast) could be attained for a given gear. Three levels of acceleration allowed for the sensitivity of the model to fluctuations in vehicle travel speed and acceleration to be characterized. Three, straight-line inertia tests were conducted at each degree of acceleration while operating in the 1st and 2nd gears of the transmission. However, inertia tests while the 2nd gear was engaged could only be conducted at levels of acceleration of "medium" and "fast" because it was difficult to attain a "slow" level acceleration. The vehicle speed had to be at least 5 m/s before the 2nd gear could be engaged

which substantially reduced the length of the test track available to conduct inertia tests in 2nd gear. Straight- line inertia tests were repeated three times at the five different combinations of acceleration and gears which resulted in a total of 15 inertia tests that were analyzed during validation. The model's accuracy was analyzed during the motion resistance, grade, and inertia component tests from the GPS and CAN data collected.

4.3.8 Uncontrolled Tests

The uncontrolled, simulated reconnaissance mission was performed on 20 December 2011 along a predetermined, on-road travel path. Simulating a reconnaissance mission typically performed by U.S. Army personnel at U.S. Army installations required careful planning prior to executing the proposed mission and vehicle movement patterns. The maneuvers performed during the controlled tests attempted to simulate the on-road and off-road maneuvers patterns observed during tracking studies at U.S. Army installations. Haugen (2002) summarizes three types of reconnaissance training missions performed by the U.S. Army, and they include the following: area security, screen line, zone reconnaissance. All three types of reconnaissance missions are performed by the U.S. Army's tactical vehicles at numerous installations. A description of each mission is given in Table 5 (Department of the Army, 2000; Haugen, 2002).

Table 5: A description of the three U.S. Army reconnaissance training missions (Source: Department of the Army, 2000; Haugen, 2002)

Mission	Description
Area Security	Provide reconnaissance and security in support of designated personnel, facilities, unit convoys, main supply routes, lines of communications, high value assets, equipment, and critical points
Screen Line	A screening force provides early warning to the main body and impedes and harasses the threat with direct and indirect fires, conducted on the front, flanks, and rear of a stationary force and to the flanks and rear of a moving force; establishes a series of operating positions and conducts patrols to ensure adequate reconnaissance and surveillance of the assigned sector; the platoon may suppress threat reconnaissance units with indirect fires in coordination with other combat elements
Zone Reconnaissance	Provide detailed information about a zone, before forces are maneuvered through the zone; provide detailed picture of how the threat plans to occupy the zone; can be terrain-oriented, force-oriented, or both; the reconnaissance platoon conducts terrain-oriented zone reconnaissance to gain detailed information about routes, terrain, and resources within the zone; the reconnaissance platoon conducts force-oriented zone reconnaissance to gain detailed information about threat forces within the zone

The test was deemed uncontrolled because the maneuvers performed during testing were dictated by the terrain conditions and the simulated mission being performed by the operator of the vehicle. Figure 8 details the travel path taken during the uncontrolled test. The operator attempted to not exceed a travel speed of 8 m/s because the military vehicles previously tracked at U.S. Army installations typically perform reconnaissance missions at low travel speeds. The maneuvers of the vehicle were determined from the operator's interpretation of the mission being performed and the terrain conditions. The operator attempted to remain in a given gear with the clutch fully engaged while using the brake pedal sparingly during the test. These factors affected the vehicle movement patterns during the uncontrolled validation test.

The distinct mobility power duty cycle characteristics for the vehicle and mission type were developed by applying the mobility power model to the GPS data collected during the

uncontrolled test. The accuracy assessment and development of the mobility power duty cycle

characteristics for the test vehicle were calculated for only the time periods when the clutch was

fully engaged and the brake pedal was not being pressed. This allowed for the drivewheel power

to be estimated from the measured engine power. The transmission was in either the 1st, 2nd, or

3rd gear during the uncontrolled test.   The power duty cycle values were estimated for the time

periods when engine power was delivered to the drivewheels and the clutch was fully engaged.

4.3.9 GPS Speed and Acceleration Offset

It was hypothesized that there may be some offset between the GPS and CAN data where the

GPS data possibly lagged the CAN data. This offset may result because the measurement of the

vehicle's change in inertia by the GPS receiver occurred some period after the power produced

by the engine. Engine power during testing was calculated from the engine speed and engine

torque values logged from certain CAN network signals. The GPS offset attempted to

compensate for any offset or delay that occurred between the observed engine power, vehicle

speed, and vehicle acceleration values calculated from the CAN data and GPS data. The Trimble

132 GPS receiver was configured to the "land" dynamic mode to optimize speed measurements

from the receiver. The Garmin 18 GPS receiver did not have an option to configure the dynamic

mode of the receiver. These factors had to be considered when comparing the theoretical

drivewheel power delivered and the predicted mobility power from the GPS data.

The GPS offset is some delay between the GPS data's measured kinematic properties (position,

speed, acceleration, turning radius, elevation) of a vehicle and the actual kinematic's that

occurred during vehicle locomotion. A positive GPS offset was defined as the GPS data lagging

the measured or observed vehicle speed, vehicle acceleration, and drivewheel power calculated from the CAN data. The first approach for determining the optimum GPS speed and acceleration offset associated with the Garmin and Trimble GPS receivers consisted of comparing the GPS data's estimated vehicle travel speed and acceleration to the calculated vehicle travel speed determined from the measured wheel speeds. The effective rolling radius (r) of the Chevrolet Equinox's wheels was determined during validation testing by measuring the distance traveled by the vehicle during a single revolution of the wheel. The effective rolling radius of all wheels during testing was 0.358 m. The calculated vehicle travel speed during straight-line maneuvers was determined by averaging the four wheel speed values (units: RPM) logged from the CAN network and applying the following equation:

$$V_{Vehicle} = (2\pi \cdot r) \cdot (n_{wheels} / 60) \tag{26}$$

Where

r is the measured rolling radius of the wheels (m),

n_{wheels} is the measured wheel speed (RPM).

Straight-line, inertia test data was used to determine the GPS speed and acceleration offset for each receiver. Taking the derivative of Equation (26) with respect to time allowed for a measured vehicle acceleration to be determined which was compared to the predicted acceleration from the GPS data. The vehicle travel speed and acceleration as a function of time was determined for 0, 1, 2 and 3 s GPS offsets and compared to the vehicle travel speed and acceleration calculated from the CAN data. The optimum GPS offset for a given receiver was the GPS offset that resulted in the maximum measured and predicted speed and

maximum/minimum accelerations occurring at the same time. Table 25 in Appendix C details the optimum GPS offsets for both GPS receivers during ten inertia tests. Figures 18 and 19 along with Figures 66 – 75 in Appendix C detail the vehicle travel speed and acceleration as a function of time at various GPS offsets during slow, medium, and fast inertia tests for the Trimble 132 and Garmin 18 GPS receivers.
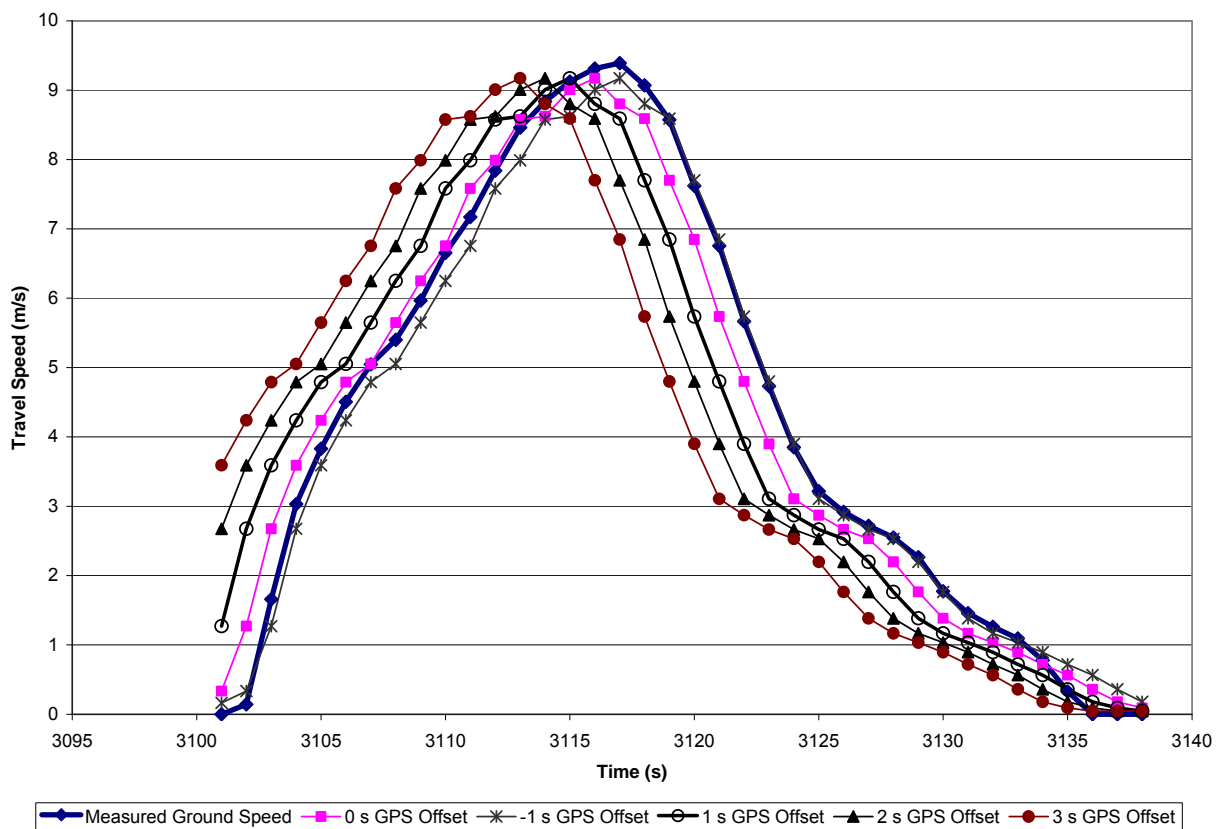
Figure 18: Vehicle travel speed at various Trimble 132 GPS offsets during a slow inertia test
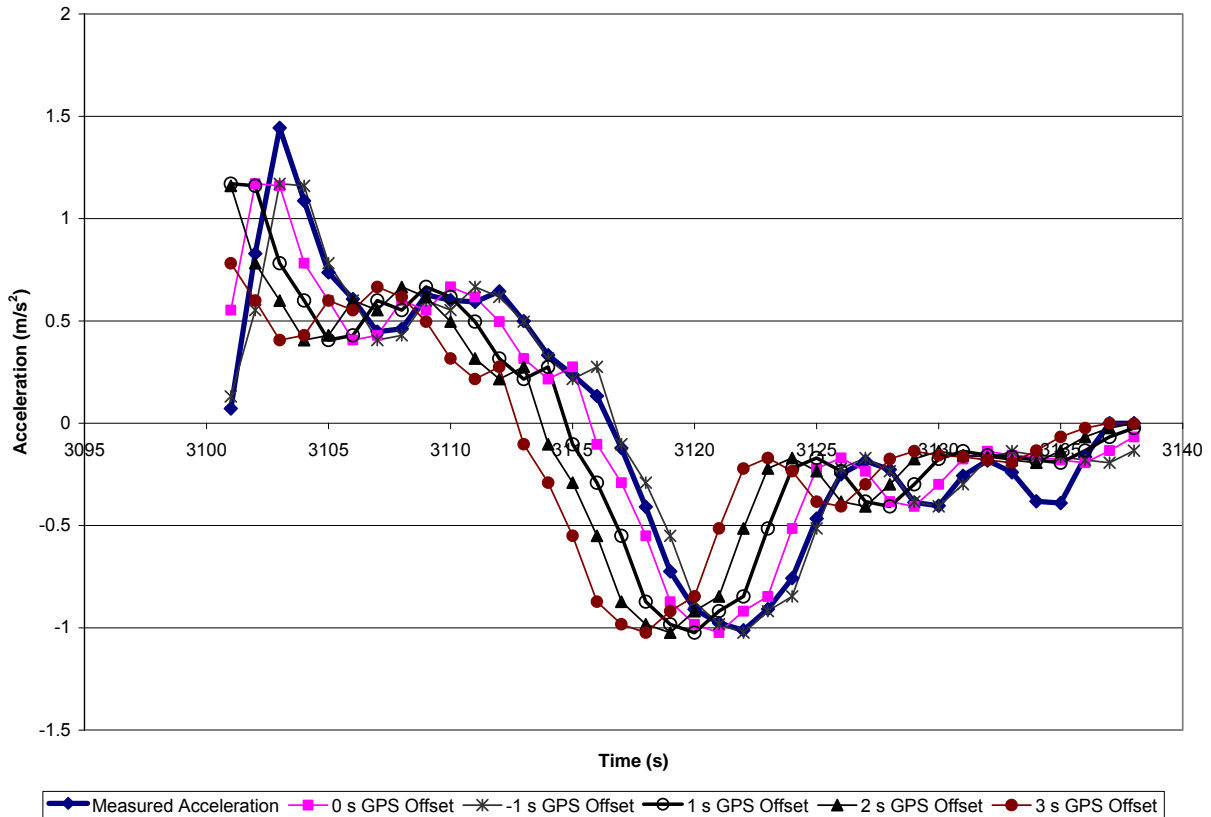
Figure 19: Vehicle acceleration at various Trimble 132 GPS offsets during a slow inertia test

The optimum GPS offset tended to increase as the level of acceleration (slow, medium, fast) increased. The optimum GPS offset for a given level of acceleration also varied depending on the GPS receiver (Garmin 18 or Trimble 132). Comparing the observed and predicted vehicle speed and acceleration values indicated that some positive, non-zero GPS offset may be needed. However, the optimum GPS offset varied for each inertia test, and it was not apparent what the correct GPS offset should be for each GPS receiver. As a result, a comparison of the predicted mobility power and the observed drivewheel power was necessary to determine the optimum GPS offset.

74

The net engine power that was delivered to the drivewheels (ie measured mobility power) was compared to the predicted mobility power from the GPS data in the second approach to further evaluate the optimum GPS offset between the two sets of data. The GPS offset that decreased the variability between the measured and predicted mobility power values during nine separate inertia tests was selected as the optimum GPS offset. A comparison of the predicted and measured mobility power at 0, 1, 2, and 3 s GPS offsets was done for nine inertia tests. Six of the tests were conducted at a degree of acceleration classified as "fast" (3 tests in 1st gear and 3 tests in 2nd gear) while three of the inertia tests were classified as "slow" (in 1st gear). Table 26 in Appendix C details the variability between the measured and predicted mobility power values at various GPS offsets for the Trimble and Garmin GPS receivers. The data for the Trimble 132 and Garmin 18 GPS receivers used in the comparison of the measured and predicted mobility power values at 0, 1, and 2 s GPS offsets are represented by Figures 76 and 77 respectively in Appendix C (Note: 3 s GPS offset data not shown due to extreme outliers).

The R-squared value associated with the measured and predicted mobility power values was used as an indicator of the variability between the measured and predicted values. A 2 s GPS offset was chosen as the optimum offset for both the Garmin and Trimble GPS receivers because this offset tended to minimize the variability between the predicted mobility power from the GPS data and the measured drivewheel power from the vehicle's CAN data. An integer GPS offset was chosen instead of some non-integer value because the GPS data was logged at a sampling rate of 1 Hz.

75

4.3.10 GPS Elevation Offset

The GPS receivers' ability to estimate the vehicle's elevation and rate of elevation change were characterized because the change in elevation of the vehicle is the principle input variable to the grade power component of the model. Static GPS data was collected at three points at the grade test location to determine the variability of the vehicle's predicted elevation from the Garmin 18 and Trimble 132 GPS receivers. The accuracy of the receiver's elevation data was first investigated by comparing the static elevation data collected for 600 s on two separate days at three points along the travel path at the test location. The 600 s of static elevation data collected at a single location during two days is shown in Figures 20 and 21 for the Trimble 132 and Garmin 18 GPS receivers respectively.
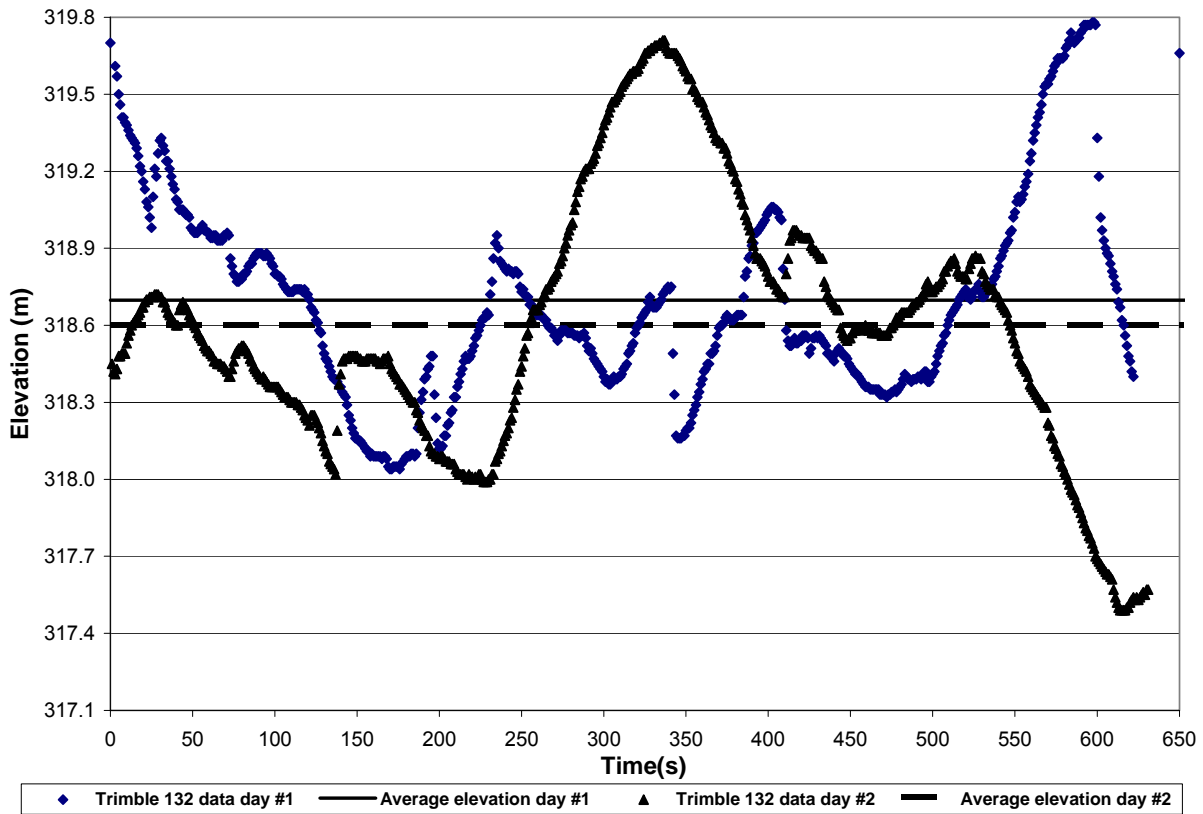
Figure 20: Static Trimble 132 elevation data during two different days at the grade test location
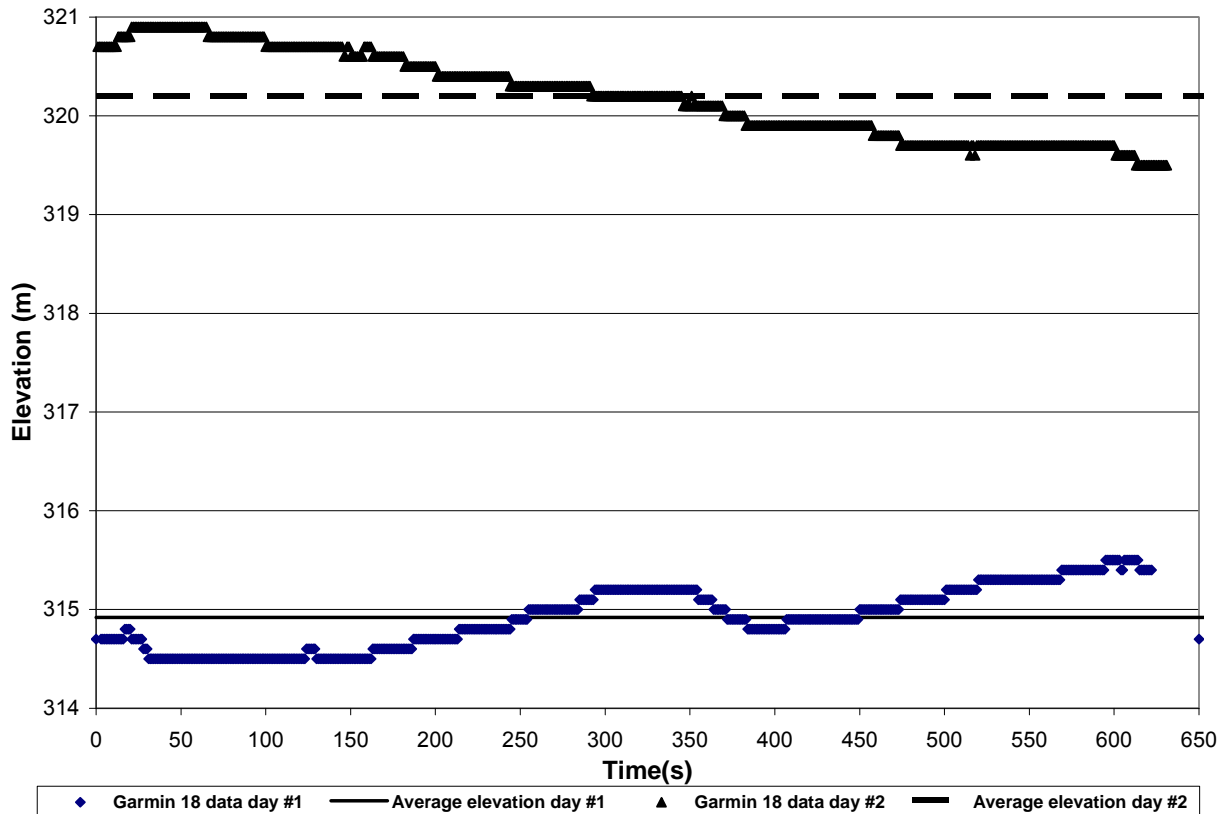
Figure 21: Static Garmin 18 elevation data during two different days at the grade test location

Figure 20 and 21 indicated that the difference between the two average elevation values was very small (< 0.1 m) for the Trimble 132 GPS receiver. The Garmin 18 receiver had approximately a 5.25 m difference between the two average elevation values. The variability of each GPS receiver during the 600 s of static data was similar, but the Trimble 132 receiver was more accurate at predicting the elevation (height above ellipsoid) of the test location. Any further use of the term elevation refers to the height above the ellipsoid.

However, the critical input parameter to the grade power component of the model was the vehicle's rate of elevation change, not the GPS elevation value. Thus the ability of each GPS receiver to accurately estimate the change in elevation of the vehicle during each grade test

needed to be investigated. Figures 22 and 23 detail the estimated vehicle elevation as a function

of the distance traveled by the vehicle from the Trimble 132 and Garmin 18 receivers

respectively during five positive grade tests.
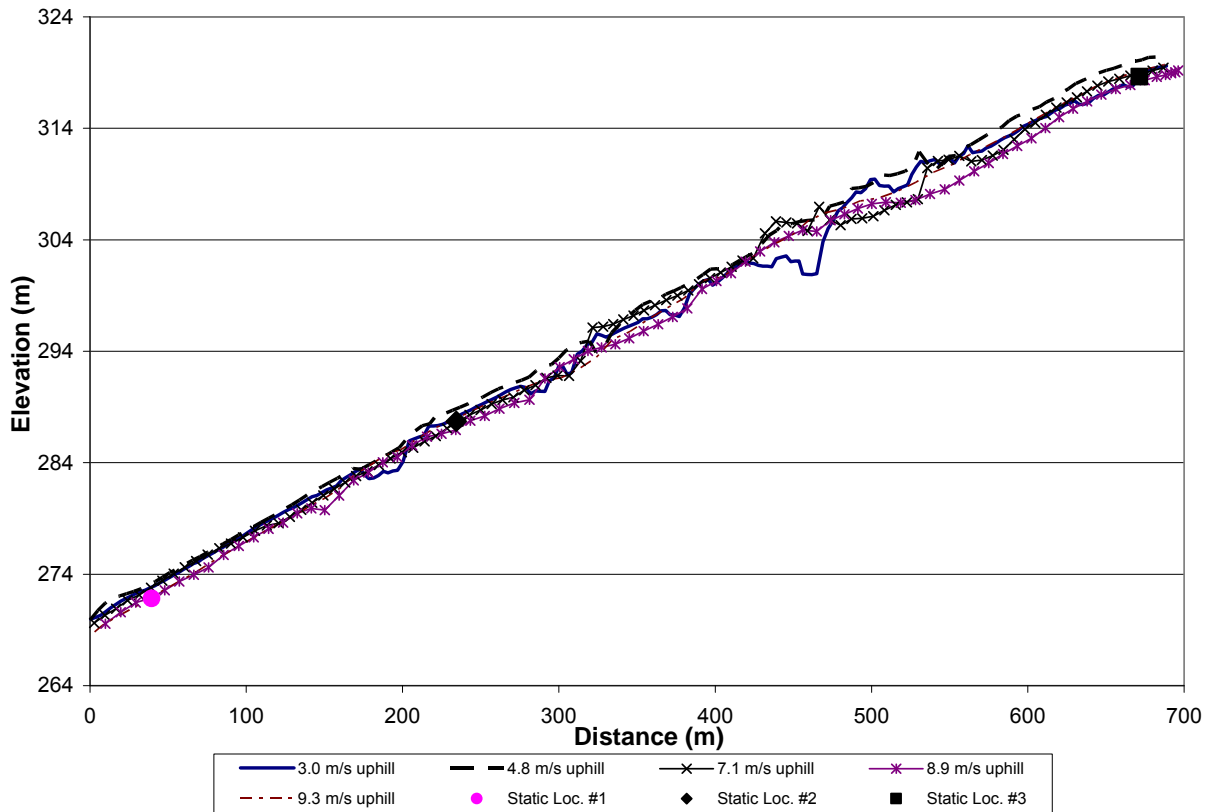
Figure 22: The change in elevation of the test vehicle as a function of distance traveled
from the Trimble 132 data during uphill grade tests at different travel speeds
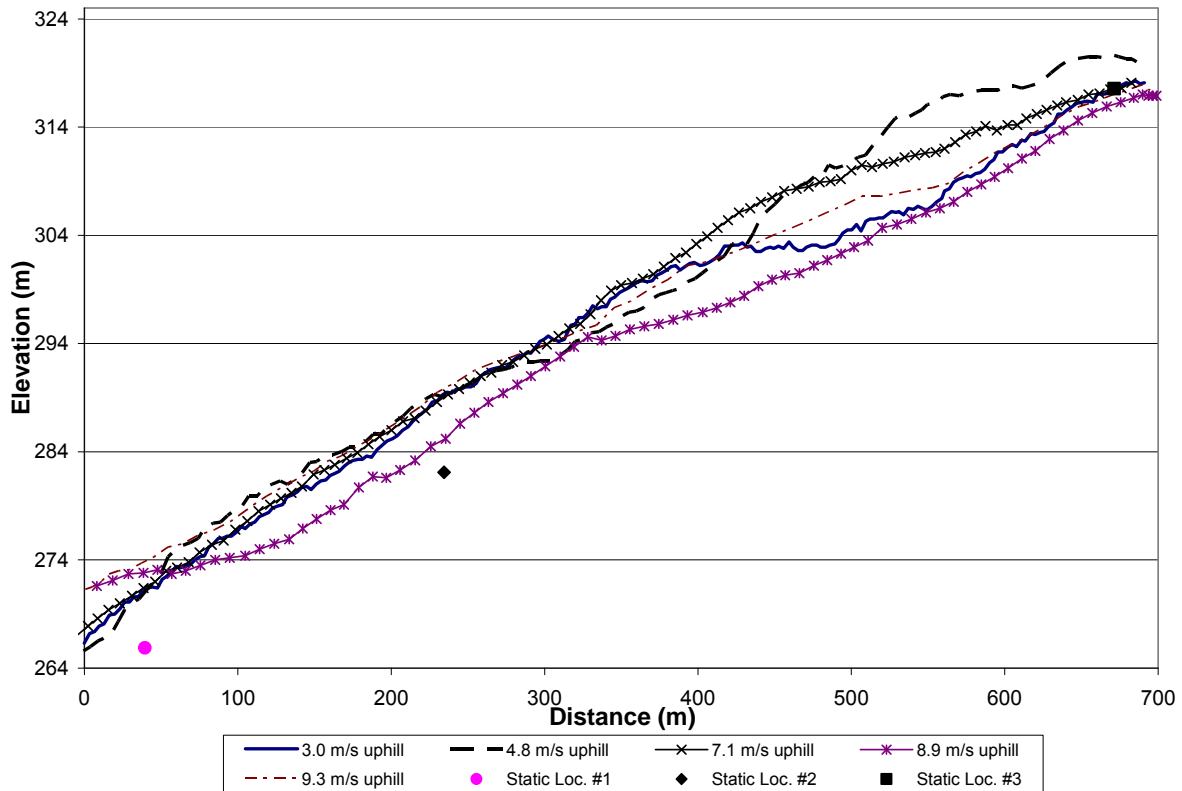
Figure 23: The change in elevation of the test vehicle as a function of distance traveled from the Garmin 18 data during uphill grade tests at different travel speeds

Figures 22 and 23 indicated that there was substantially greater variability from the Garmin 18 GPS receiver's rate of elevation change data compared to the Trimble 132 receiver. The Trimble 132 GPS receiver had a greater degree of accuracy at predicting the average elevation of the vehicle. The greater accuracy of the Trimble 132 receiver was indicated from the curves seen in Figure 22. The dynamic elevation values during each test for the Trimble 132 receiver were within 1.3 m of the static elevation values for the three locations estimated from 600 s of static GPS data. The Garmin 18 receiver's dynamic elevation values differed up to 8.3 m from the static elevation value. The elevation and associated change in elevation values during each test appeared to be more consistent across each grade test for the Trimble 132 receiver. The Garmin 18 GPS receiver had greater variability of the elevation values between each test. This indicated

that Garmin 18 receiver might be less accurate at estimating the vehicle's rate of elevation change.

Any offset or delay associated with the GPS elevation data was determined by comparing the uphill and downhill elevation values at static location #2. An indicator of a GPS elevation offset would have been if the downhill elevation values tended to be greater than the associated elevation value while the vehicle was traversing uphill. Table 6 summarizes the elevation values while traversing uphill and downhill during five separate grade tests.

Table 6: A comparison of the elevation data (height above ellipsoid) obtained from the Garmin 18 and Trimble 132 GPS receivers while traversing uphill and downhill during five grade tests

Test No.	Garmin 18 GPS receiver		Trimble 132 GPS receiver	
	Elevation (m)		Elevation (m)	
	Downhill	Uphill	Downhill	Uphill
1	288.9	289.5	289.39	288.10
2	285.1	289.4	288.52	288.70
3	288.5	289.3	287.19	287.71
4	289.2	285.2	288.05	286.94
5	291.9	289.5	286.92	287.81

The average elevation at this location was estimated to be 282.1 and 287.72 m for the Garmin 18 and Trimble 132 GPS receivers respectively. The average elevation values were estimated from static elevation data collected at the location on 15 February 2012 and 18 February 2012. The results summarized in Table 6 led to a 0 s GPS elevation offset being chosen for both GPS receivers since no distinct trends were observed in the data analyzed such as the downhill elevation values being greater than the uphill values.

4.4 Results and Discussion

GPS data was acquired from the Trimble 132 and Garmin 18 GPS receivers during the controlled and uncontrolled tests to validate the model. The Garmin 18 receiver is typically the GPS receiver used with the Vehicle Tracking System (VTS) to track military vehicles during training missions. This GPS receiver is used with the VTS units because it is a compact, low-power, and cost-effective receiver that can be easily mounted so that it does not interfere with the training mission. The Trimble 132 GPS receiver represents a more accurate GPS receiver. The results from the controlled and uncontrolled tests are first presented for the Trimble 132 GPS receiver because it represents the best available receiver for validating the model during testing. The results from the Garmin 18 receiver are an indicator of the model's accuracy when data from the GPS receiver typically used to track military vehicles is applied to the model. The further use of the term "measured drivewheel power" refers to the calculated drivewheel power values estimated from the engine speed and engine torque messages transmitted on certain 11 bit CAN signals. The absolute average percent error values provided in this section were calculated by dividing the magnitude of the difference between the discrete predicted and measured values by the magnitude of the measured value while averaging all of these discrete terms.

4.4.1 Controlled Tests

Validation of the model required that controlled tests be performed for each component of the model. The predicted net mobility power value was compared to the total indicated or measured drivewheel power value that was determined from the CAN data logged during validation of each model component. Accuracy assessment while validating each component of the model

81

was conducted by comparing the total measured and predicted power values, rather than comparing the component measured and predicted power values for validation. In other words, component validation occurred by comparing the total predicted values from the GPS data, not each component value, to the net, measured drivewheel power values. The results presented were generated using a 2 s GPS speed and acceleration offset (ie lag) and a 0 s GPS elevation offset for both GPS receivers. Equation (11) was used to predict the vehicle's acceleration from the discrete GPS speed data, and a simple 5 s running average was used to filter the GPS elevation data. Sections 4.3.9 and 4.3.10 provide a detailed description of the methods used to determine the correct GPS speed and acceleration offset. A *.m MATLAB file given in Appendix B was used to convert the 25 Hz engine speed, engine torque, and wheel speed data logged from the signals transmitted on the test vehicle's CAN network during testing to the GPS data's 1 Hz sampling rate. Power dissipated by the engine's accessory components and the drivetrain frictional losses were accounted for when estimating the discrete measured drivewheel power values. Section 4.3.2 provides the procedure used to convert the 25 Hz CAN data, and the process for estimating drivewheel power is provided in Sections 4.3.3 – 4.3.6.

4.4.1.1 Motion Resistance Tests

It was critical that the appropriate GPS speed offset was determined before validating the motion resistance component of the model. The 24 straight-line motion resistance tests performed allowed for the accuracy and variability of the motion resistance component of the model to be characterized. There was a fault in the Trimble 132 GPS data stored to the Serial Data Recorder(SDR) during the straight-line, 6.6 m/s travel speed tests in 1st gear, and this resulted in four of the six tests at this travel speed being excluded from the analysis of the Trimble 132 data.

The error in the GPS data occurred for 80 s, and the data collected after this fault was not affected. Thus only 20 of the 24 straight-line motion resistance tests were analyzed from the Trimble 132 GPS data while the data from the Garmin 18 receiver was analyzed for all 24 tests. The statistics for the 20 straight-line motion resistance tests are summarized in Table 7, and a comparison of the discrete predicted and measured power values at the five average travel speeds is represented in Figure 24 for the Trimble 132 GPS receiver.

Table 7: A summary of the results for the Trimble 132 GPS receiver during 20 straight-line motion resistance tests

Test No.	Gear	Test Duration (s)	Avg. Travel Speed (m/s)	Avg. Predicted Power (kW)	Avg. Measured Power (kW)	Predicted Power Std. Dev. (kW)	Measured Power Std. Dev. (kW)	Measured vs. Predicted Power RMSE (kW)
1	1	54	2.4	0.29	1.09	0.8	1.2	1.2
2	1	45	2.6	0.46	0.82	0.6	0.7	0.7
3	1	45	2.6	0.38	0.57	0.8	1.0	0.7
4	1	40	2.7	0.42	0.50	0.6	0.6	0.6
5	1	46	2.7	0.55	0.40	0.7	0.6	0.7
6	1	44	2.7	0.36	0.41	0.7	0.6	0.6
7	1	24	4.6	1.23	0.05	2.0	2.1	1.4
8	1	23	4.8	0.25	-0.39	1.5	0.7	1.3
9	1	23	4.7	0.70	-0.47	1.2	0.8	1.4
10	1	24	4.8	0.83	-0.09	1.1	0.5	1.3
11	1	25	4.8	0.65	-0.35	0.7	0.5	1.1
12	1	23	4.8	0.68	-0.03	1.1	0.6	1.1
13	1	16	6.5	2.41	1.95	4.6	0.8	1.4
14	1	16	6.7	0.56	0.19	2.2	0.9	1.8
15	2	16	6.8	1.24	1.09	6.5	5.6	2.2
16	2	14	6.6	0.33	-0.23	1.9	1.5	1.2
17	2	15	6.9	1.35	0.56	1.7	1.6	1.3
18	2	16	6.9	1.12	0.52	2.1	2.0	1.4
19	2	17	6.8	0.91	0.49	3.0	1.9	1.8
20	2	16	6.8	0.73	0.28	2.4	1.8	1.4

Figure 24: The discrete predicted mobility power values from the Trimble 132 GPS receiver during 20 straight-line motion resistance tests compared to the measured drivewheel power

The majority of the discrete predicted and measured power values did not exceed 4 kW in

magnitude, and the discrete data was concentrated about the origin. The standard deviation of the

discrete measured and predicted power values revealed that the power values estimated from the

Trimble 132 GPS data typically had more variation than the drivewheel power values calculated

from the CAN data. The Root Mean Square Error (RMSE), an indicator of the magnitude of the

variability of the discrete predicted power values, tended to only increase slightly as the average

travel speed of the vehicle increased. The slight increase in RMSE indicated that the magnitude

of the variability relative to the measured power values may have decreased assuming that the

motion resistance power increased as the vehicle travel speed increased. Any slight wind that may have existed during the tests would have also been another source of variability.

The measured and predicted discrete power values tended to fluctuate above and below 0 kW of power, but the values were skewed slightly positive. The average measured and predicted power values in Table 7 further indicated that the discrete values were skewed positive. The positive power requirement during the tests appeared to increase slightly as the average travel speed increased. It was previously thought that the power requirement during the motion resistance tests would be a small, positive value that increased with travel speed. The discrete negative predicted and measured values were not expected during the motion resistance tests. The test site had a minimal grade, but a slight grade of the surface was present for stormwater drainage at the test site. This factor introduced another possible source of variability during the motion resistance tests because the grade may have increased the range of the measured power values, both positive and negative.

The small fluctuations in the vehicle travel speed during the motion resistance tests were one reason why the discrete positive and negative values occurred. The fluctuations of the travel speed and subsequent power values that exceeded 4 kW in magnitude may also have been due to the difficulty in maintaining a constant, slow travel speed during the motion resistance tests. A power value greater than positive 4 kW may have occurred because the operator increased the throttle position at a certain time to attempt to maintain a constant travel speed. The increase in the throttle position resulted in a greater measured power, but the operator may have exceeded the target travel speed. Any slight negative acceleration during the motion resistance tests

resulted in braking from the engine which produced a negative measured power since the

drivetrain was directly coupled to the engine during all tests. The brake pedal was not pressed

during any of the motion resistance tests. Exceeding the travel speed may have caused the less

than -4 kW values where the operator may have had the throttle at the idle position while the

engine braked or slowed down the vehicle. The negative average power values estimated from

the Trimble 132 data may have also been to due to errors in the GPS elevation data.

The statistics for the 24 straight-line motion resistance tests are summarized in Table 8, and a

comparison of the discrete predicted and measured power values at the five levels of average

travel speed and two levels of turning radii is represented in Figure 25 for the Garmin 18 GPS

receiver.

Table 8: A summary of the results for the Garmin 18 GPS receiver during 24 straight-line motion resistance tests

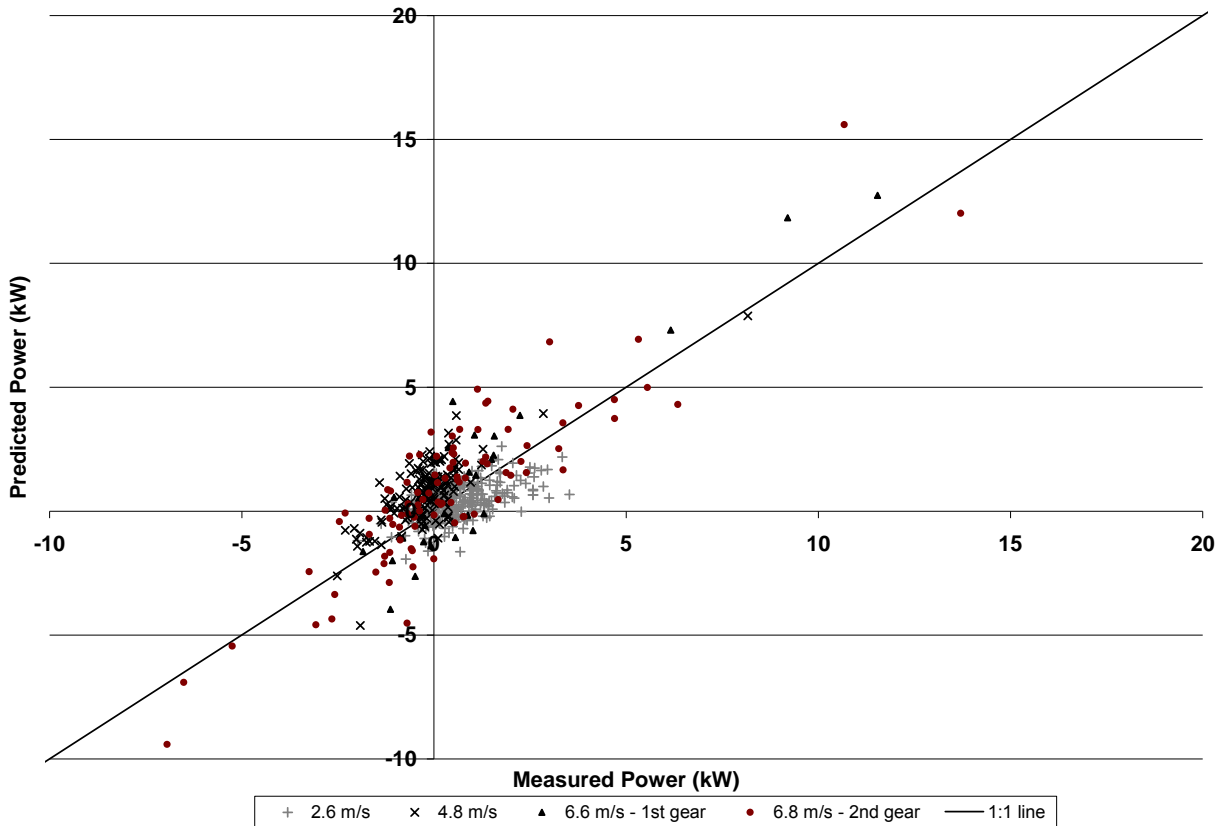| Test No.	Gear	Test Duration (s)	Avg. Travel Speed (m/s)	Avg. Predicted Power (kW)	Avg. Measured Power (kW)	Predicted Power Std. Dev. (kW)	Measured Power Std. Dev. (kW)	Measured vs. Predicted Power RMSE (kW)
1	1	54	2.4	0.13	1.09	1.2	1.2	1.7
2	1	45	2.6	0.87	0.82	1.7	0.7	1.7
3	1	45	2.6	-0.78	0.57	1.4	1.0	2.2
4	1	40	2.7	0.19	0.50	1.5	0.6	1.6
5	1	46	2.7	-0.06	0.40	1.6	0.6	1.8
6	1	44	2.7	-0.09	0.41	1.5	0.6	1.6
7	1	24	4.6	1.38	0.05	2.9	2.1	1.8
8	1	23	4.8	-0.47	-0.39	1.3	0.7	1.2
9	1	23	4.7	0.14	-0.47	1.6	0.8	1.6
10	1	24	4.8	-0.49	-0.09	1.6	0.5	1.5
11	1	25	4.8	1.36	-0.35	1.4	0.5	2.1
12	1	23	4.9	-0.76	-0.03	1.1	0.6	1.5
13	1	16	6.5	2.95	1.95	4.5	0.8	1.8
14	1	15	6.4	-3.25	0.25	2.3	1.5	3.7
15	1	16	6.6	0.36	0.25	3.0	1.4	1.9
16	1	15	6.8	-1.72	-0.02	2.7	1.5	2.5
17	1	15	6.8	2.95	0.40	4.3	1.1	4.1
18	1	16	6.7	0.06	0.19	1.8	0.9	1.0
19	2	16	6.8	1.45	1.10	6.8	5.6	1.8
20	2	14	6.7	-1.86	-0.23	2.7	1.5	2.6
21	2	15	6.9	1.35	0.56	2.2	1.6	1.6
22	2	16	6.9	-0.84	0.52	2.7	2.0	1.8
23	2	17	6.9	-0.12	0.49	4.1	1.9	2.5
24	2	16	6.8	0.34	0.28	2.1	1.8	1.8

Figure 25: The discrete predicted mobility power values from the Garmin 18 GPS receiver during 24 straight-line motion resistance tests compared to the measured drivewheel power

The straight-line motion resistance results from the Garmin 18 GPS data had similar trends and statistics, but the variability of the predicted mobility power values increased slightly compared to the Trimble 132 data's results. The discrete data points in Figure 25 are not as concentrated along the 1:1 line at a point slightly above the origin. The data points greater than 5 kW in magnitude also tended to lie closer to the 1:1 line compared to the same points calculated from the Garmin 18 data. The average RMSE value of all of the straight-line tests from the Garmin 18 data was approximately 37% greater than the average RMSE value from the Trimble 132 data. These quantitative measures were a confirmation of the qualitative conclusions drawn from Figure 24 and Figure25.

The statistics for the five constant turning radius motion resistance tests are summarized in Table 9, and a comparison of the discrete predicted and measured power values at the five levels of average travel speed and turning radii is represented in Figure 26 for the Trimble 132 GPS receiver. The average predicted and measured power during the 20 straight-line and five constant turning radius motion resistance tests are represented in Figure 27.

Table 9: A summary of the results for the Trimble 132 GPS receiver during five constant turning radius motion resistance tests

Test No.	Gear	Test Duration (s)	Avg. Travel Speed (m/s)	Avg. Turning Radius (m)	Avg. Predicted Power (kW)	Avg. Measured Power (kW)	Predicted power Std. Dev. (kW)	Measured power Std. Dev. (kW)	Meas. vs. Pred. Power RMSE (kW)
1	1	61	2.2	4.9	0.29	1.23	0.83	0.88	1.2
2	1	103	2.4	9.2	0.35	0.62	0.53	0.51	0.7
3	1	60	3.2	4.9	0.64	0.65	0.90	0.90	0.7
4	1	96	3.5	9.5	0.55	-0.19	1.34	0.83	1.5
5	1	55	5.0	9.4	0.92	1.39	2.31	1.32	1.7
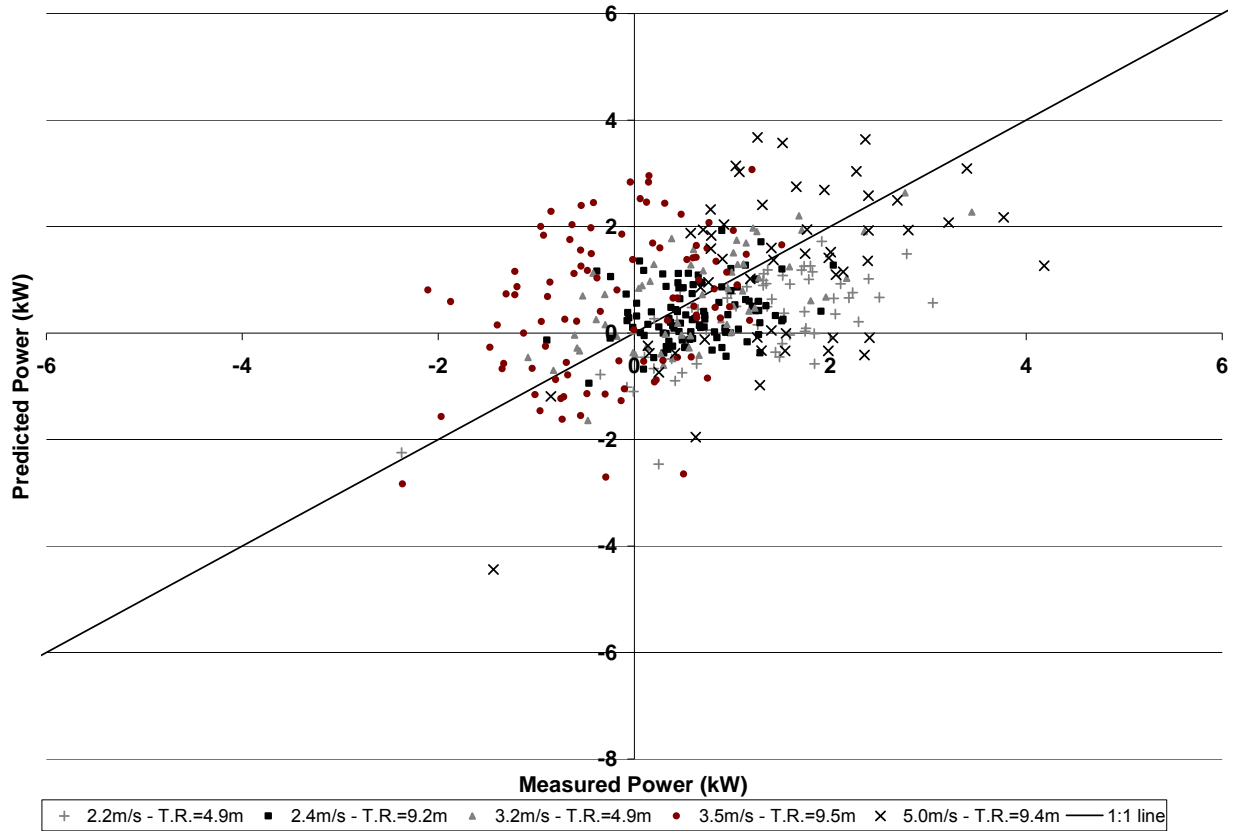
Figure 26: The discrete predicted mobility power values from the Trimble 132 GPS receiver during five constant turning radius motion resistance tests compared to the measured drivewheel power
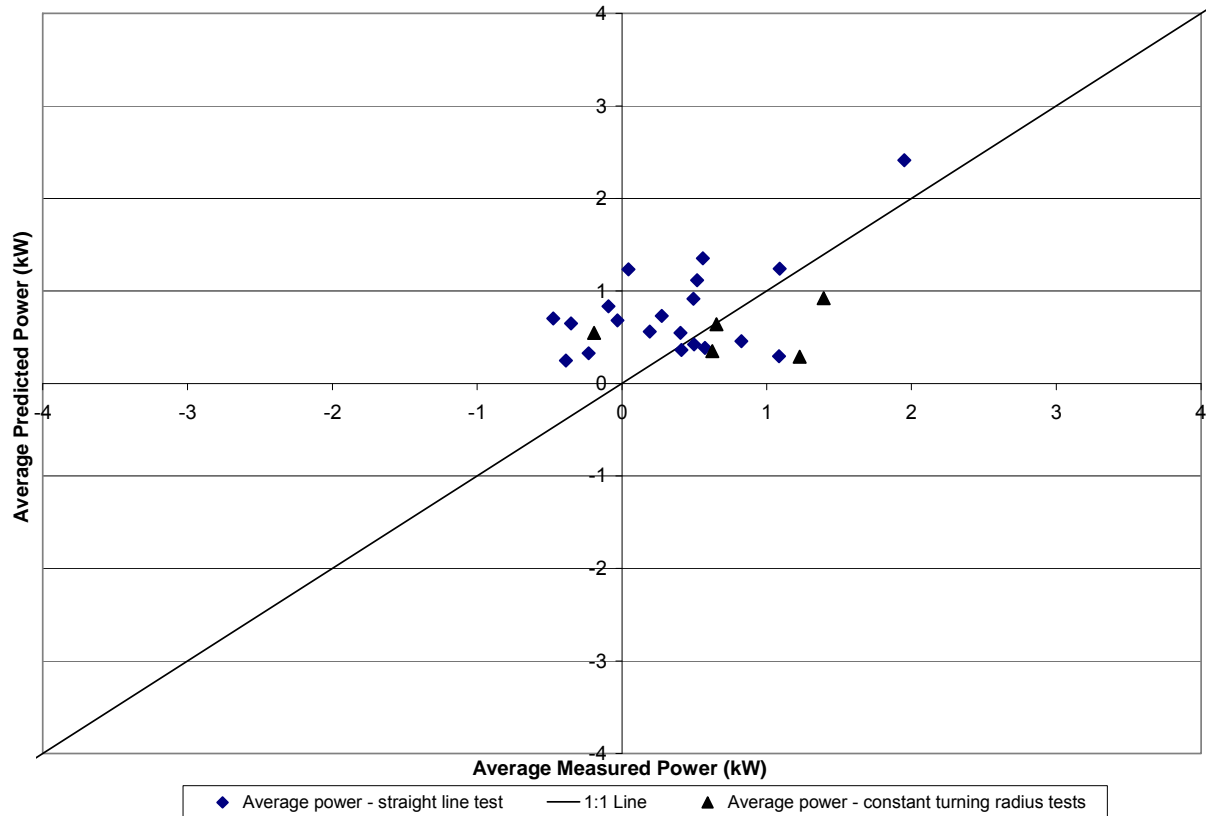
Figure 27: The predicted average mobility power from the Trimble 132 GPS receiver compared to the measured average drivewheel power during the 20 straight-line and five constant turning radius motion resistance tests

The data from the constant turning radius tests resulted in similar trends seen during the straight-line tests. The variability of the predicted values was similar, but there were no values that exceeded approximately 4.3 kW in magnitude. The RMSE values during the turning radius tests ranged between 0.7 and 1.7 kW, and the values were similar to the values calculated for the straight-line tests. The discrete data points were concentrated about the origin, but the discrete power values tended to be more positive compared to the straight-line motion resistance tests. The negative measured power values may have been due to the inaccuracies associated with estimating drivewheel power from the calculated engine power values. The constant turning radius average power values in Figure 27 indicated that the constant turning radius tests had a

slightly greater non-zero, positive power requirements than the straight-line tests. The measured

and predicted power during the constant turning radius tests tended to increase as the vehicle

travel speed increased and the vehicle turning radius decreased. These trends confirmed the

assumptions underlying the Vehicle-Terrain Interaction (VTI) model that assumes motion

resistance increases as the steering angle of the wheel increases.

The statistics for the five constant turning radius motion resistance tests are summarized in Table

10, and a comparison of the discrete predicted and measured power values at the five levels of

average travel speed and turning radii is represented in Figure 28 for the Garmin 18 GPS

receiver. The average predicted and measured power during the 24 straight-line and five

constant turning radius motion resistance tests are represented in Figure 29.

Table 10: A summary of the results for the Garmin 18 GPS receiver during five constant turning radius motion resistance tests

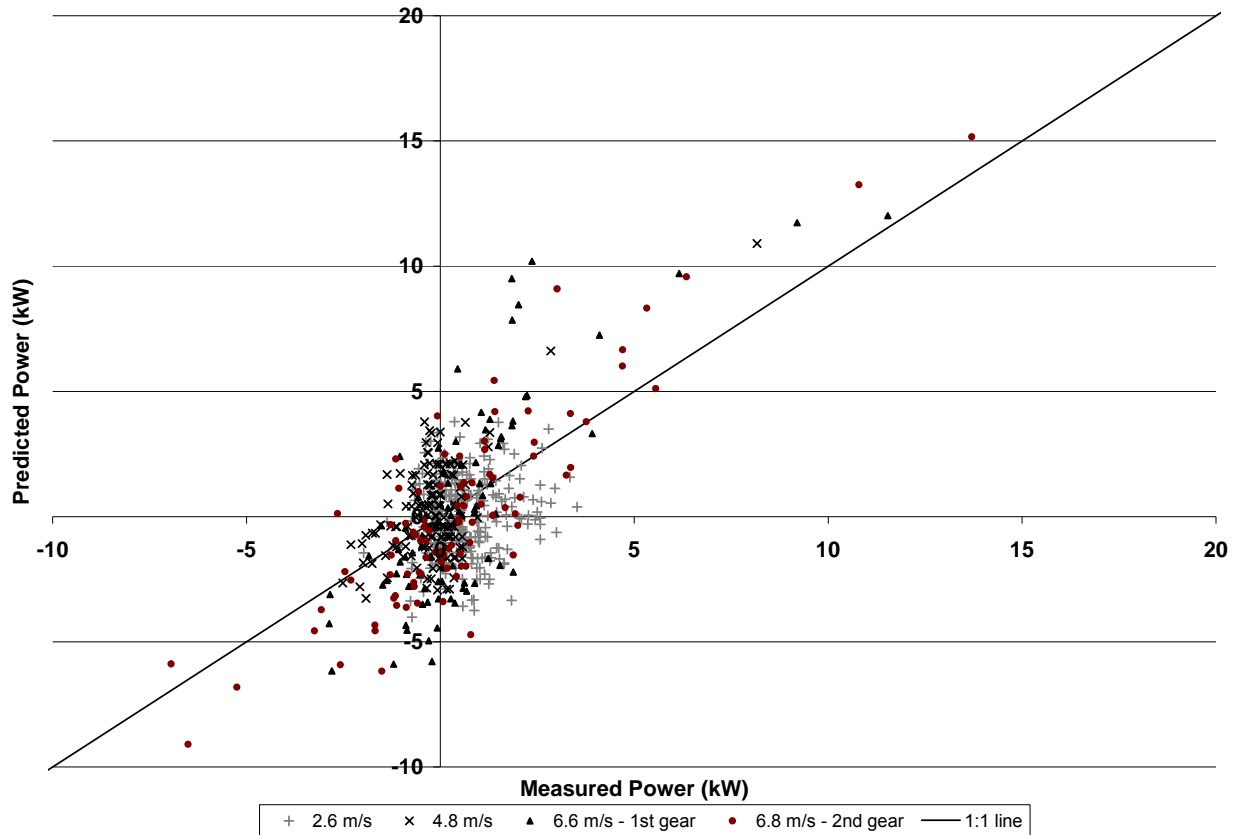| Test No.	Gear	Test Duration (s)	Avg. Travel Speed (m/s)	Avg. Turning Radius (m)	Avg. Predicted Power (kW)	Avg. Measured Power (kW)	Predicted power Std. Dev. (kW)	Measured power Std. Dev. (kW)	Meas. vs. Pred. Power RMSE (kW)
1	1	61	2.3	6.5	0.96	1.23	1.41	0.88	1.7
2	1	103	2.5	15.7	0.14	0.62	2.00	0.51	1.9
3	1	60	3.3	5.3	0.19	0.65	1.54	0.90	1.2
4	1	96	3.6	11.6	0.90	-0.19	2.29	0.83	2.5
5	1	55	5.1	9.9	1.59	1.39	2.39	1.32	2.2
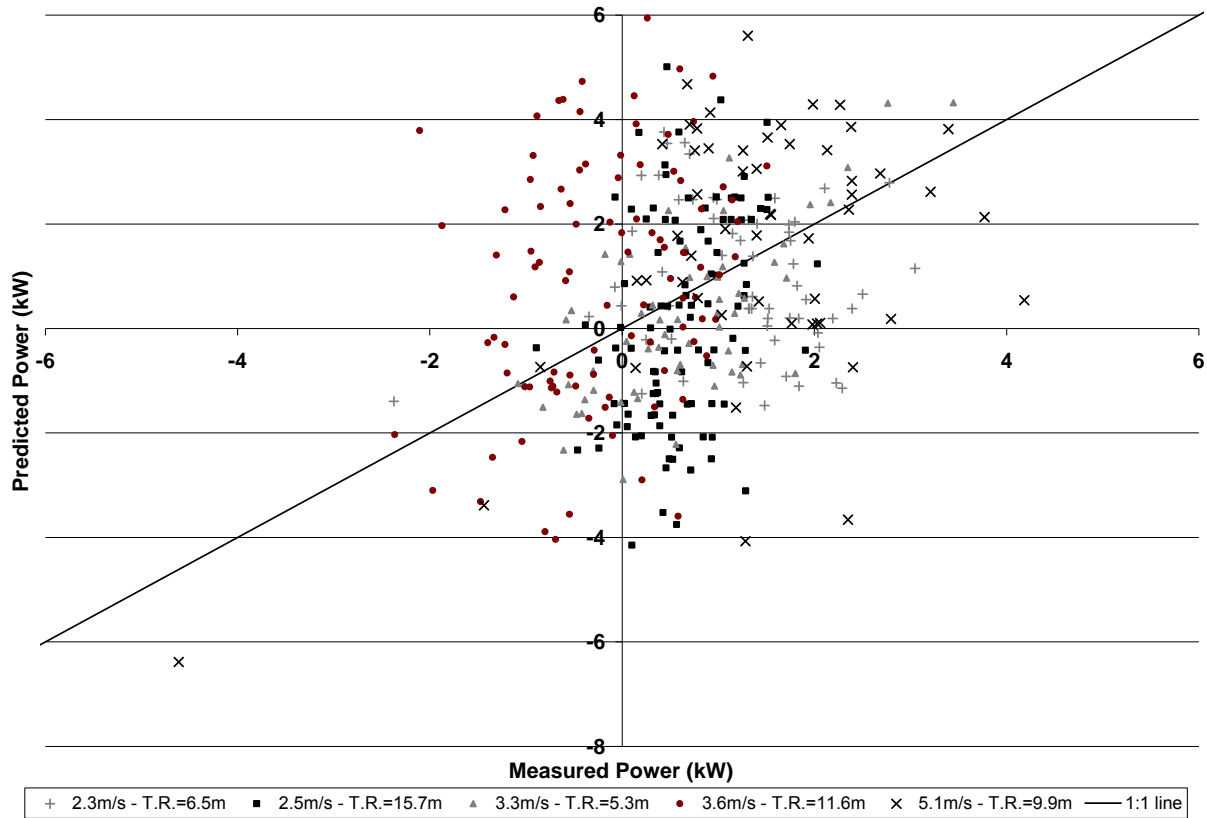
Figure 28: The discrete predicted mobility power values from the Garmin 18 GPS receiver during five constant turning radius motion resistance tests compared to the measured drivewheel power
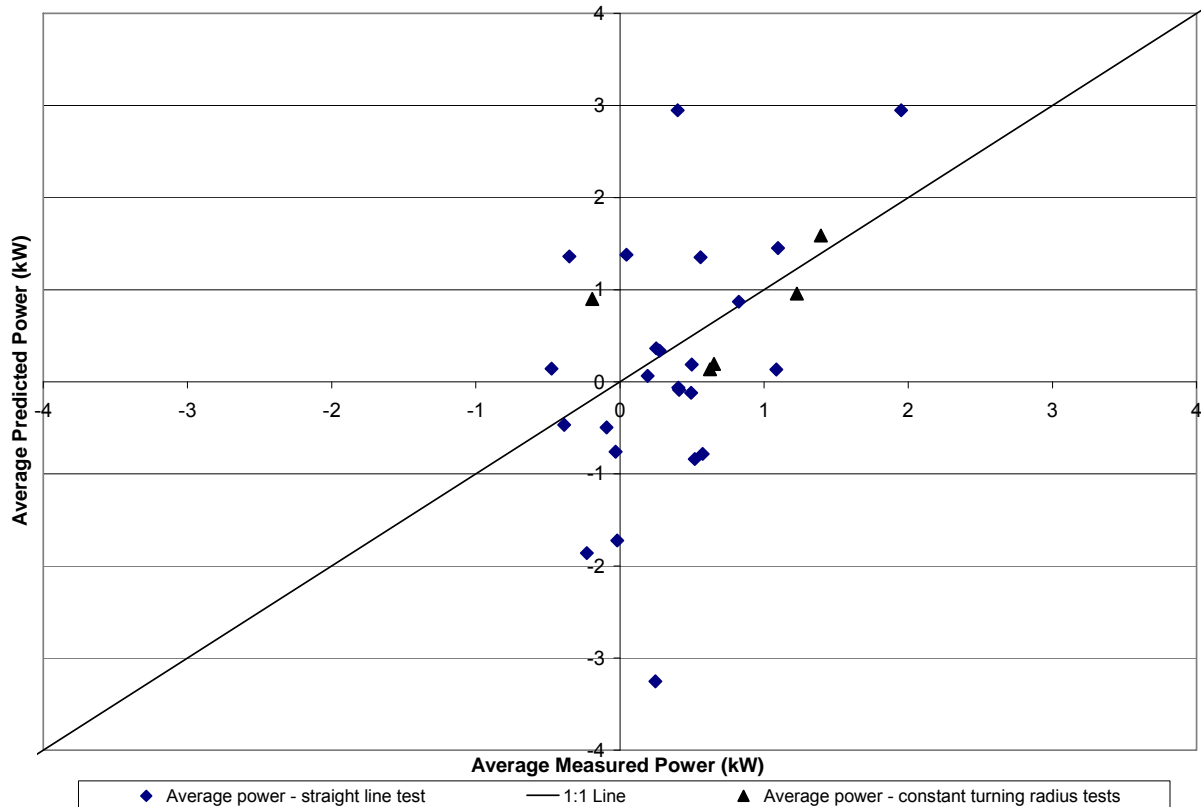
Figure 29: The predicted average mobility power from the Garmin 18 GPS receiver compared to the measured average drivewheel power during the 24 straight-line and five constant turning radius motion resistance tests

The variability of the Garmin 18 GPS receiver during the constant turning radius tests also tended to be greater than the variability of the Trimble 132 receiver's results. The Garmin 18 receiver's discrete data points were less concentrated near the 1:1 line. The Garmin 18 receiver had 22 discrete data points that had predicted mobility power values greater than 4 kW in magnitude, compared to only two discrete data points from Trimble 132 data. The average RMSE value of all of the constant turning radius tests from the Garmin 18 data was approximately 39% greater than the average RMSE value from the Trimble 132 data. The Trimble 132 tended to provide a better estimate of the vehicle's required mobility power during the five constant turning radius tests.

The turning radius estimated from the GPS data was an important input parameter during the constant turning radius tests because the steered wheel angle values needed to apply Equation (4) were estimated from the predicted turning radius. The Trimble 132 receiver resulted in a higher level of accuracy being attained during the constant turning radius tests because the spatial position of each GPS point allowed for a more accurate estimate of the vehicle's turning radius. The actual turning radius of each test was approximately 5 and 10 m while the discrete turning radius values estimated from the Garmin 18 data exceeded these values by up to approximately 10 m. The greater variability that was associated with the Garmin 18 data's turning radius estimates was one possible source of the increased variability of the Garmin 18 receiver compared to the Trimble 132 receiver during the constant turning radius tests.

The average power values during the straight-line and constant turning radius motion resistance tests further confirmed the greater accuracy that was attained with the Trimble 132 GPS receiver. It was estimated that 10 of the 24 straight-line tests had negative power requirements from the Garmin 18 data compared to zero for the Trimble 132 receiver. The average power values from the Trimble 132 receiver were more concentrated along the 1:1 line just above the origin. The results from the straight-line and constant turning radius motion resistance tests indicated that the results from the Trimble 132 receiver had less variability than the Garmin 18 receiver's results while the estimates of the discrete power requirements were reasonable.

The motion resistance ratio estimated from the Vehicle Terrain Interaction (VTI) model for the Chevrolet Equinox's tires used during validation testing was compared to the coefficient of

rolling resistance (analogous to motion resistance ratio) provided by the tire manufacturer. The VTI model estimated the motion resistance ratio of the vehicle to be 0.00773 while the estimated ratio at the rated inflation pressure from the tire manufacturer was 0.00675. The percent difference between the two motion resistance values was 14.6%. This indicated that the VTI model's estimated motion resistance ratio was in reasonable agreement with ratio provided by the manufacturer. The close agreement between the two values gives validity to the assumption made that a firm pavement terrain should use a *CI* of 4137 kPa when applying Equation (2) from the VTI model. The VTI model provided for a more flexible model while the model predicted that the motion resistance ratio of the wheel increased as the vehicle turning radius decreased. Furthermore, the VTI model is more suitable for estimating the motion resistance of military vehicles operating in on-road and off-road terrains where the terrain's measured *CI* value can vary substantially.

4.4.1.2 Grade Tests

Nine grade tests were conducted at average travel speeds of approximately 3.3, 4.8, 7.1, 9.3, and 11.4 m/s. Evaluating the accuracy of the GPS receivers' ability to estimate the vehicle's rate of elevation increase was critical to characterizing the grade power component of the model. Figure 30 compares the vehicle's predicted rate of elevation change from the two GPS receivers during a 10.8 m/s constant speed grade test.
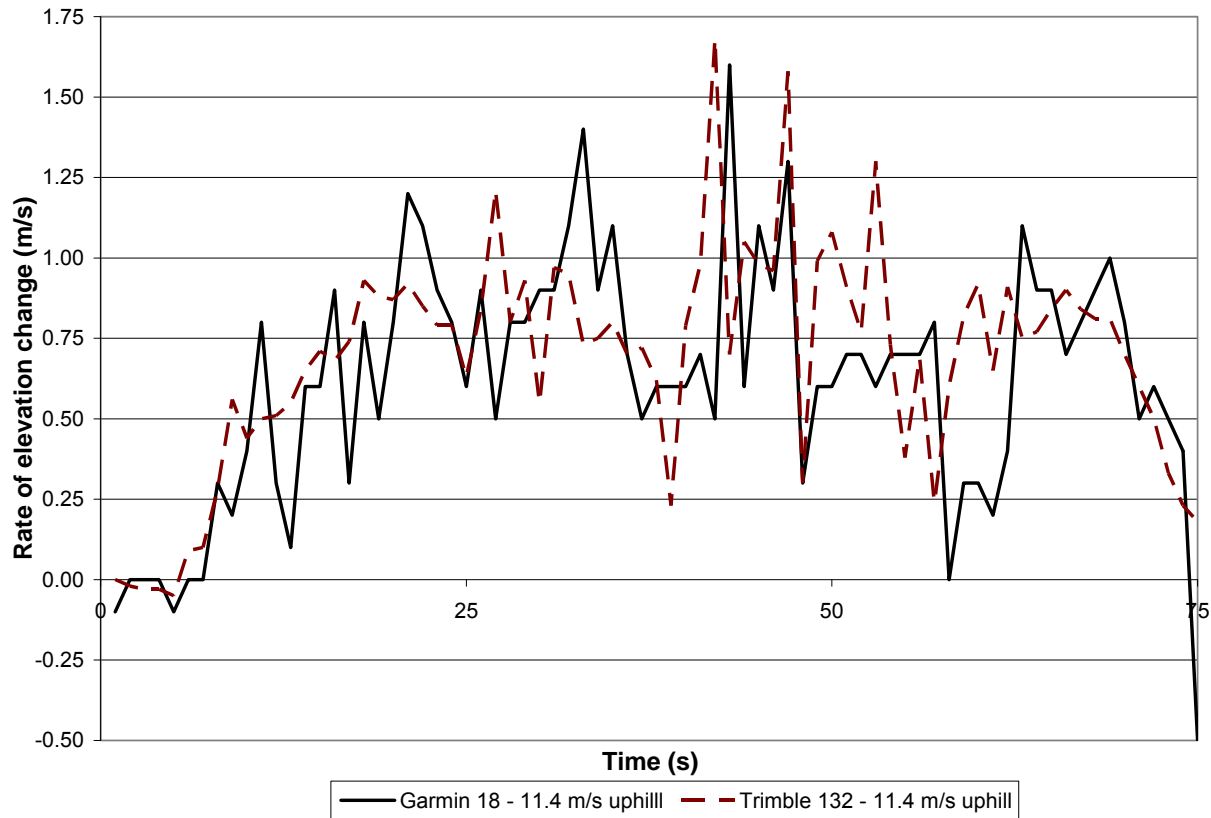
Figure 30: Elevation change estimated from the Garmin 18 and Trimble 132 GPS receivers during a 11.4 m/s uphill grade test

The Trimble 132 GPS receiver's data during the constant speed tests resulted in a smaller amount of variability associated with the vehicle's predicted rate of elevation change. The standard deviation of the elevation change during this test was 0.27 and 0.34 m/s for the Trimble 132 and Garmin 18 GPS receivers respectively. Figure 30 indicated that filtering of the rate of elevation change data was necessary to smooth the data for both receivers due to the rapid fluctuations in the magnitude of the elevation change between the discrete data points. The elevation change estimated from the Garmin 18 receiver's data may have been more variable than the Trimble 132 receiver's data, but a simple 5 s running average filter was used to smooth both GPS receivers change in elevation data. Comparing the predicted mobility power using several types of change

in elevation filters further emphasized the need to smooth the change in elevation data. Figure 31 and 32 provide a comparison between the filtered and unfiltered predicted mobility power values and the measured drivewheel power for the Trimble 132 and Garmin 18 receivers respectively.
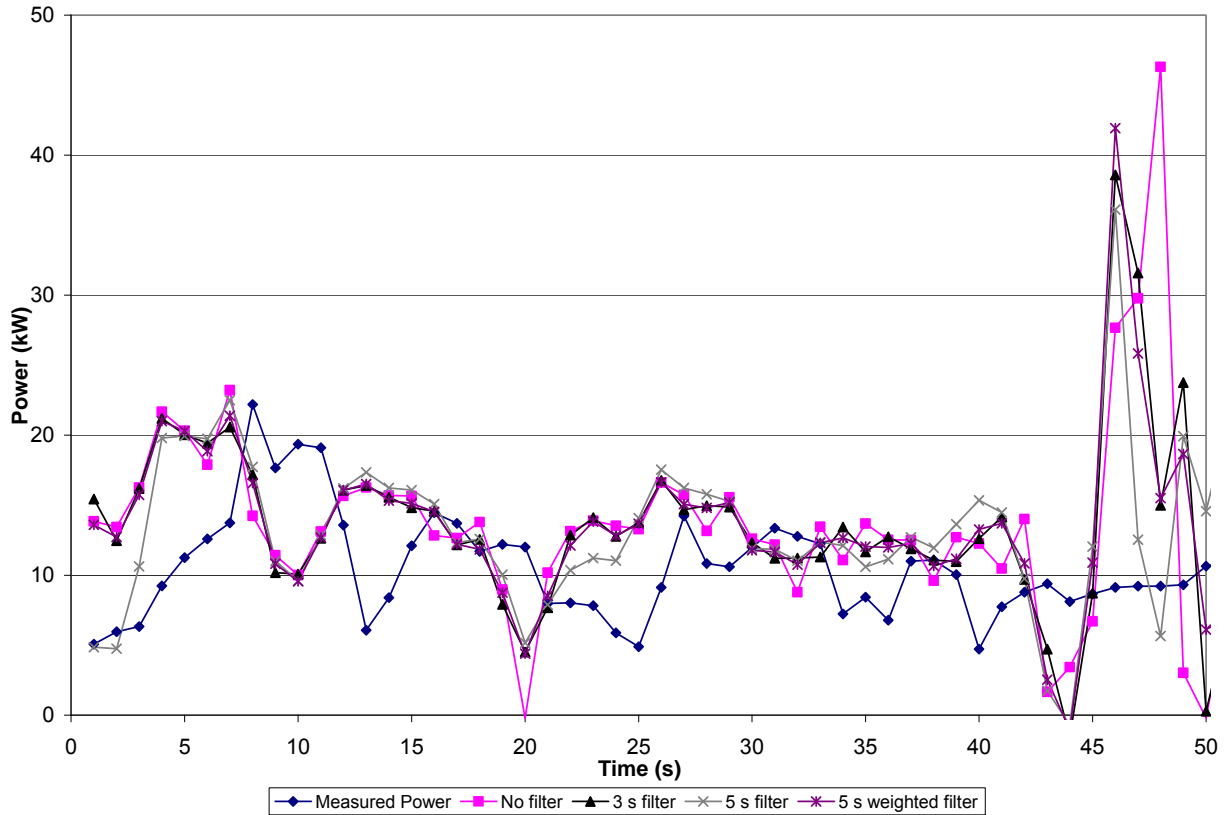
Figure 31: The predicted mobility power using different change in elevation filters Trimble 132 GPS data during a 7.1 m/s travel speed grade test
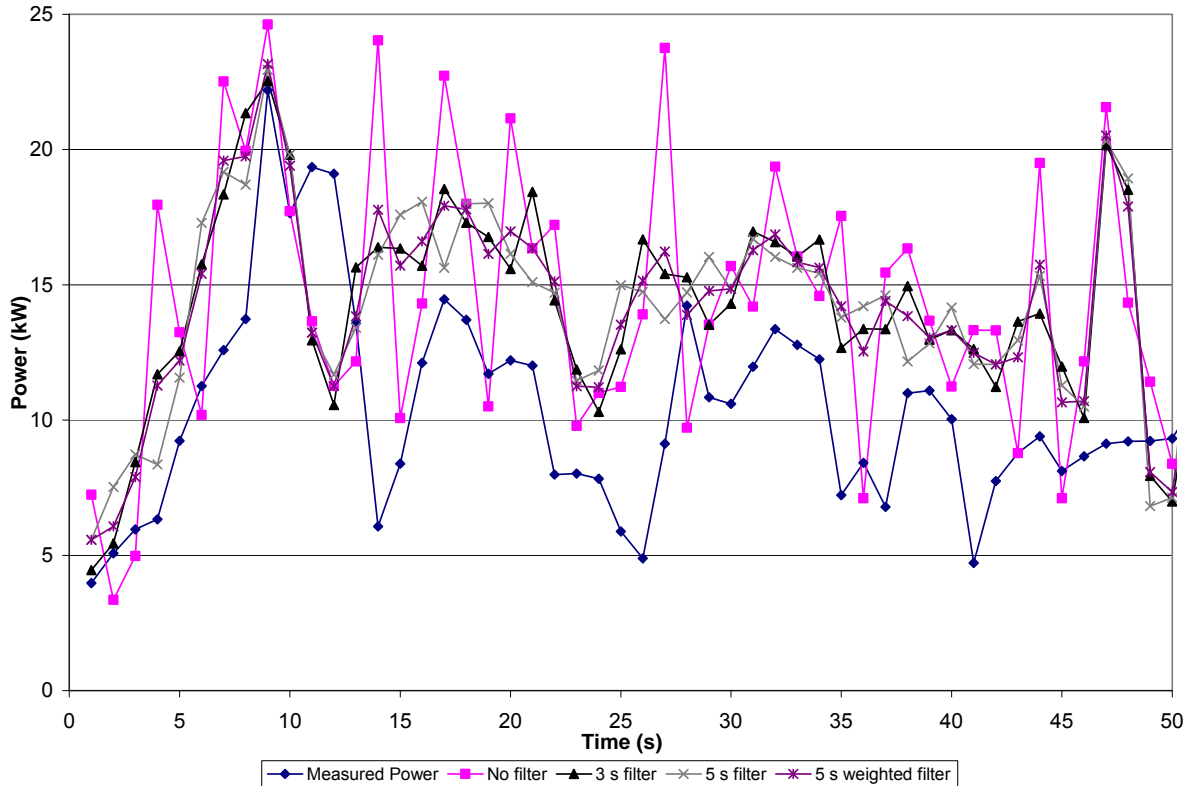
Figure 32: The predicted mobility power using different change in elevation filters
Garmin 18 GPS data during a 7.1 m/s travel speed grade test

The predicted mobility power without using an elevation filter resulted in predicted values that

tended to oscillate above and below the measured drivewheel power values when the Garmin 18

receiver data was used. The measured drivewheel power values refer to the calculated

drivewheel power values estimated from the engine speed and engine torque messages

transmitted on certain 11 bit CAN signals. The oscillations of the predicted values from the

Trimble 132 data appeared to be significantly smaller in magnitude when no filter was used.

This trend was observed during all of the grade tests, independent of the average travel speed.

The 5 s running average filter was applied to the change in elevation data to smooth the change

in elevation data and reduce the oscillating characteristics of the predicted mobility power

curves. This 5 s filter was used to estimate the discrete predicted mobility power values during the nine grade tests.

The statistics and results for the nine grade tests are summarized in Tables 11 and 12 respectively, and a comparison of the discrete predicted and measured power values at the five average travel speeds is given by Figure 33 for the Trimble 132 GPS receiver. The average predicted and measured power values during the nine grade tests are represented in Figure 34.

Table 11: A summary of the Trimble 132 GPS receiver data collected during the nine grade tests

Test No.	Gear	Test Duration (s)	Avg. Travel Speed (m/s)	Avg. dh / dt (m/s)	Avg. Predicted Percent Grade
1	1	232	3.1	0.22	7.2%
2	1	186	3.6	0.27	7.4%
3	1	216	3.1	0.23	7.5%
4	1	142	4.8	0.36	7.6%
5	1	101	7.1	0.52	7.3%
6	1	90	7.2	0.52	7.3%
7	2	75	9.3	0.66	7.1%
8	2	56	11.5	0.86	7.5%
9	2	44	11.3	0.81	7.2%

Table 12: A summary of the results and statistics from the Trimble 132 GPS receiver during the nine grade tests

Test No.	Avg. Predicted Power (kW)	Avg. Predicted Power Std. Dev. (kW)	Avg. Measured Power (kW)	Avg. Measured Power Std. Dev. (kW)	Absolute Average Percent Error	Measured vs. Predicted Power RMSE (kW)	Power CV RMSE
1	5.08	4.07	5.06	1.00	58.5%	4.2	0.83
2	6.23	3.32	5.65	1.38	50.3%	3.4	0.61
3	5.43	3.87	5.12	0.98	56.8%	3.9	0.77
4	8.39	3.09	8.50	2.81	48.2%	3.8	0.45
5	12.19	6.77	9.98	3.82	80.2%	7.7	0.77
6	12.34	5.61	11.93	2.54	42.8%	5.8	0.49
7	16.23	5.14	16.41	4.66	37.6%	7.0	0.43
8	20.18	8.59	21.29	8.60	33.7%	7.4	0.35
9	21.05	8.58	21.51	5.86	37.4%	3.9	0.18
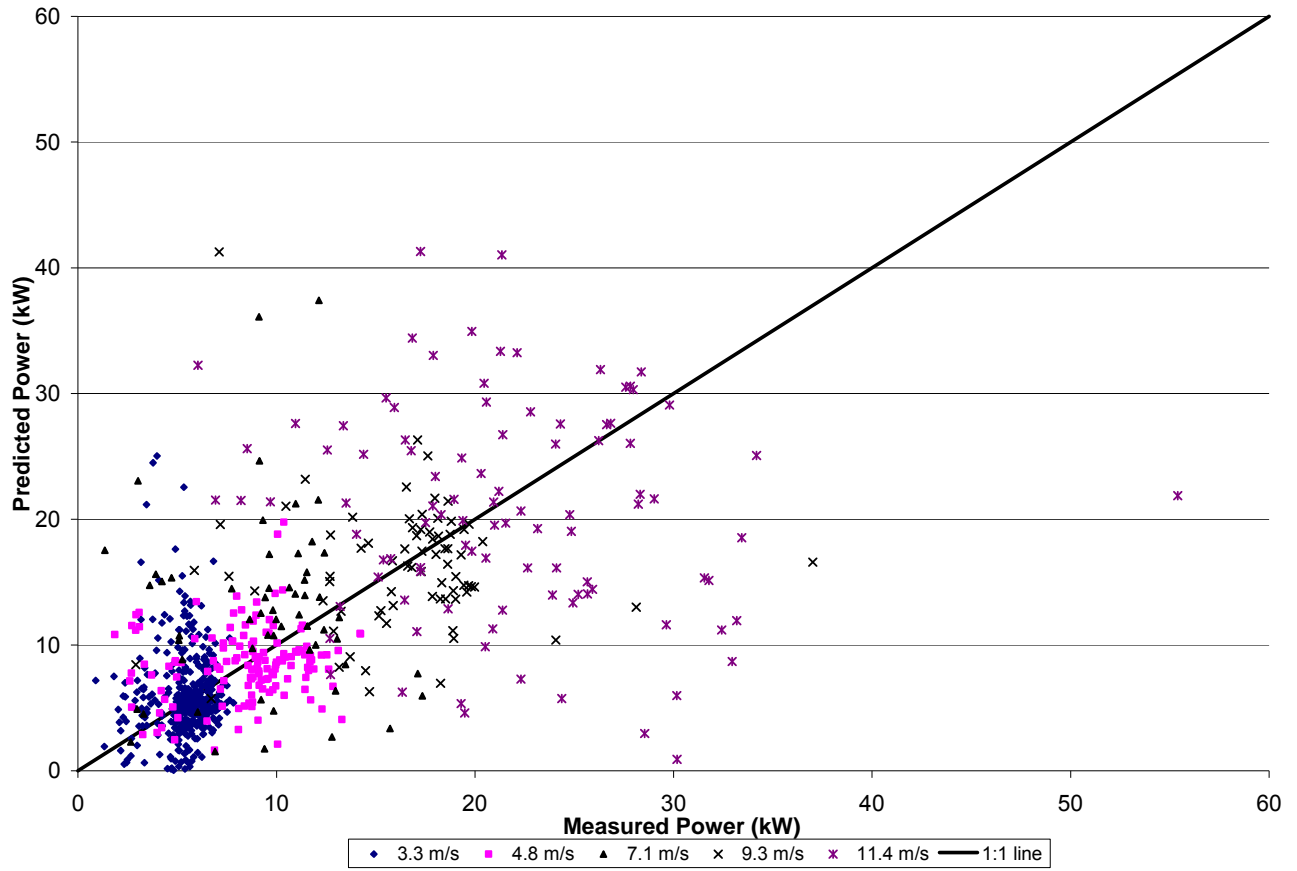
Figure 33: The discrete predicted mobility power values from the Trimble 132 GPS receiver during nine grade tests compared to the measured drivewheel power

Figure 34: The predicted average mobility power from the Trimble 132 GPS receiver during nine grade tests compared to the measured average drivewheel power

The statistics in Table 12 and the variability of the model indicated by Figures 33 and 34 led to the conclusion that there was a moderate level of variability between the discrete measured and predicted power values during the grade tests. The discrete data points for a given travel speed tended to be equally scattered above and below the 1:1 line in Figure 33. The magnitude of the predicted discrete and average power values increased as the average vehicle travel speed increased. The predicted average power requirement during all nine grade tests had an absolute average percent error of 6% which indicated the model was very accurate at predicting the average power requirements. The absolute average percent error values were calculated by dividing the magnitude of the difference between the discrete predicted and measured values by the magnitude of the measured value while averaging all of these discrete terms. A lower level

of accuracy was attained when estimating the discrete power requirements during the grade test, as indicated by an absolute average percent error of 50%. The maximum discrete and average predicted mobility power values were approximately 39 and 20% of the rated engine power respectively during the nine grade tests.

The absolute average percent error, RMSE, and Coefficient of Variation of the RMSE (CV RMSE) values were used as an indicator of the models accuracy at predicting the discrete mobility power values during the nine grade tests. CV RMSE is the RMSE normalized to the average of the measured values, and it provided an indication of the variability of the model relative to the average measured drivewheel power. These measures of accuracy indicated that the model tended to attain a higher level of accuracy during the grade tests performed at higher average travel speeds. The CV RMSE values tended to decrease as the average vehicle travel speed increased. The variability of the model's predicted power value was minimized during the grade test performed at an average travel speed of 11.3 m/s. The absolute average percent error and CV RMSE values for this test were 37.4% and 0.18 respectively. These values starkly differ compared to the absolute average percent error and CV RMSE values for the 3.1 m/s average travel speed grade test which were 58.5% and 0.83 respectively.

The statistics and results for the nine grade tests are summarized in Tables 13 and 14, and a comparison of the discrete predicted and measured power values at the five average travel speeds is given in Figure 35 for the Garmin 18 GPS data. The average predicted and measured power values during the nine grade tests are represented in Figure 36 for the Garmin 18 GPS data.

Table 13: A summary of the Garmin 18 GPS receiver data collected during the nine grade tests

Test No.	Gear	Test Duration (s)	Avg. Travel Speed (m/s)	Avg. dh / dt (m/s)	Avg. Predicted Percent Grade
1	1	232	3.0	0.24	7.8%
2	1	186	3.6	0.28	7.7%
3	1	216	3.0	0.21	7.0%
4	1	142	4.8	0.39	8.2%
5	1	101	7.1	0.51	7.3%
6	1	90	7.2	0.43	5.9%
7	2	75	9.2	0.56	6.1%
8	2	56	11.5	0.86	7.5%
9	2	44	11.2	0.74	6.6%

Table 14: A summary of the results and statistics from the Garmin 18 GPS receiver during the nine grade tests

| Test No.	Avg. Predicted Power (kW)	Avg. Predicted Power Std. Dev. (kW)	Avg. Measured Power (kW)	Avg. Measured Power Std. Dev. (kW)	Absolute Average Percent Error	Measured vs. Predicted Power RMSE (kW)	Power CV RMSE
1	5.42	2.86	5.08	1.00	44.8%	2.69	0.53
2	6.40	4.97	5.65	1.38	32.1%	5.16	0.91
3	5.00	4.23	5.10	0.98	64.6%	4.14	0.81
4	9.15	4.88	8.45	2.81	62.4%	5.18	0.61
5	12.23	5.78	10.04	3.82	58.9%	6.01	0.60
6	9.97	4.91	11.95	2.54	41.5%	5.77	0.48
7	14.40	8.12	16.54	4.66	52.2%	10.39	0.63
8	19.97	11.15	21.08	8.60	37.3%	11.62	0.55
9	19.31	9.99	21.58	5.86	31.4%	3.51	0.16
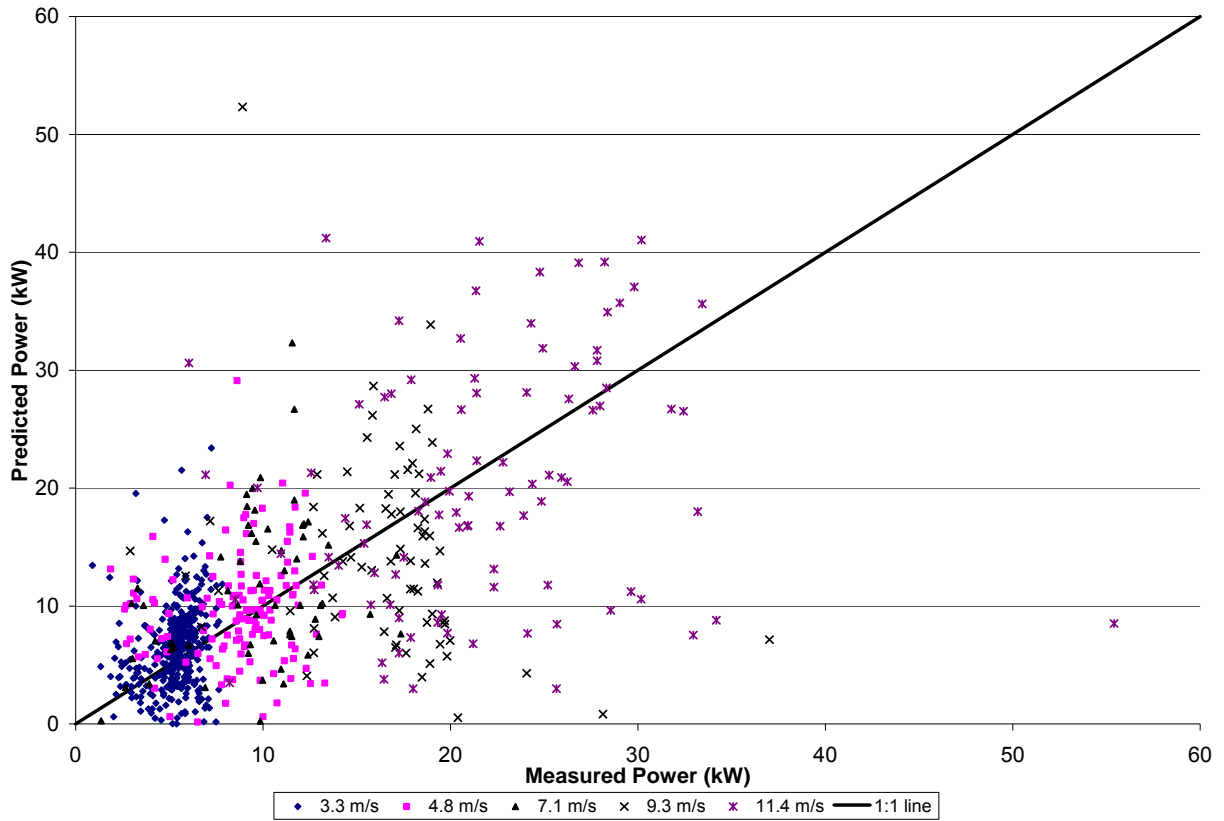
Figure 35: The discrete predicted mobility power values from the Garmin 18 GPS receiver during nine grade tests compared to the measured drivewheel power
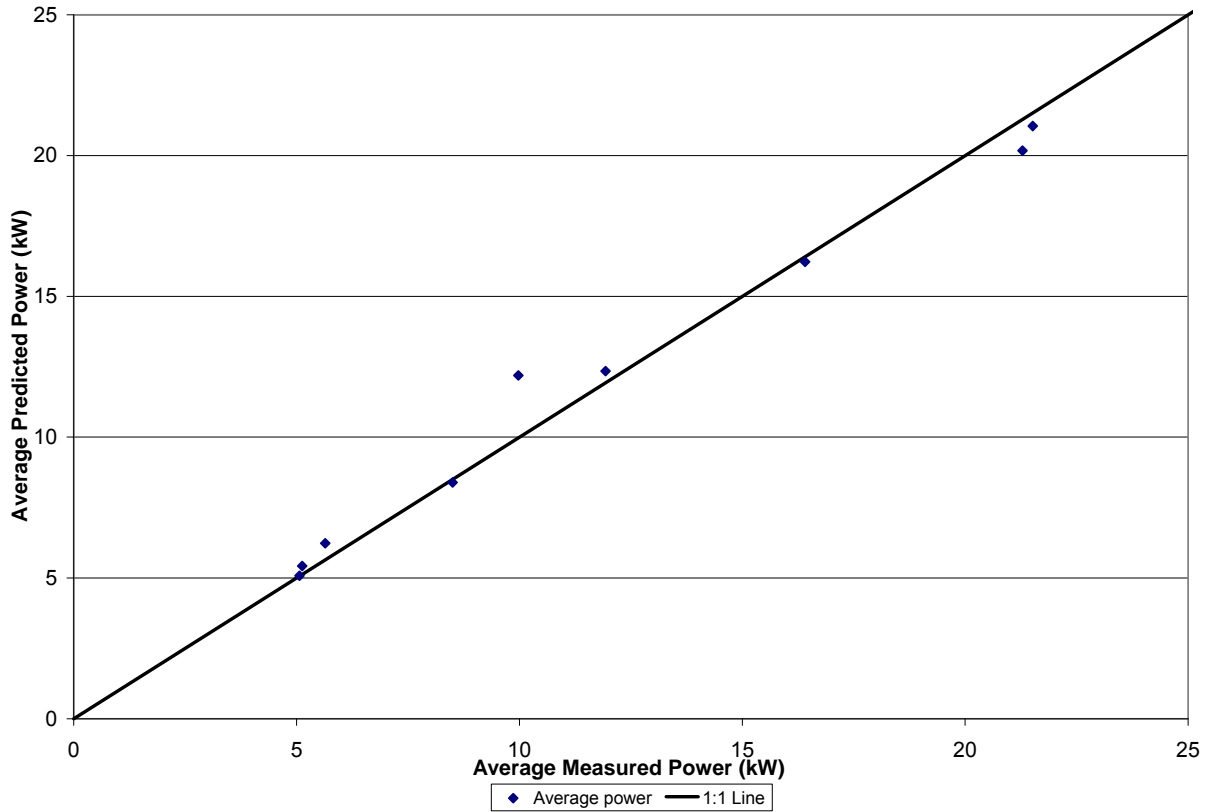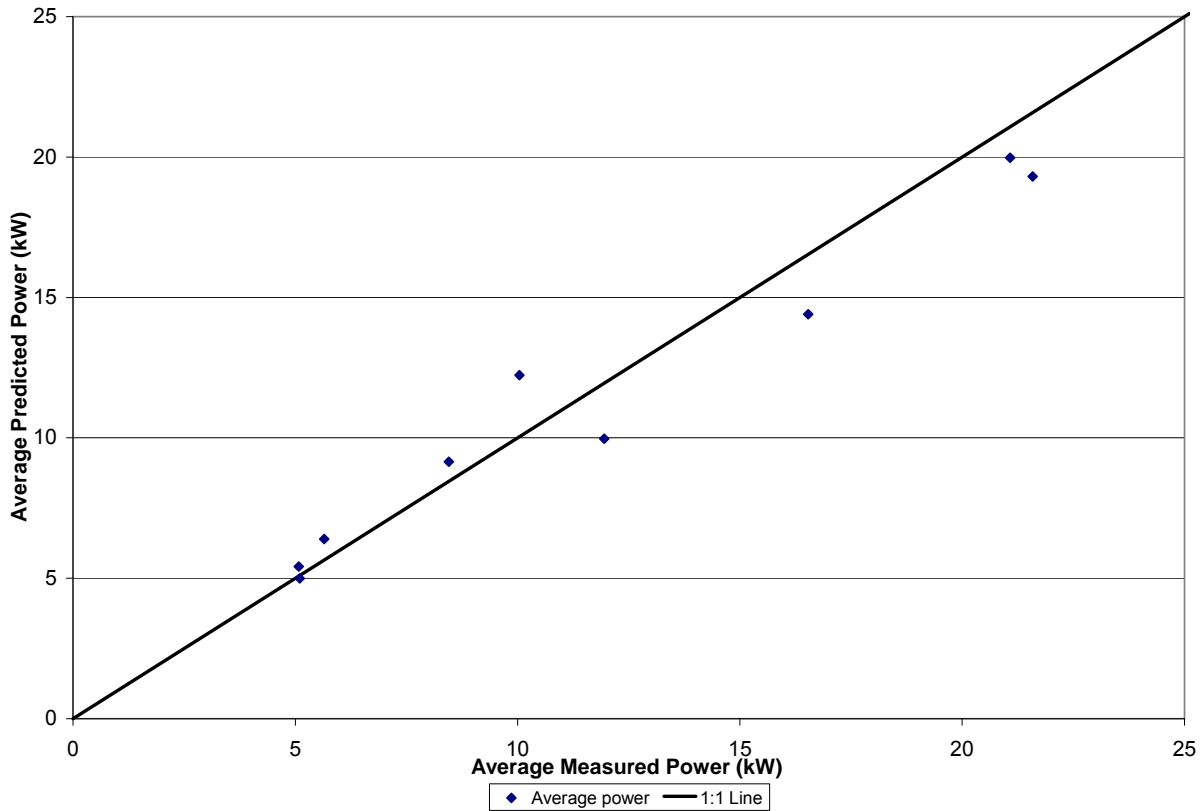
Figure 36: The predicted average mobility power from the Garmin 18 GPS receiver
during nine grade tests compared to the measured average drivewheel power

The discrete data represented in Figure 35 indicated that the Garmin 18 GPS receiver data

slightly decreased the model's accuracy during the nine grade tests compared to the results from

the Trimble 132 data. The Garmin 18 receiver's discrete data points tended to have more

outliers while the points appeared to be slightly less concentrated near the 1:1 line. The RMSE

and CV RMSE values calculated for each test indicated that the model had a small increase in

the variability when the Garmin 18 GPS receiver's data was used. However, both receivers

provided reasonable estimates of the discrete predicted power requirements during the grade

tests. Furthermore, the model attained a high level of accuracy when estimating the average

power requirements for the data from both GPS receivers while the Trimble 132 receiver was

slightly more accurate.

106

Any difference in the model's accuracy between the Trimble 132 and Garmin 18 receivers' results was attributed to the Trimble 132 GPS receiver's ability to more accurately estimate the vehicle's rate of elevation change. The Trimble 132 GPS receiver data provided for smoother estimates of the vehicle's elevation change with fewer rapid changes in the magnitude of the elevation change, as indicated by Figures 30 – 32. The estimated average percent grade during the tests allowed for the variability of the predicted percent grade traversed to be characterized across each test. The average percent grade values for the Garmin 18 GPS receiver were between 5.9 and 8.0% while the average percent grades from the Trimble 132 receiver ranged between 7.1 and 7.6%. The standard deviation of the Garmin 18 receiver's average percent grade values was approximately 550% greater than the 0.14% standard deviation of the percent grade estimated from the Trimble 132 GPS receiver.

The results from the Trimble 132 and Garmin 18 GPS receiver data collected indicated that the model had moderate level of variability associated with the estimated discrete mobility power values during the nine grade tests. However, a high degree of accuracy and a substantially decreased level of variability were achieved by the model when predicting the test vehicle's average power requirement.

4.4.1.3 Inertia Tests

The 15 straight-line inertia tests allowed for the accuracy and variability of the inertia power component of the GPS-based mobility power model to be characterized. Three tests were conducted at a degree of acceleration of "slow" while the 1st gear of the transmission was

engaged. Six tests each were conducted at degrees of acceleration of "medium" and "fast" where half of the tests had the 1st gear engaged and the other tests were in 2nd gear.

The accuracy of the model at predicting the power required to vary the inertia of the test vehicle was strongly dependent on the estimated vehicle speed and acceleration values obtained from the GPS data. The results presented were generated using a 2 s GPS speed and acceleration offset (ie lag), and Sections 4.3.9 and 4.3.10 provide a detailed description of the methods used to determine the correct GPS speed and acceleration offset. The derivative of the discrete GPS speed data was taken with respect to time to determine the vehicle's predicted acceleration. The acceleration calculated from the discrete GPS speed data was identified possibly as a significant source of variability in estimating the test vehicle's inertia power requirements because numerically differentiating the discrete GPS speed data may have amplified any noise in the GPS speed data. Figures 37 and 38 summarize a comparison of the average measured and predicted acceleration during each inertia test for the Trimble 132 and Garmin 18 GPS receivers. The measured acceleration values were calculated from the discrete measured wheel speed data. The measured or calculated vehicle travel speed was computed from the discrete measured wheel speed data via Equation (26) from Section 4.3.9, and the derivative was taken with respect to time to calculate the discrete measured acceleration values.
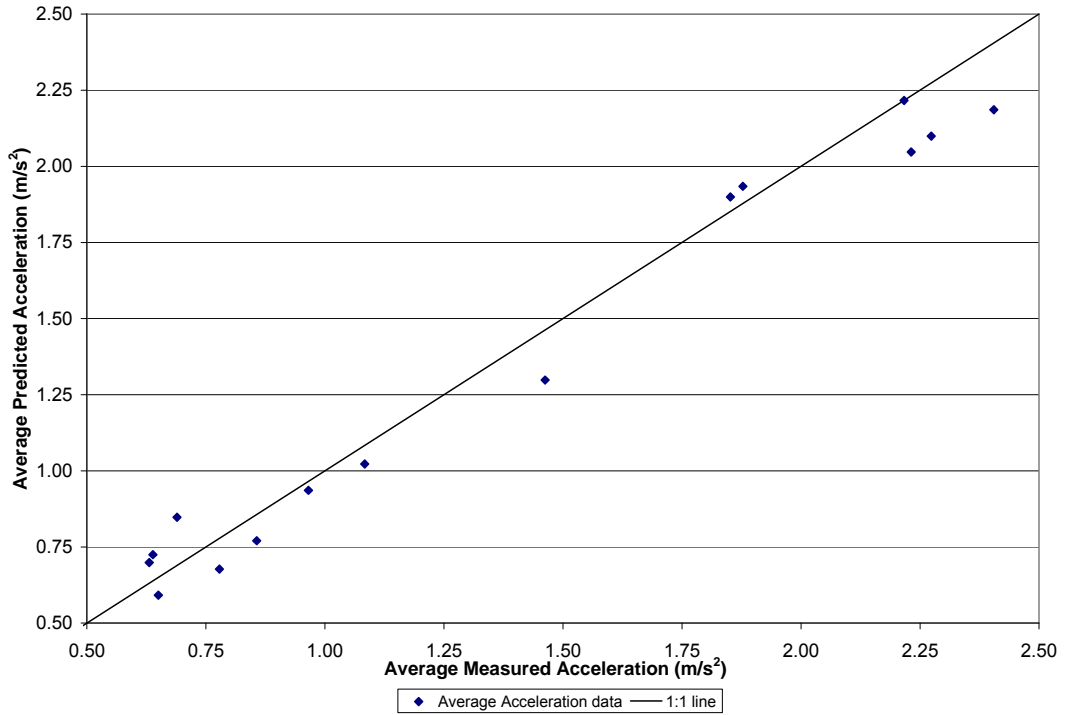
Figure 37: The average predicted vehicle acceleration from the Trimble 132 GPS receiver during 15 inertia tests compared to the measured acceleration
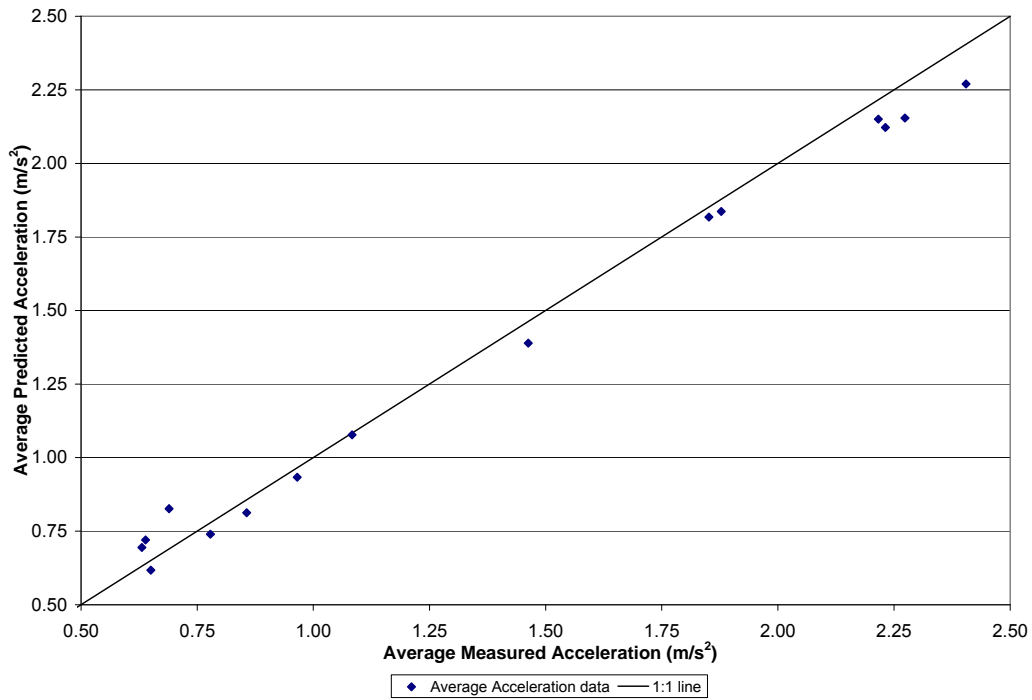
Figure 38: The average predicted vehicle acceleration from the Garmin 18 GPS receiver during 15 inertia tests compared to the measured acceleration

109

Figures 37 and 38 indicated that the Trimble 132 and Garmin 18 receivers accurately predicted the vehicle's average acceleration during the 15 inertia tests. The GPS receivers tended to slightly underestimate the vehicle's average acceleration during the inertia tests except during tests with a slow degree of acceleration. The average predicted acceleration RMSE values were 0.42 and 0.30 m/s^2 for the Trimble 132 and Garmin 18 receivers respectively. The Garmin 18 GPS receiver had slightly less variability associated with estimating vehicle acceleration, despite the greater precision of the Trimble 132 GPS.

The differences in the estimated vehicle acceleration values from the two receivers were attributed to a few significant factors. The proprietary method for estimating the discrete speed value for each GPS point is different for each GPS receiver manufacturer. The various methods available for estimating and filtering the GPS speed data was the primary reason why there were differences between the GPS receivers. One method may over-smooth or under-smooth the vehicle speed data more than the other. The derivative of the discrete speed data was taken to determine the vehicle's acceleration. Taking the derivative of the vehicle speed data to determine vehicle acceleration may have amplified the magnitude of the error associated with the speed data. One source of error may have been the inaccuracy associated with the rotational speed sensor for each wheel. The measured straight-line vehicle acceleration was calculated from the wheel speed CAN data, and the accuracy of these sensors was unknown. Another factor to consider was the 2 s GPS offset used in the analysis. The 2 s GPS offset may have been biased or more applicable to one receiver compared to the other. The Trimble 132 receiver may have

110

provided for better estimates of vehicle acceleration at some other non-integer GPS offset that

was not analyzed (ie 0.5, 1.5, 2.5 s GPS offset).

The 15 straight-line inertia tests conducted allowed for validation and an accuracy assessment of

the inertia component the model. The results and statistics from the Trimble 132 GPS data for

the 15 inertia tests are detailed in Tables 15 and 16, and the relationship between the measured

and predicted values are given in Figure 39. The average predicted acceleration Root Mean

Square Error (RMSE) values are also provided in Table 15. The average RMSE value was a

maximum during Test Number 12 while the RMSE was minimized during Test Number 13.

There was minimal variability across the three acceleration RMSE values during the inertia tests

conducted at a given level of acceleration and gear.

Table 15: A summary of the Trimble 132 GPS receiver data collected during the 15
inertia tests

Test No.	Gear	Degree of Acceleration	Test Duration (s)	Measured vs. Predicted Acceleration RMSE (m/s^2)
1	1	Slow	10	0.53
2	1	Slow	9	0.51
3	1	Slow	8	0.59
4	1	Medium	4	0.41
5	1	Medium	4	0.39
6	1	Medium	4	0.47
7	2	Medium	6	0.30
8	2	Medium	7	0.31
9	2	Medium	6	0.43
10	1	Fast	5	0.55
11	1	Fast	10	0.65
12	1	Fast	8	0.68
13	2	Fast	8	0.10
14	2	Fast	8	0.27
15	2	Fast	7	0.13

Table 16: A summary of the results and statistics from the Trimble 132 GPS receiver during the 15 inertia tests

Test No.	Avg. Predicted Power (kW)	Avg. Predicted Power Std. Dev. (kW)	Avg. Measured Power (kW)	Avg. Measured Power Std. Dev. (kW)	Absolute Average Percent Error	Measured vs. Predicted Power RMSE (kW)	Power CV RMSE
1	10.1	3.69	8.9	3.49	29%	2.29	0.26
2	9.1	3.02	7.9	1.95	35%	2.90	0.37
3	10.2	4.45	10.2	2.82	27%	2.86	0.28
4	30.1	6.37	23.1	3.25	45%	18.64	0.41
5	14.6	3.93	12.0	3.21	43%	17.97	0.35
6	21.7	4.75	17.6	3.99	32%	16.81	0.33
7	16.3	2.61	16.5	3.09	46%	10.65	0.44
8	19.1	10.62	20.7	6.21	43%	11.63	0.42
9	28.4	2.68	25.2	6.03	38%	12.05	0.36
10	33.7	23.15	24.3	16.79	30%	8.12	0.35
11	36.9	29.15	27.8	21.75	26%	3.62	0.30
12	43.2	27.91	33.9	19.35	26%	5.83	0.33
13	63.1	18.52	45.4	17.94	15%	3.26	0.20
14	65.2	18.12	51.3	21.08	38%	10.80	0.52
15	65.4	21.53	51.0	18.09	19%	4.54	0.18

Figure 39: The discrete predicted mobility power values from the Trimble 132 GPS receiver during 15 inertia tests compared to the measured drivewheel power

The results indicated that the GPS-based model provided very reasonable estimates of the

required mobility power of the vehicle during the 15 inertia tests. CV RMSE is the RMSE

normalized to the average of the measured values, and it provided an indication of the variability of the model relative to the average measured drivewheel power. The maximum predicted discrete mobility power value during the 15 inertia tests was approximately 84% of the rated engine power. This discrete value represented the greatest predicted and measured power requirement for the test vehicle during all of the controlled tests. The three inertia tests conducted at a fast degree of acceleration while the 2nd gear of the transmission was engaged (ie Test Numbers 13 – 15) had the lowest absolute average percent error and Coefficient of Variation of the RMSE (CV RMSE) values between the estimated mobility power and the measured drivewheel power. The absolute average percent error values were calculated by dividing the magnitude of the difference between the discrete predicted and measured values by the magnitude of the measured value while averaging all of these discrete terms. The absolute average percent error and CV RMSE values during the three inertia tests conducted at a medium level of acceleration in 2nd gear (ie Test Numbers 7 – 9) were on average approximately 37% greater than the values calculated for the fast inertia tests in 2nd gear. In general, the model provided accurate estimates of the discrete power requirements during the 15 inertia tests. The average predicted and measured mobility power requirement values for the 15 inertia tests are summarized in Figure 40 for the Trimble 132 GPS receiver.
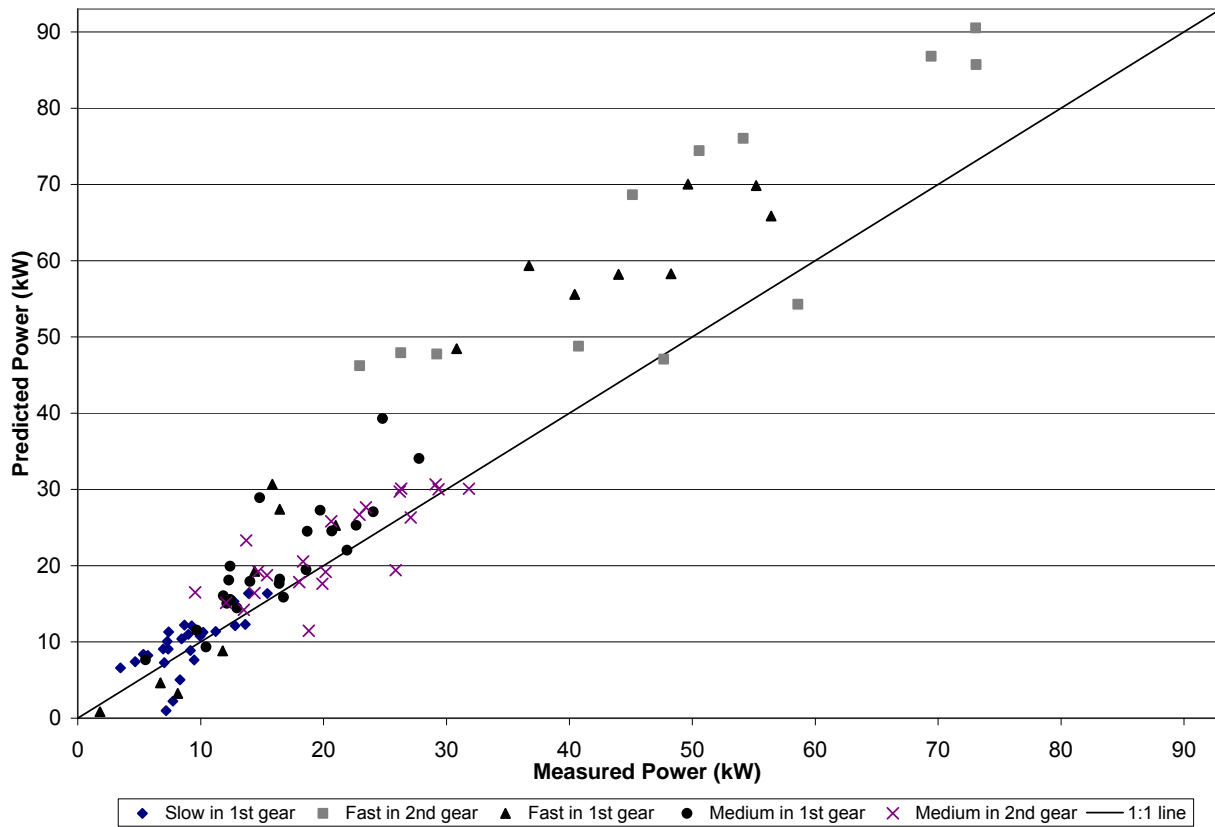
Figure 40: The predicted average mobility power from the Trimble 132 GPS receiver during 15 inertia tests compared to the measured average drivewheel power

The average power values predicted from the mobility power model for the 15 inertia tests were very similar to the average measured power delivered to the drivewheels of the test vehicle. The maximum average predicted mobility power values was approximately 58% of the rated engine power during the 15 inertia tests. The model tended to slightly overestimate the average power requirement during the 15 inertia tests. This trend may have been attributed to the equivalent mass term that was used in Equation (13) to estimate the power requirement from the inertia component of the model. The m_{eq} term depended on the gamma value (γ) value for the gear that was engaged during an inertia test. Some unknown difference between the m_{eq} predicted from the model and the vehicle's actual m_{eq} in a given gear was one possible source of the model's

114

tendency to overestimate the mobility power requirements of the vehicle. The γ values provided

for the vehicle to estimate m_{eq} may have needed to be recalibrated for the vehicle configuration

tested since the model tended to slightly overestimate the power requirements despite

underestimating the average vehicle acceleration. Figure 40 indicated that the model tended to

predict the average power requirements with a high level of accuracy during the 15 inertia tests

from the Trimble 132 GPS data.

Tables 17and 18 along with Figures 41 and 42 detail the results obtained using data collected

from the Garmin 18 GPS receiver for the 15 inertia tests conducted.

Table 17: A summary of the Garmin 18 GPS receiver data collected during the 15 inertia tests

Test No.	Gear	Degree of Acceleration	Test Duration (s)	Measured vs. Predicted Acceleration RMSE (m/s^2)
1	1	Slow	10	0.51
2	1	Slow	9	0.50
3	1	Slow	8	0.62
4	1	Medium	4	0.55
5	1	Medium	4	0.61
6	1	Medium	4	0.65
7	2	Medium	6	0.05
8	2	Medium	7	0.06
9	2	Medium	6	0.07
10	1	Fast	5	0.13
11	1	Fast	10	0.15
12	1	Fast	8	0.16
13	2	Fast	8	0.15
14	2	Fast	8	0.15
15	2	Fast	7	0.16

Table 18: A summary of the results and statistics from the Garmin 18 GPS receiver during the 15 inertia tests

Test No.	Avg. Predicted Power (kW)	Avg. Predicted Power Std. Dev. (kW)	Avg. Measured Power (kW)	Avg. Measured Power Std. Dev. (kW)	Absolute Average Percent Error	Measured vs. Predicted Power RMSE (kW)	Power CV RMSE
1	10.5	3.87	8.9	3.49	48%	3.54	0.40
2	8.3	3.34	7.9	1.95	38%	3.29	0.42
3	10.8	5.19	10.2	2.82	39%	3.99	0.39
4	27.8	5.13	23.1	3.25	22%	6.91	0.30
5	14.0	3.45	12.0	3.21	27%	3.22	0.27
6	20.2	5.86	17.6	3.99	22%	5.28	0.30
7	15.2	2.20	16.5	3.09	12%	3.13	0.19
8	22.3	5.31	20.7	6.21	22%	4.55	0.22
9	25.8	5.50	25.2	6.03	6%	1.83	0.07
10	27.6	22.36	24.3	16.79	36%	6.59	0.27
11	32.5	29.35	27.8	21.75	42%	8.30	0.30
12	39.3	30.44	33.9	19.35	41%	10.71	0.32
13	60.0	16.02	45.4	17.94	41%	16.42	0.36
14	59.3	13.67	51.3	21.08	38%	14.81	0.29
15	62.2	18.43	51.0	18.09	28%	14.09	0.28
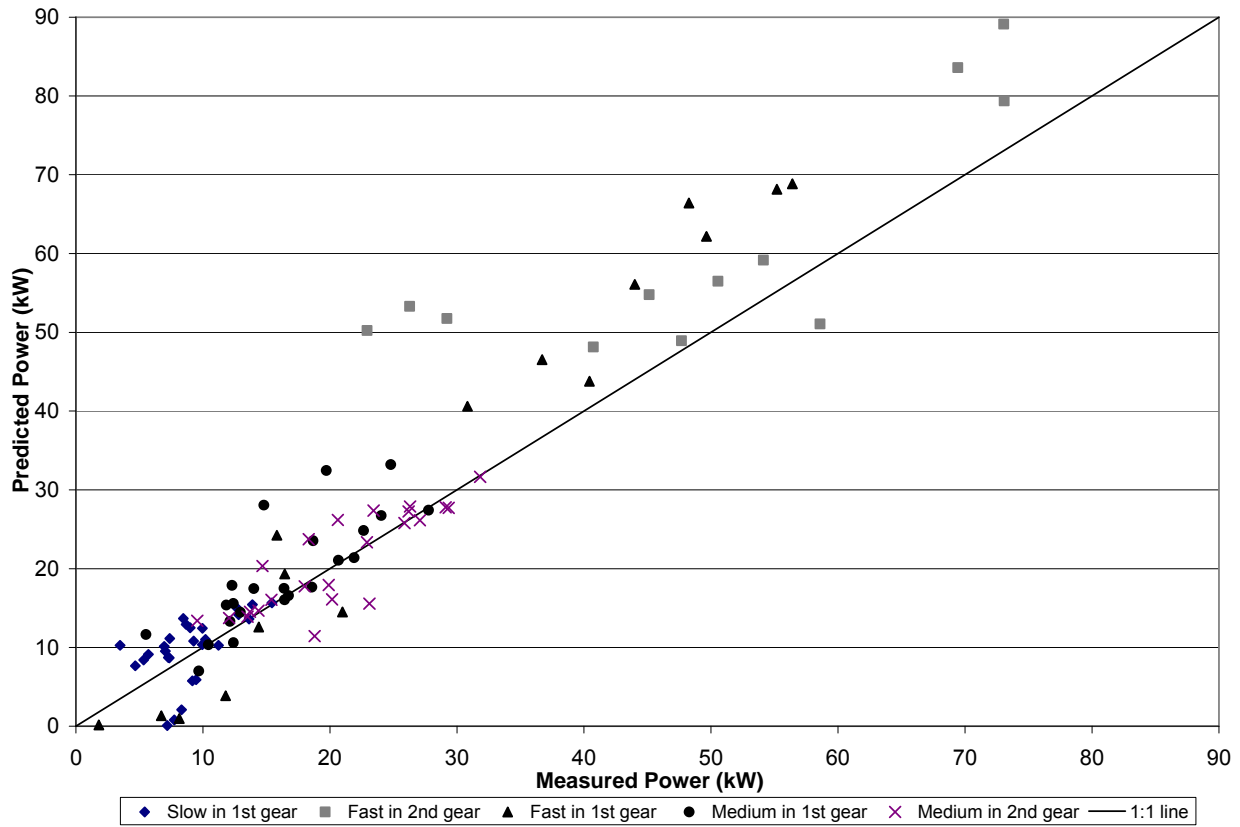
Figure 41: The discrete predicted mobility power values from the Garmin 18 GPS receiver during 15 inertia tests compared to the measured drivewheel power
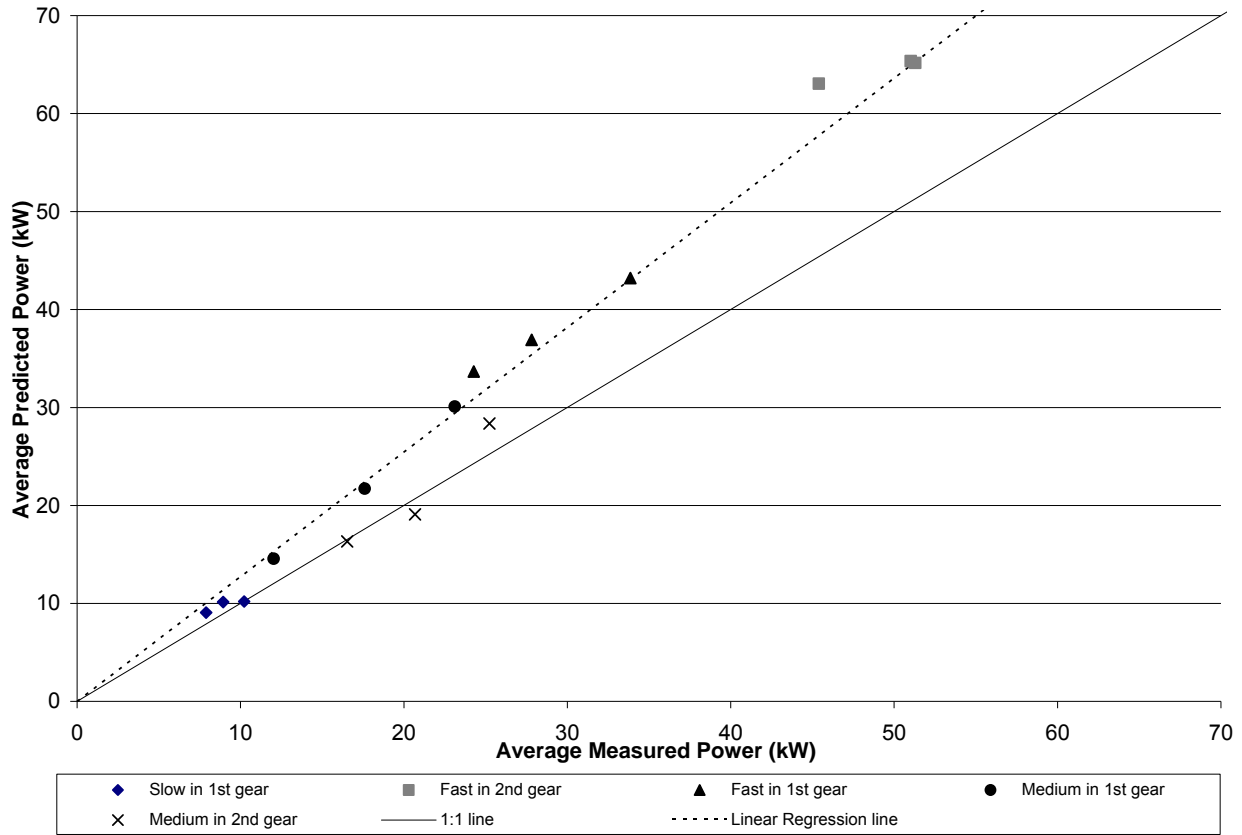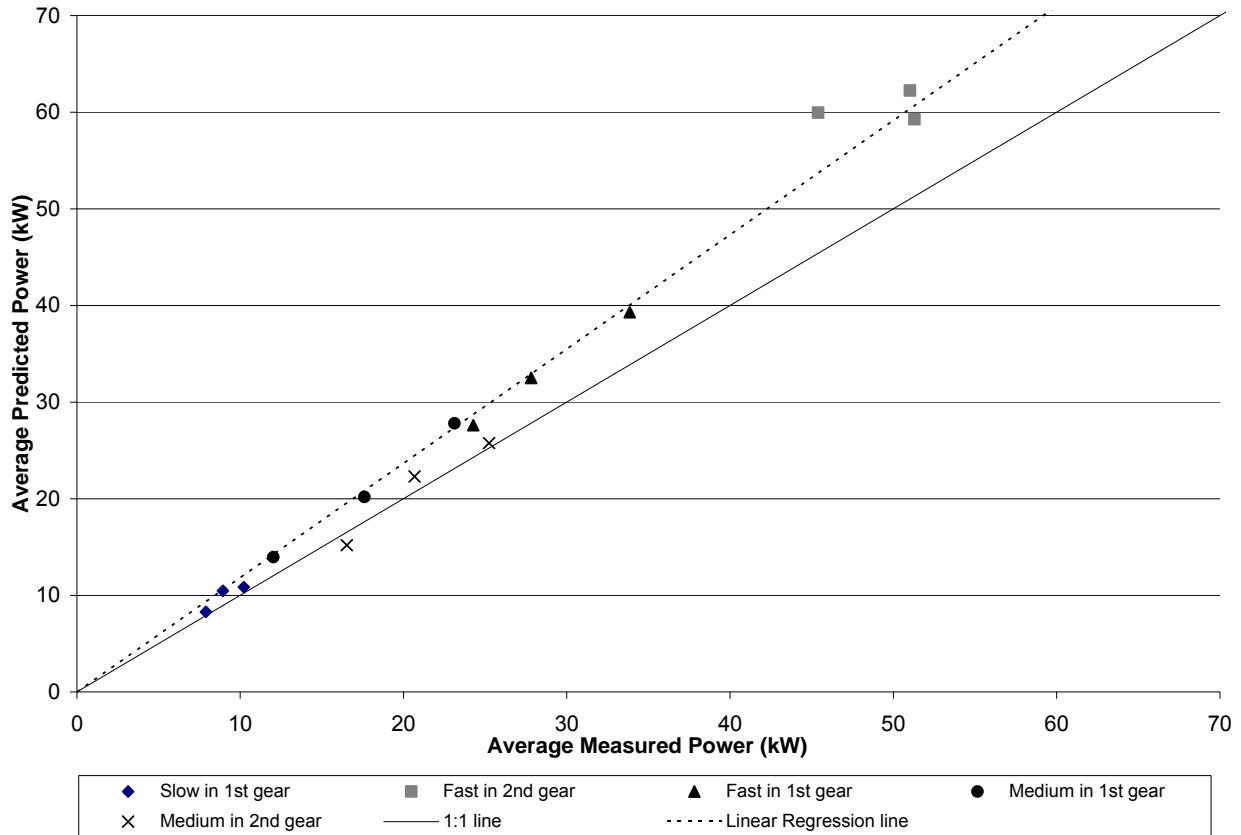
Figure 42: The predicted average mobility power from the Garmin 18 GPS receiver during 15 inertia tests compared to the measured average drivewheel power

The trends of the model using the Garmin 18 GPS receiver data were similar to the trends described for the Trimble 132 receiver. The model continued to slightly overestimate the power requirements of the vehicle during the inertia tests when the Garmin 18 data was used. The variability of the predicted mobility power values decreased slightly when the Garmin 18 GPS receiver data was used because there was less variability associated with the predicted vehicle acceleration values from the Garmin 18 GPS receiver. The decrease in variability may have resulted from the 2 s GPS offset that was used. The decrease in variability of the predicted power values from the Garmin 18 GPS receiver was indicated by the scatter of the discrete data

117

points in Figure 41. The absolute average percent error and CV RMSE also tended to decrease slightly with the Garmin 18 GPS receiver.

The least-squares linear regression lines shown in Figures 40 and 42 for the Trimble 132 and Garmin 18 GPS receivers respectively were developed from the average predicted and measured power values while the intercept of the regression line was set to zero. The coefficient of determination value (R^2) for the least-squares linear regression lines were 0.98 for both GPS receivers. The model tended to overestimate the average power requirement of the test vehicle during the inertia tests, and the slope of the linear regression lines further reinforced this conclusion. The slope of the linear regression lines were 1.27 and 1.18 for the Trimble 132 and Garmin 18 receivers respectively. The linear regression slopes for the Trimble 132 and Garmin 18 receivers indicated that a 27 and 18% respectively reduction in the gamma (γ) values used in Equation (12) from Section 3.6.2 to calculate the inertia component of the model allowed for the model to be calibrated for the test vehicle and the given GPS receiver. Figures 43 and 44 detail a comparison of the average predicted mobility power and drivewheel power values after reducing the gamma values used for the GPS data from Trimble 132 and Garmin 18 receivers by 27 and 18% respectively.
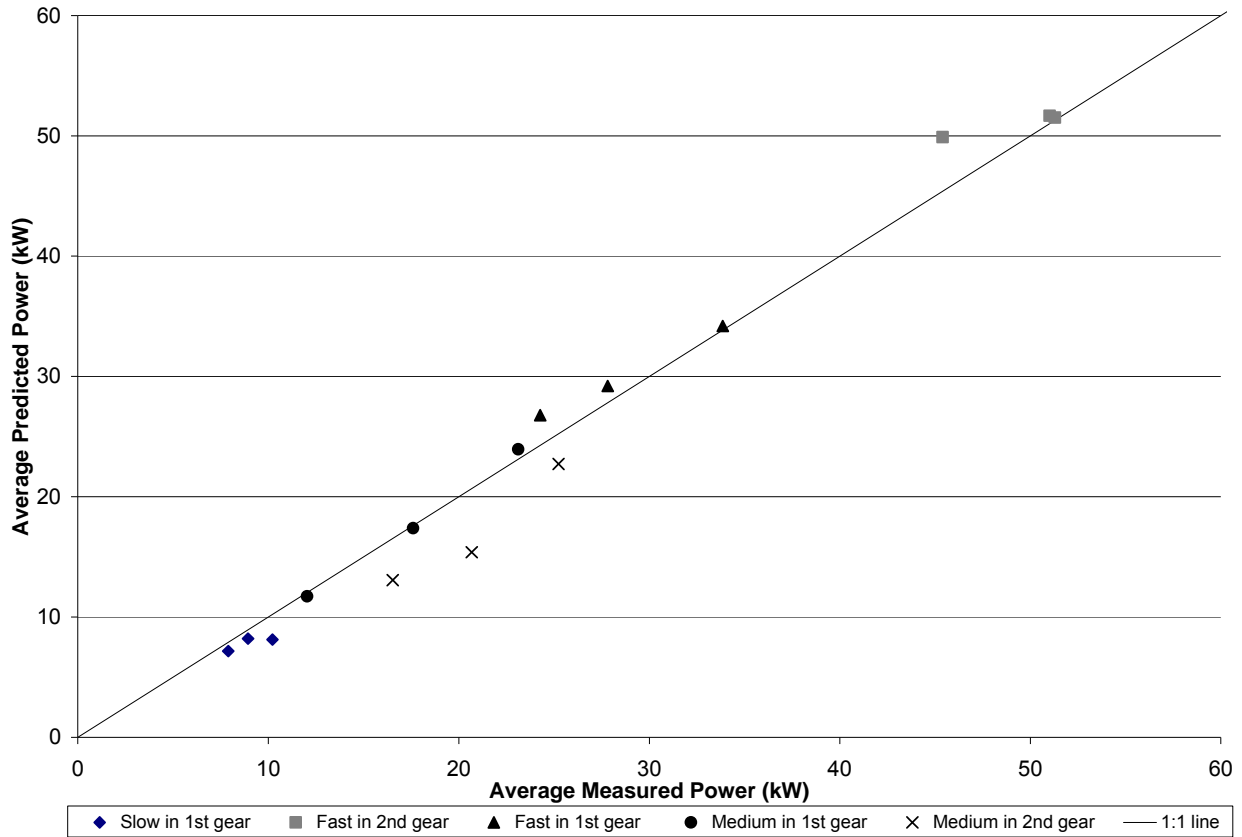
Figure 43: The predicted average mobility power from the Trimble 132 GPS receiver using calibrated drivetrain gamma (γ) values during 15 inertia tests compared to the measured average drivewheel power
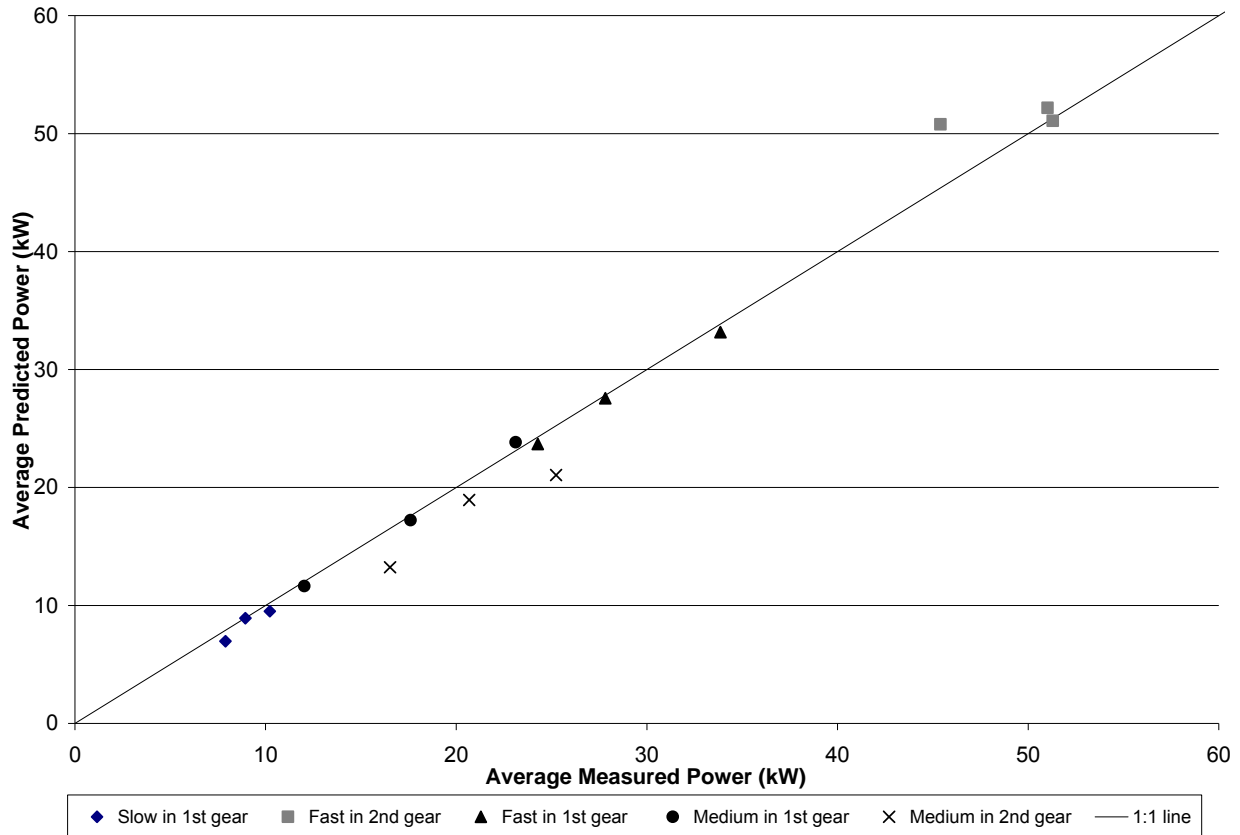
Figure 44: The predicted average mobility power from the Garmin 18 GPS receiver using calibrated drivetrain gamma (γ) values during 15 inertia tests compared to the measured average drivewheel power

Reducing the gamma values used to estimate the inertia component of the model decreased the variability between the average predicted mobility power and the drivewheel power values. The absolute average percent error and RMSE values between the average predicted and measured values were both decreased by 74% for the Trimble 132 GPS receiver. The absolute average percent error and RMSE values between the average predicted and measured values were decreased by 81 and 71% for the Garmin 18 receiver.

The inertia test results indicated that the model had an acceptable amount of variability associated with the estimated discrete mobility power values from both the Trimble 132 and Garmin 18 GPS receiver data collected. The GPS receivers accurately estimated the average acceleration of the vehicle during 15 inertia tests. A high degree of accuracy and a decreased level of variability were achieved by the model when predicting the test vehicle's average power requirement during the inertia tests from the Trimble 132 and Garmin 18 GPS data.

4.4.2 Uncontrolled Test – Simulated Reconnaissance Mission

The uncontrolled test performed attempted to simulate the vehicle movement patterns of U.S. Army vehicles during reconnaissance missions. Approximately 2400 s of test data was collected during the uncontrolled test while engine power was delivered to the drivewheels for only 2100 s of the test. The results are only for the durations when the clutch was fully engaged and transmitting engine power to the drivewheels through the 1st, 2nd, or 3rd gear of the transmission. The statistics from the uncontrolled test are summarized in Table 19 for each gear, and the discrete measured and predicted values are shown in Figure 45 for the Trimble 132 GPS receiver. Figure 8 in Section 4.2.1 illustrates the discrete predicted mobility power values during a portion of uncontrolled test from the Trimble 132 GPS data. A thematic map is given in Figure 46 showing the estimated absolute error between the measured and predicted discrete power values estimated from the Trimble 132 GPS data. The absolute error values were determined by calculating the magnitude of the difference between the discrete predicted and measured values.

Table 19: A summary of the results and statistics from the Trimble 132 GPS data during the uncontrolled tests

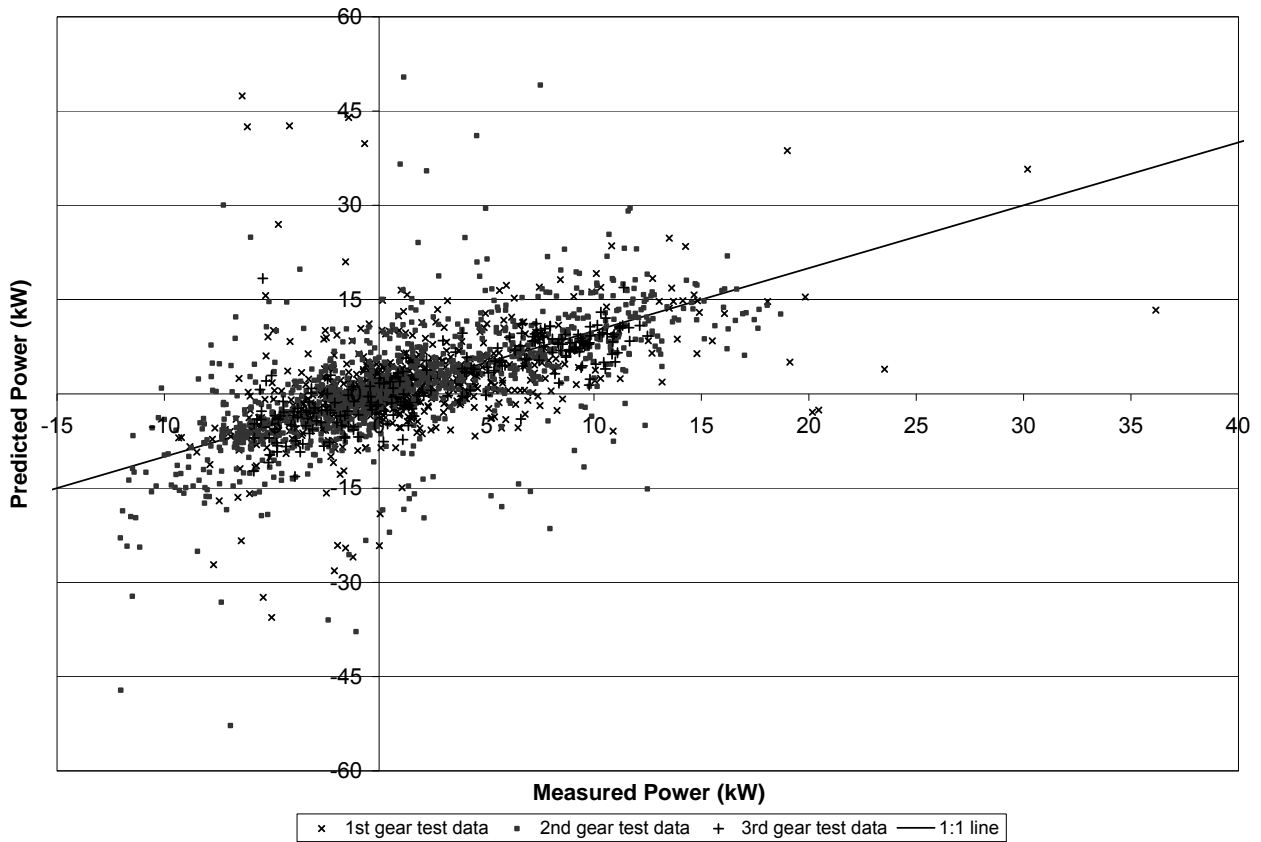| Gear	Duration (s)	Avg. Travel Speed (m/s)	Avg. Absolute Elevation Change (m/s)	Avg. Predicted Positive Power (kW)	Avg. Measured Positive Power (kW)	Measured vs. Predicted Power RMSE (kW)
1	757	3.7	0.17	5.0	3.6	6.86
2	1128	7.8	0.28	7.1	5.9	6.95
3	218	9.4	0.21	6.6	6.7	3.59
	Average:	6.5	0.23	6.3	5.2	6.57

Figure 45: The discrete predicted mobility power values from the Trimble 132 GPS receiver during uncontrolled compared to the measured drivewheel power
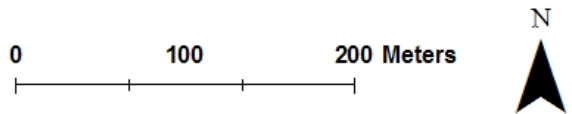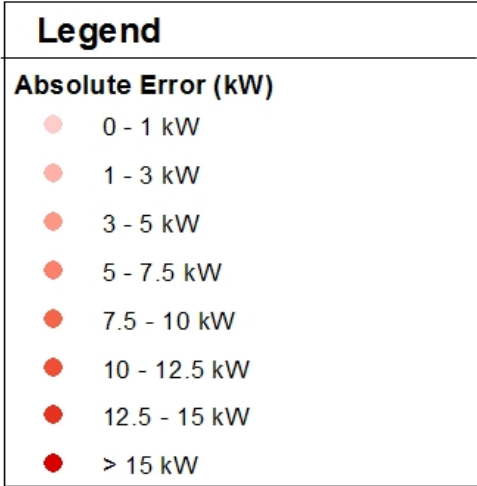
122
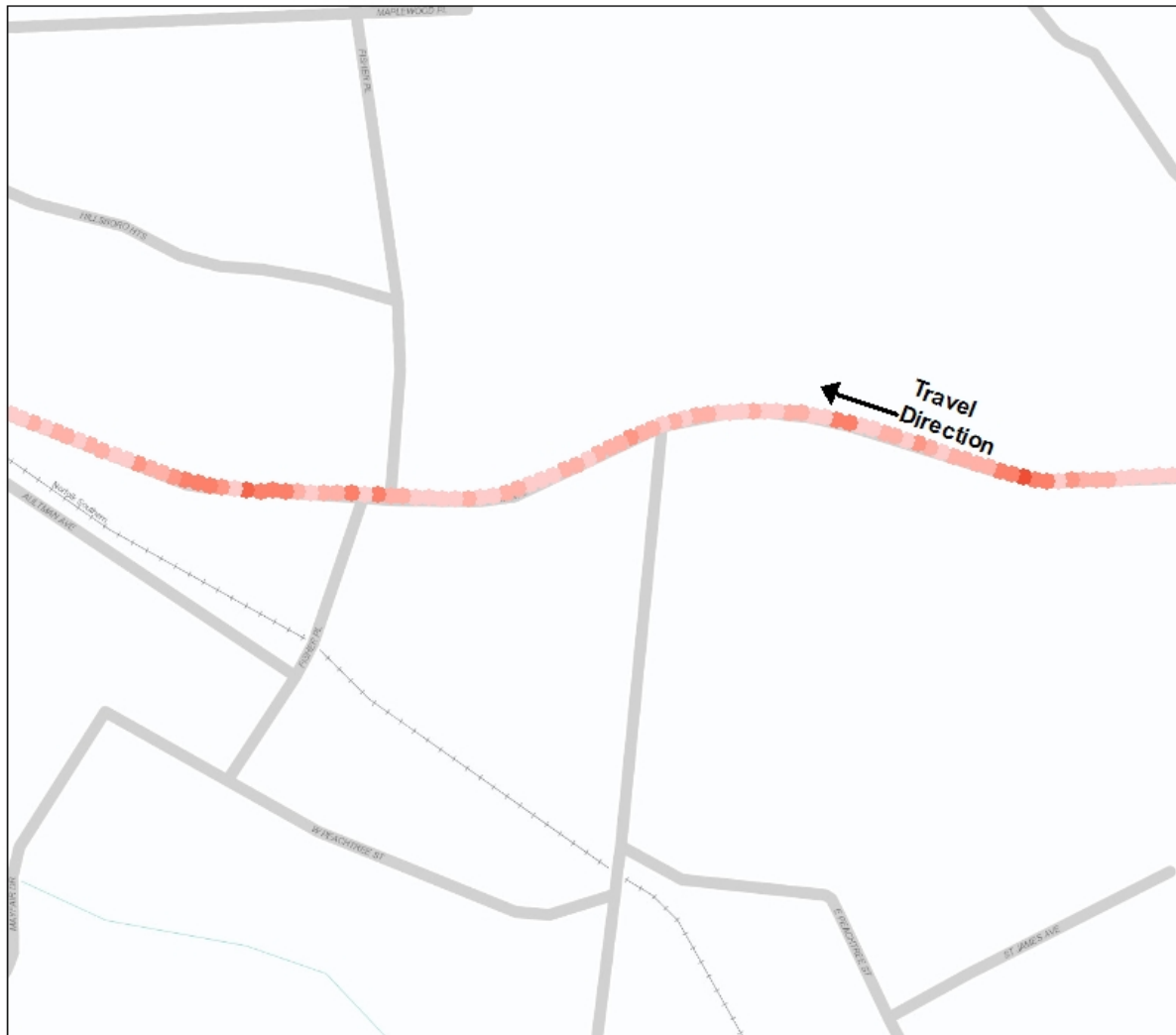
Figure 46: The absolute error of the model's predicted mobility power requirement from the Trimble 132 data compared to the measured drivewheel power during the uncontrolled test

There was a moderate level of variability between the discrete measured and predicted power values. No outliers were identified from the discrete Trimble 132 data in Figure 45. Reasonable estimates of the discrete negative and positive power requirements were predicted from the mobility power model. The majority of the discrete positive and negative power values were less than 25 kW. The average positive predicted and measured power requirements in each gear were between 5.0 – 6.6 kW and 3.6 – 6.7 kW respectively. The absolute average percent error of the positive power requirements during the reconnaissance mission was approximately 20%. The absolute average percent error values were calculated by dividing the magnitude of the difference between the discrete predicted and measured values by the magnitude of the measured value while averaging all of these discrete terms. The model tended to slightly overestimate the power requirement of the test vehicle during the uncontrolled test.

In general, the power requirement was less than 5 kW for the portion of the uncontrolled test represented in Figure 8 from Section 4.2.1. The discrete predicted positive power requirement during the uncontrolled test tended to be less than 17% of the rated engine power. The travel path shown in Figure 8 attempted to simulate a military vehicle while performing a reconnaissance mission. The two on-road looping travel paths represented in Figure 8 were similar to previously observed movement patterns during reconnaissance missions. The on-road loops performed during the uncontrolled test were an attempt to simulate the off-road movement patterns of military vehicles during reconnaissance missions when the military personnel maneuver in new off-road terrain after leaving a main road or trail. In general, the power requirement of the test vehicle during these simulated off-road maneuvers was less than the

124

power requirement while traversing the on-road terrain. The lower mobility power requirements during the simulated off-road movements were due to a reduced travel speed that typically did not exceed 3 m/s. The simulated on-road movement patterns shown in Figure 8 had discrete values that exceeded 20 kW in magnitude which was due to the vehicle's greater travel speed, acceleration, and percent grade traversed during the simulated on-road maneuvers.

The discrete absolute error values in Figure 46 varied substantially, and the spatial location appeared to affect the variation of the predicted mobility power requirement. Approximately 10 – 20 discrete GPS points in a row tended to have similar absolute error values. The similar values were, in general, either greater than 10 kW or less than 3 kW. This implied the accuracy of the model was affected by the GPS signal quality where the signals transmitted from the satellites may have been blocked by the surrounding environment. The travel path resulted in some of the satellites' signals being blocked from tree cover, houses, or other structures in the surrounding environment. After further investigation of the Trimble 132 GPS data, it was confirmed that the signals from certain satellites became blocked during the uncontrolled test. This was indicated by the GPS receiver losing communication with three of the seven satellites when the vehicle was traversing the path represented on the far left side of Figure 46. At this point, the Dilution of Precision (DOP), a measure of the quality of the position of the satellites relative to the receiver's location, increased from approximately 1.2 to 6.3. This information confirmed that the poor GPS signal quality was one source of the increased absolute average error during the uncontrolled test. The GPS quality indicators should be taken into consideration when estimating mobility power from GPS data. The accuracy of the mobility power estimates may increase substantially if the GPS quality is poor.

The correlation coefficient can be used as an indicator of the strength of a linear relationship between two variables. The correlation coefficient was calculated between the Dilution of Precision (DOP) value acquired from the GPS data and the absolute error estimated from the model's predicted discrete mobility power values. This correlation coefficient value provided for an indication of the ability of the GPS data's DOP values to be used to estimate the accuracy of the model. The correlation coefficients for the Garmin 18 and Trimble 132 GPS receivers were -0.04 and 0.38 respectively during the uncontrolled tests. The correlation coefficient for the Garmin 18 receiver indicated that the DOP values from this GPS receiver could not be used as a measure of the accuracy of the model. However, the DOP values from the Trimble 132 receiver allowed for a moderate correlation between the DOP and the absolute error of the model. Thus the Trimble 132 receiver's DOP values can be used as an indicator of the accuracy of the model. The Garmin 18 GPS receiver's DOP values tended to range between 0.9 and 1.4 while the Trimble 132 receiver's DOP values ranged between 0.9 and 9.2. The standard deviations of the DOP values for the Garmin 18 and Trimble 132 receivers were 0.06 and 1.3 respectively. The DOP values from the Garmin 18 receiver remained constant as the model's accuracy decreased while the Trimble 132 receiver's DOP values tended to increase as the variability of the model increased. In general, it is suggested that future applications of this model should be applied to GPS data with good quality and DOP values less than 2.5. The Garmin 18 and Trimble 132 GPS receiver DOP values as a function of time during the uncontrolled test are represented in Figure 47. The absolute error of the predicted discrete mobility power values as DOP varied during the uncontrolled test is represented by Figure 48 and 49 for the Trimble 132 and Garmin 18 GPS receivers respectively.
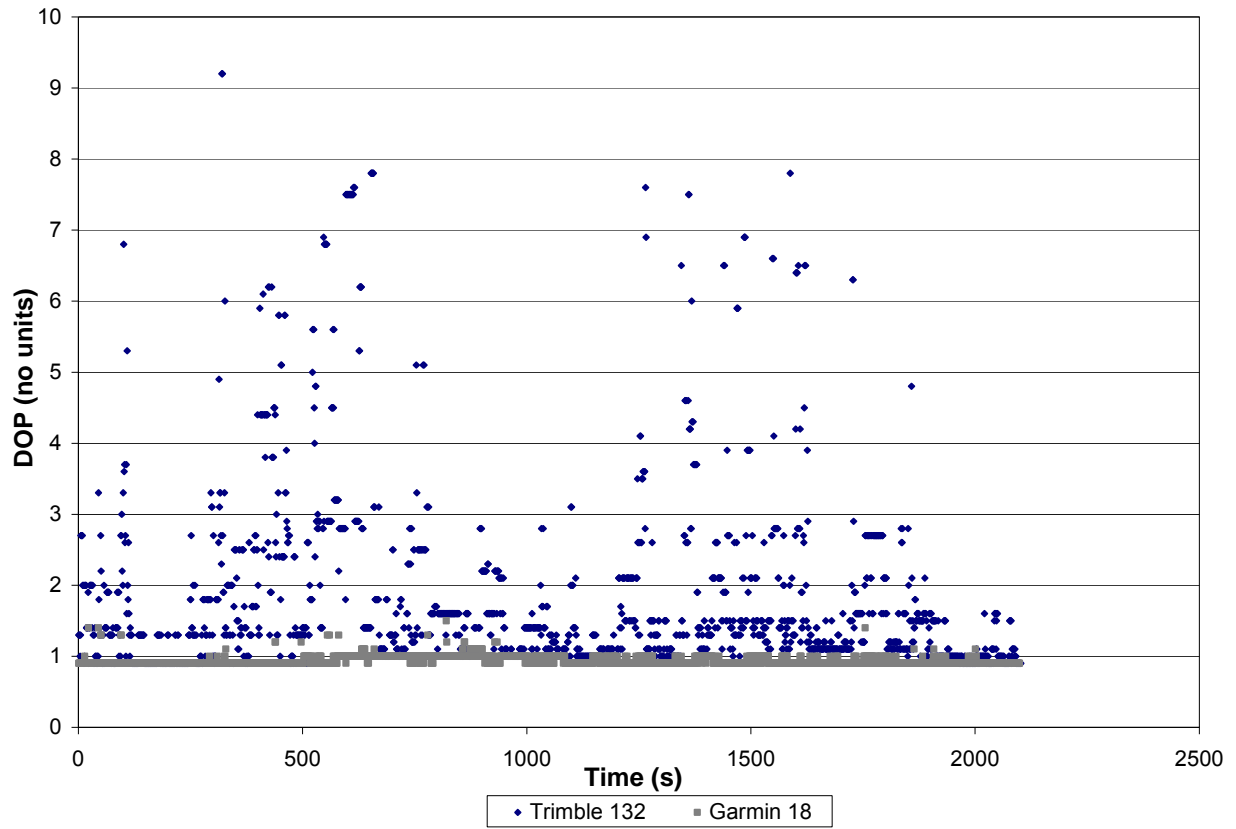
Figure 47: The Dilution of Precision (DOP) from the Trimble 132 and Garmin 18 GPS receivers during the uncontrolled test
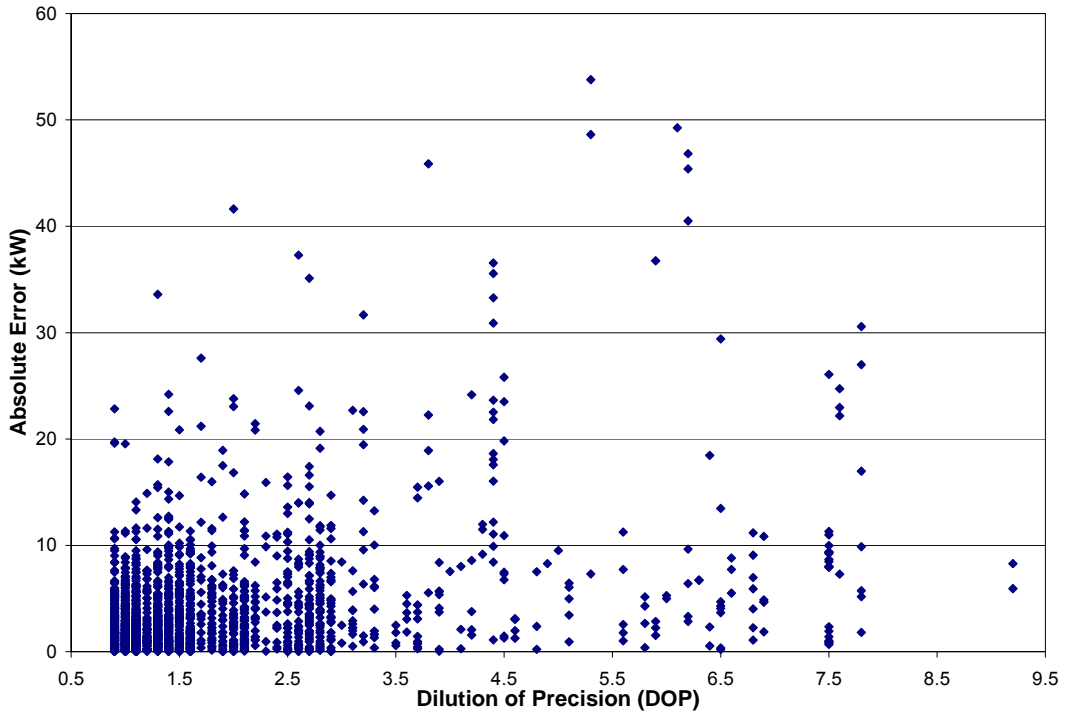
Figure 48: The predicted mobility power absolute error as a function of the Trimble 132 GPS receiver's Dilution of Precision (DOP) values
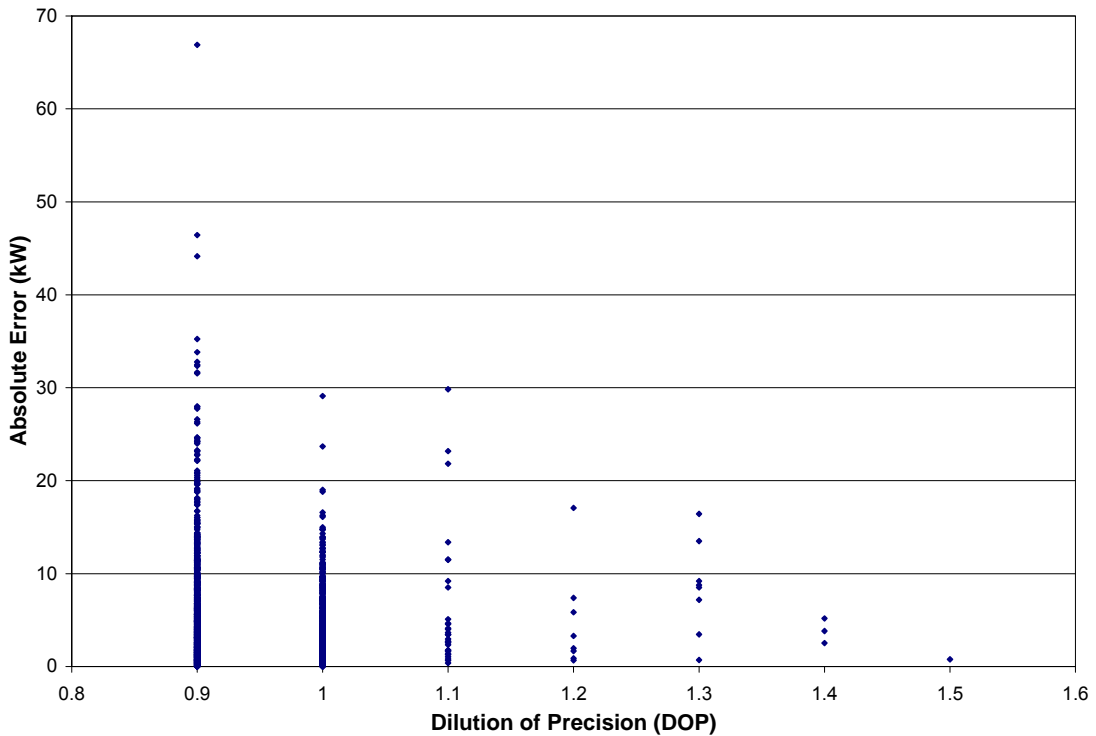
Figure 49: The predicted mobility power absolute error as a function of the Garmin 18 GPS receiver's Dilution of Precision (DOP) values

The model's greater accuracy in 3rd gear may be due to the accuracy associated with the measured power value. The measured power value was determined from the logged engine speed and torque values found in certain CAN signals. The accuracy of the estimated torque value may have been dependent on the load of the engine which was why the accuracy of measured power value may have varied depending on the gear and subsequent load on the engine. The greater variability about the origin represented in Figure 45 may be attributed to the inaccuracy of the engine torque measurement when the engine was under minimal load.

It was critical to characterize the model's ability to accurately estimate the mission-specific power duty cycle values for a given vehicle. Reasonable predictions of the power duty cycle values from the GPS-based model would indicate the approach can be used by on-road and off-road vehicle design engineer's to estimate power requirements. The measured and predicted power duty cycle values for each duty cycle range during the uncontrolled test are given in Figure 50 for the Trimble 132 GPS receiver.
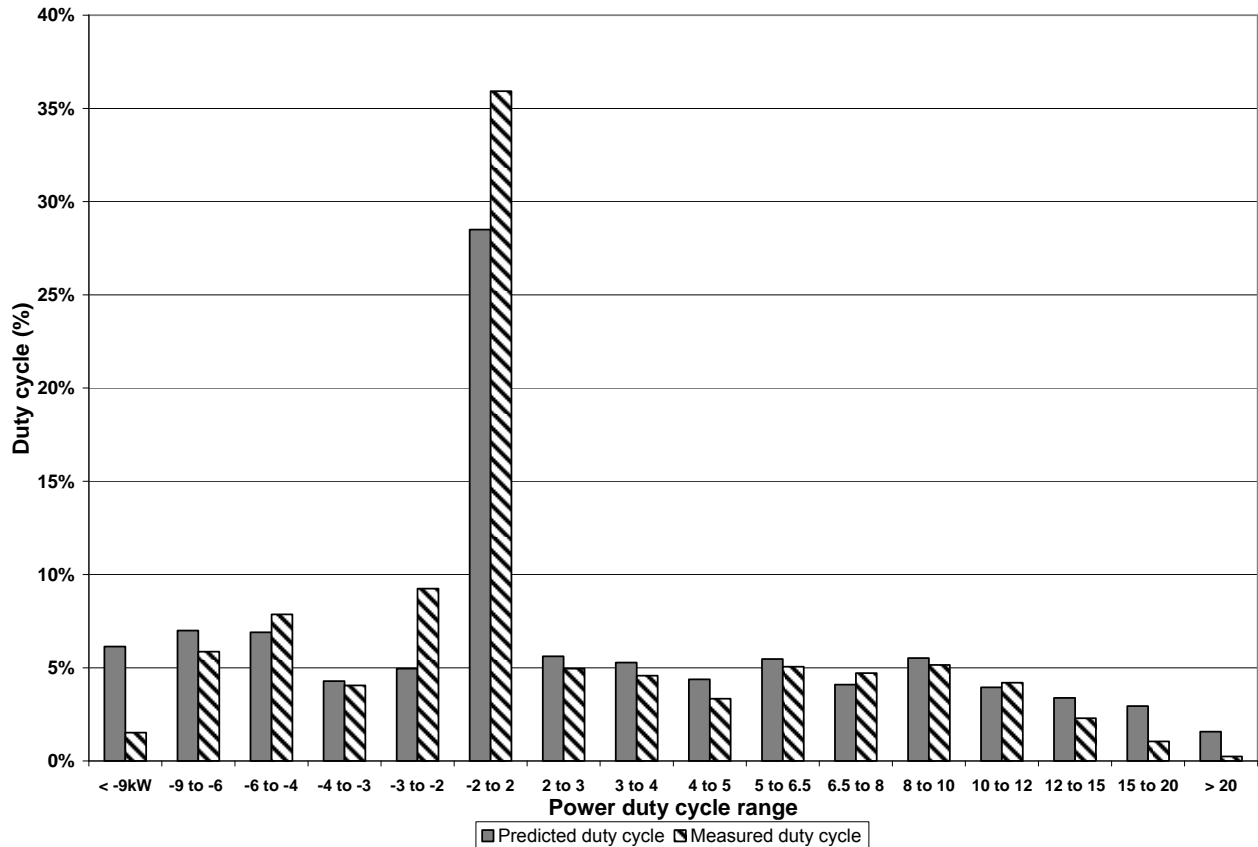
Figure 50: The predicted power duty cycle values from the Trimble 132 receiver compared to the measured duty cycle values

There was a reasonable level of agreement between the measured and predicted duty cycle values during the uncontrolled test. The variability of the predicted mobility power duty cycle values was minimized when estimating the seven duty cycle ranges that were between 2 and 12 kW. The absolute average percent error for the duty cycles between 2 and 12 kW was approximately 14%. This indicated that the model was able to estimate the positive power duty cycles that were less than 12 kW with a small amount of variability during the uncontrolled test. The model tended to over predict the values of the duty cycles greater than 12 kW and less than -9 kW. The absolute average percent error increased to approximately 560% for the largest positive power duty cycle, greater than 20 kW. The absolute average error of the negative power

130

duty cycle ranges tended to increase as the duty cycle range increased in magnitude. The predicted -2 to 2 kW duty cycle value was significantly different than the measured -2 to 2 kW duty cycle. This indicated that the model had less accuracy in predicting the less than 2 kW in magnitude, positive and negative, power requirements during the uncontrolled test.

The predicted average positive power requirement from each component of the model during the uncontrolled test was calculated to characterize the fraction of the total positive power requirement that was due to each resistive force. This information allows for the change in the motion resistance, grade, inertia, and aerodynamic drag power components due to the mission and terrain-type to be characterized. However, only the maximum 20% of the discrete positive predicted mobility power values were used in the analysis because the maximum power requirement in the given operating conditions is of principle interest when determining the appropriate size of a vehicle's power source. The inertia and grade components of the model were averaged over only the positive values of each component where the negative and zero component values were not used to estimate the average positive power requirement. For this reason, the sum of the values for all of the components do not sum to the total mobility power requirement. Figure 51 summarizes the average positive power requirement for total mobility power and each component of the model along with one standard deviation bars for the maximum 20% of the discrete positive mobility power values.
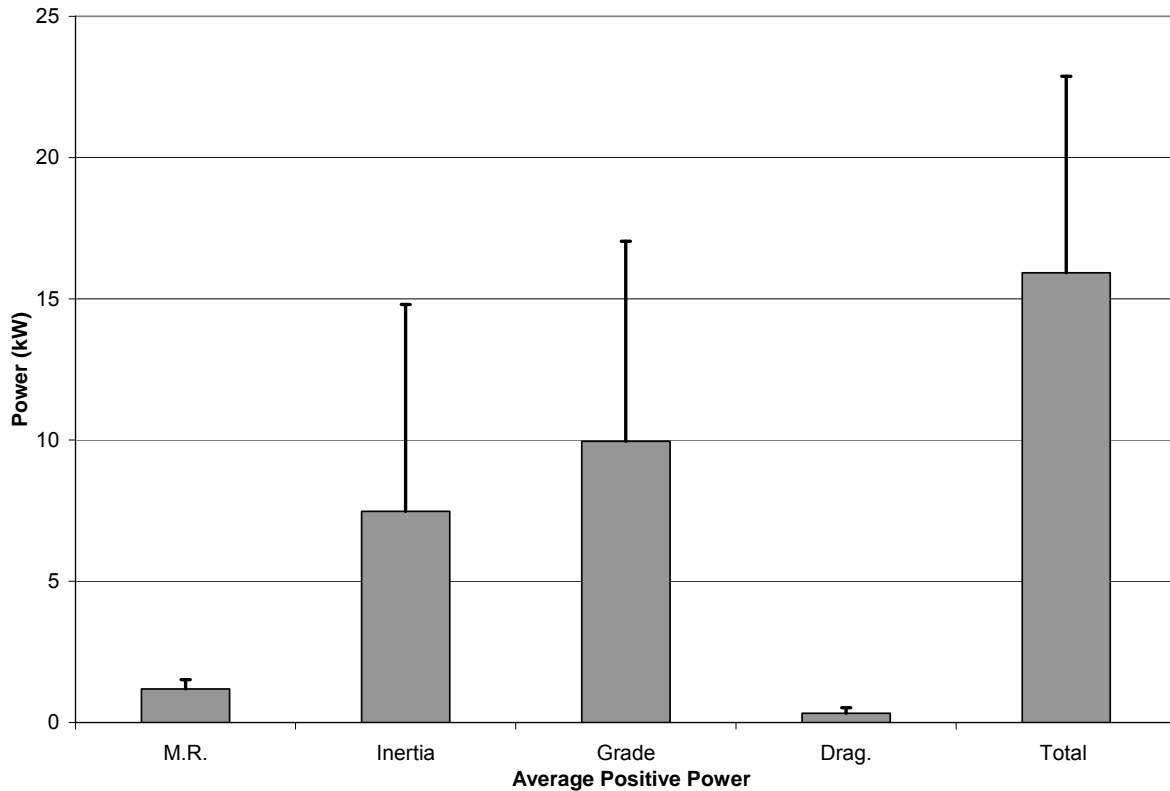
Figure 51 : The predicted peak 20% average positive power requirement of the components of the model and the total average positive power with one standard deviation the bars from the Trimble 132 GPS receiver during the uncontrolled test

The average positive power requirement for the vehicle during the uncontrolled test was approximately 15.9 kW from the Trimble 132 receiver's. The grade component of the model resulted in the greatest average positive power requirement from any component because the average positive grade during the uncontrolled test was 3.5%. The inertia component had the second greatest average positive power requirement with a value of 7.5 kW, followed by the motion resistance and aerodynamic drag components. The standard deviation of the inertia component was the greatest of any component with a value of 7.3 kW. This was due to the test vehicle's 0.37 m/s^2 average positive acceleration, estimated from the discrete GPS data. The variation in the vehicle travel speed was partially due to the 3.5% average grade traversed by the

132

test vehicle. The mobility power model was applied to the Garmin 18 GPS receiver data

collected during the uncontrolled test. Table 20 and Figure 52 detail the results from the Garmin

18 GPS receiver during the uncontrolled test.

Table 20: A summary of the results and statistics from the Garmin 18 GPS data during the uncontrolled tests

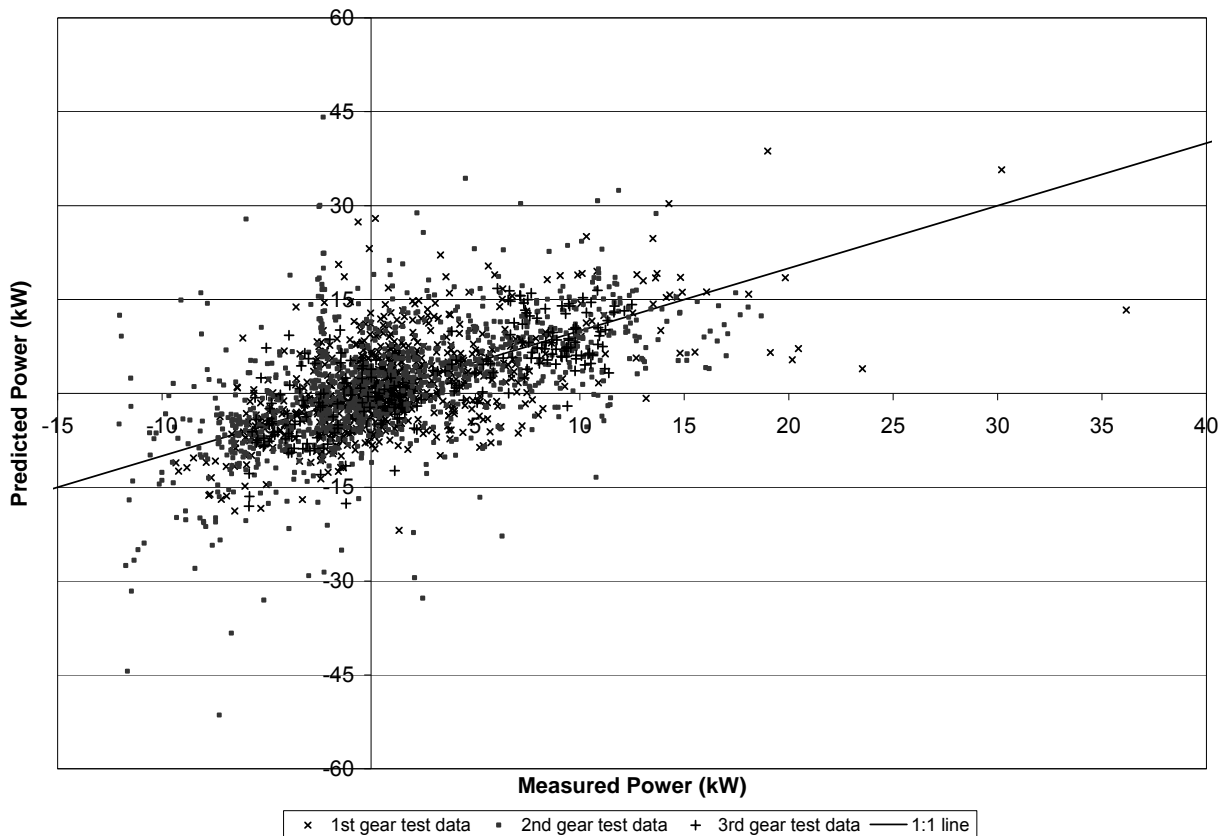| Gear	Duration (s)	Avg. Travel Speed (m/s)	Avg. Absolute Elevation Change (m/s)	Avg. Predicted Positive Power (kW)	Avg. Measured Positive Power (kW)	Measured vs. Predicted Power RMSE (kW)
1	757	3.6	0.22	6.6	3.7	6.24
2	1125	7.8	0.30	7.8	5.8	8.12
3	218	9.4	0.27	7.3	6.7	4.80
	Average:	6.5	0.26	7.3	5.1	7.10

Figure 52: The discrete predicted mobility power values from the Garmin 18 GPS receiver during uncontrolled compared to the measured drivewheel power

Of the 2100 total discrete data points, three data points are not shown in Figure 52 because they exceeded 75 kW in magnitude and were identified as outliers. Subsequently, they were removed from the statistical analysis summarized in Table 20. The difference between the measured and predicted power values for these three discrete values substantially exceeded the calculated RMSE value multiplied by two. The three discrete data points were removed for this reason. The justification for removing these outliers is analogous to the Chauvenet's criterion for removing outliers from normally distributed data based on the mean and standard deviation of a dataset. Chauvenet's criterion states that if the difference between a discrete value and the mean of a normally distributed data set exceeds the standard deviation multiplied by two then the discrete value can be considered an outlier (Ross, 2003). The outliers were the result of poor estimates of vehicle acceleration from the GPS speed data. The predicted vehicle acceleration values during a 3 s span were 7 and -8 m/s^2 which exceeded the levels of vehicle acceleration that occurred during the uncontrolled test.

The Garmin 18 data slightly decreased the accuracy of the predicted discrete and average power requirements during the uncontrolled test. The absolute percent error of the average positive power requirement during the uncontrolled test increased to 41% for the Garmin 18 receiver compared to 20% for the Trimble 132 receiver. The model's Root Mean Square Error (RMSE) value from the Garmin 18 data during the entire uncontrolled test was increased by approximately 8% compared to the Trimble 132 data. The greater accuracy of the Trimble 132 receivers' elevation estimates (height above ellipsoid) was identified as a possible reason for the increased variability from the Garmin 18 receiver. The predicted mobility power duty cycle values from the Garmin 18 receiver are compared to the measured duty cycles in Figure 53, and

134

the average maximum 20% positive power values and one standard deviation bars are

represented in Figure 54.
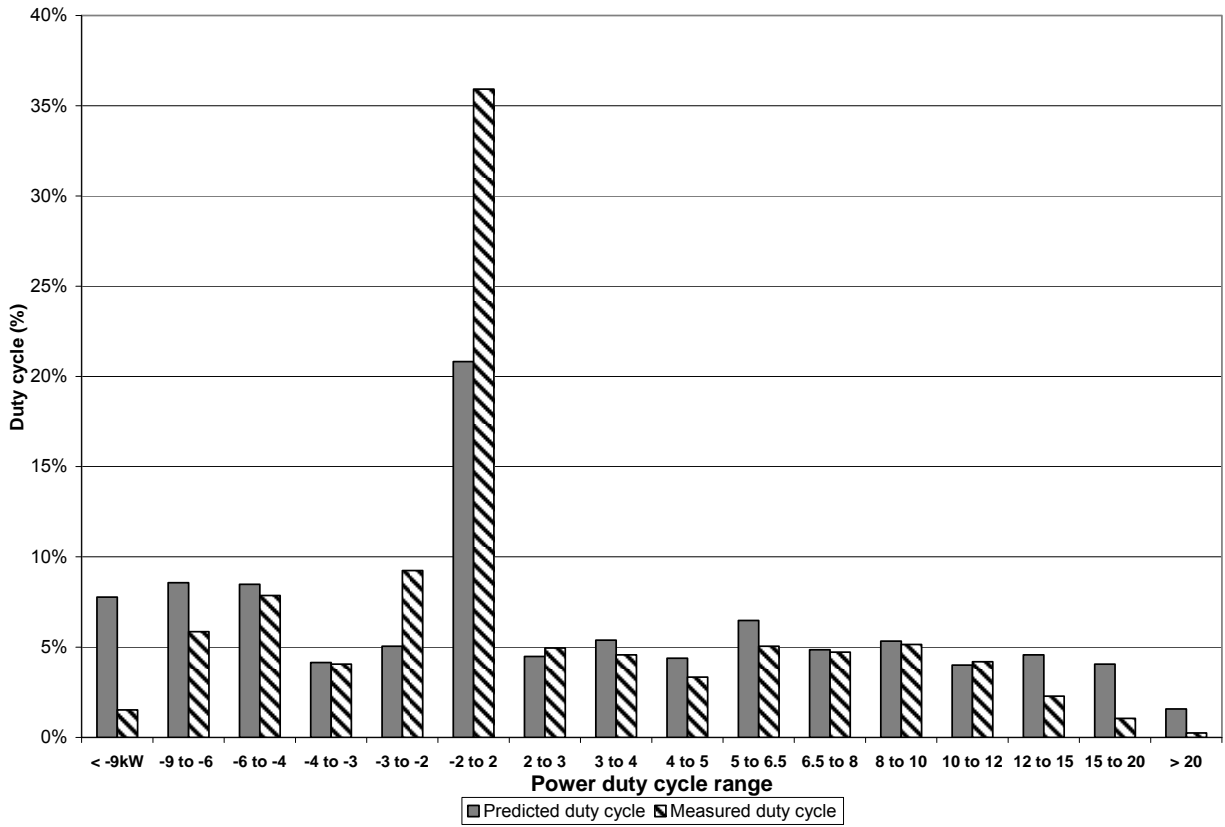
Figure 53: The predicted power duty cycle values from the Garmin 18 receiver compared to the measured duty cycle values
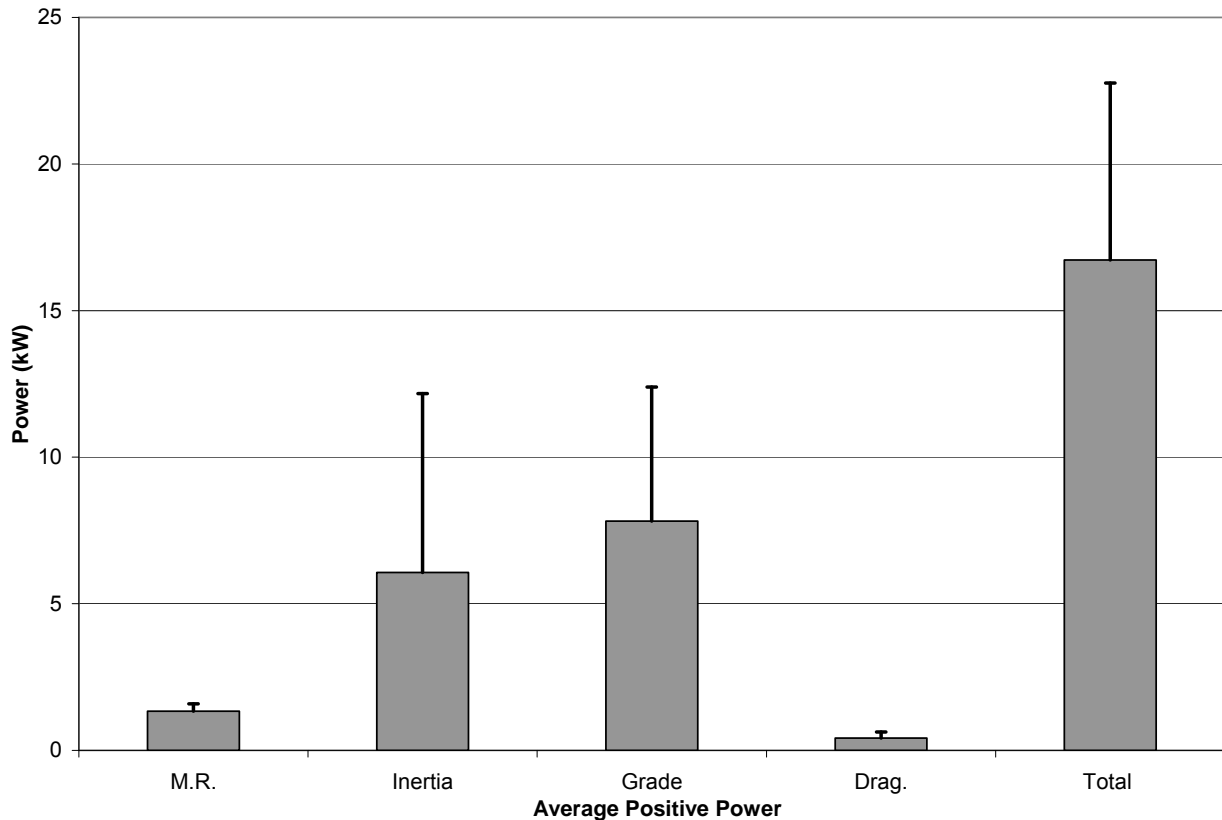
Figure 54: The predicted peak 20% average positive power requirement of the components of the model and the total average positive power with one standard deviation the bars from the Garmin 18 GPS receiver during the uncontrolled test

The predicted power duty cycle values from the Garmin 18 receiver were similar to the duty cycles estimated from the Trimble 132 data. The absolute average percent error for the duty cycles between 2 and 12 kW was 14%, approximately equal to the value calculated for the Trimble 132 results. The absolute average errors of the predicted negative ($< -2kW$) and positive ($> 2kW$) duty cycle values increased by approximately 32 and 18% respectively. The predicted -2 to 2 kW mobility power range had a 21% increase in the absolute percent error.

The test vehicle's average positive power requirement during the uncontrolled test was estimated to be approximately 16.7 kW from the Garmin 18 data. The percent error of the predicted average positive mobility power value was approximately 43% from the Garmin 18 receiver data compared to 37% for the Trimble 132 receiver. The estimate of the average positive grade and inertia power requirements during the uncontrolled test were 22 and 18% less in magnitude respectively from the Garmin 18 data. The standard deviation values of the total and component positive power values were similar for both GPS receivers.

Figure 55 represents another way of comparing the duty cycle trends estimated from the Trimble 132 and Garmin 18 GPS data to the measured power duty cycle. The "percent power greater than" value for a given power value represents the fraction of the total discrete data points that are greater than the given discrete point. This allowed for the measured duty cycle curve to be compared to the predicted duty cycle curves from the Trimble 132 and Garmin 18 GPS data.
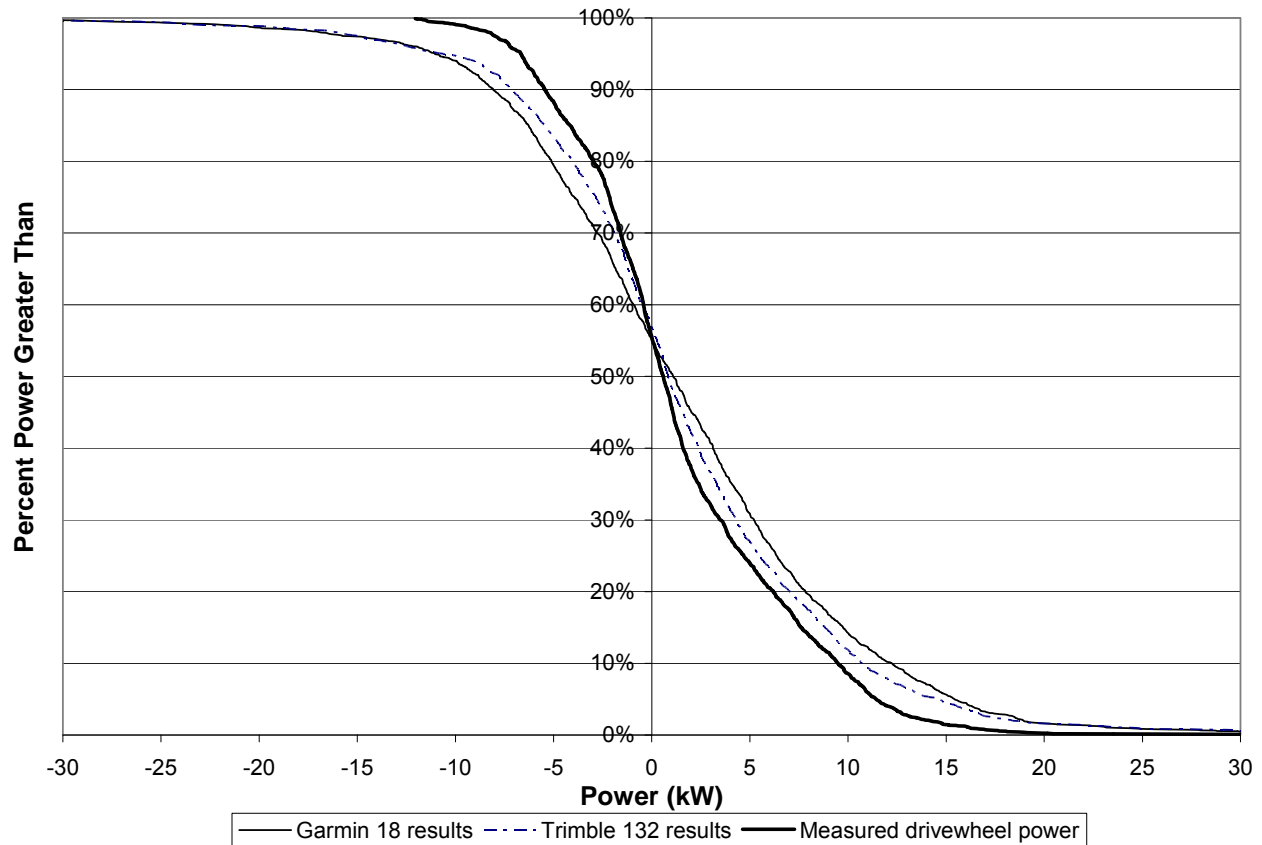
Figure 55: The predicted mobility power duty cycle curves from the Trimble 132 and Garmin 18 GPS data compared to the measured drivewheel power duty cycle during the uncontrolled test

Approximately 55% of the measured power requirement during the uncontrolled test was greater than 0 kW. The model was able to predict that approximately 56% of the power requirement during the test was greater than 0 kW from both GPS receivers. The deviation between the measured and predicted curves tended to increase as the magnitude of the power value increased. The curve generated from the Trimble 132 data was more similar to the measured duty cycle curve in Figure 55, compared to the Garmin 18 duty cycle curve. The Trimble 132 data was more accurate at estimating the characteristics of the duty cycle curve in the positive power region in comparison to estimating the curve's trends in the negative power region. The duty

cycle curve estimated from the Garmin 18 GPS data had similar trends for both the positive and negative power regions of the curve. Figure 55 indicated that the Trimble 132 and Garmin 18 GPS receivers estimated the characteristics of the duty cycle curve during the uncontrolled test with an acceptable level of accuracy. In the future, the predicted duty cycle curves may continue to approach the measured duty cycle curves as the accuracy of GPS data improves while providing improved estimates of the dynamic vehicle parameters necessary for application of the mobility power model.

The results from the Trimble 132 and Garmin 18 GPS receiver data collected during the uncontrolled test were a validation of the entire model in a scenario that simulated a U.S. Army reconnaissance mission. A moderate level of accuracy was achieved from the model using Trimble 132 and Garmin 18 GPS data. Reasonable estimates of the test vehicle's average power were attained with the Garmin 18 receiver. The average positive power requirement estimated from the Trimble 132 data had a high level accuracy when compared to the measured average drivewheel power.

Chapter 5: Applications

The controlled and uncontrolled tests that were performed validated the mobility power model, and the results indicated that a Vehicle Tracking System (VTS) equipped with a Garmin 18 GPS receiver can be used to provide reasonable estimates of a vehicle's power duty cycle characteristics. Quantifying the mobility power duty cycles of military vehicles from historical GPS tracking data may provide design engineers with a useful approach for characterizing the actual, in-field power duty cycles of military vehicles. Quantifying the in-field power duty cycles may represent a potentially useful tool for hybrid military vehicle design. The U.S. Army's Stryker vehicles were tracked with VTS units while conducting training missions at the Fort Lewis and Pohakuloa Training Area (PTA) military installations in 2005 and 2009 respectively. The mobility power duty cycles' of three Stryker vehicles were estimated from GPS tracking data for the missions conducted at each installation.

5.1 Materials

The VTS system described in Section 4.2.2 was used to track the Stryker vehicles operating at the two U.S. military installations. The mobility power model was used to predict the power duty cycles from historical GPS data. A cone penetrometer was used to measure the soil's Cone Index value (*CI)* during off-road maneuvers at PTA (Howard, 2011).

5.1.1 Stryker Vehicle Specifications

The GPS data from the U.S. military's Stryker Infantry Carrier Vehicle (ICV) was used to characterize the power duty cycles at the two military installations. The Stryker is an 8-wheeled,

17,237 kg vehicle that is powered by a 261 kW V-8 diesel engine. General dimensions of the

vehicle are shown in Figure 56. The maximum travel speed of the vehicle is 27 m/s. The

vehicle is either 4 or 8-wheel drive; during maneuvers, the vehicle was operated in as a 4-wheel

drive vehicle. The vehicle is equipped with a Central Tire Inflation System (CTIS) that allows

the operator to vary the inflation pressure of all tires simultaneously according to the terrain

conditions (Ayers et al., 2009; Potteti, 2009). All wheels were equipped with Michelin X tires.

The inflation pressure of the tires remained a constant 483 kPa during the 2005 and 2009 Stryker

maneuvers. The tire parameters necessary for applying Equation (2) are given in Figure 57 while

the tire deflection represented in Figure 57 was at a 483 kPa inflation pressure. Wong (2010)

indicated that large military vehicles typically have a drag coefficient value (C_D) of

approximately 1.0, and this value was assumed to be the approximate drag coefficient of the
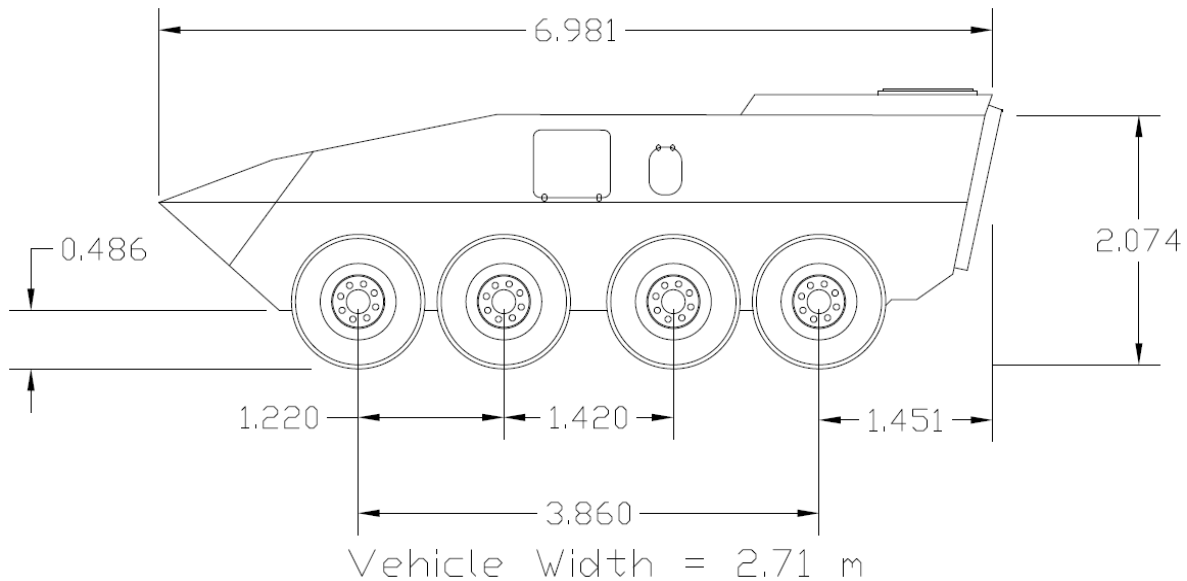
Stryker vehicle (Wong, 2010).

Figure 56: Stryker vehicle geometry (units: meters)
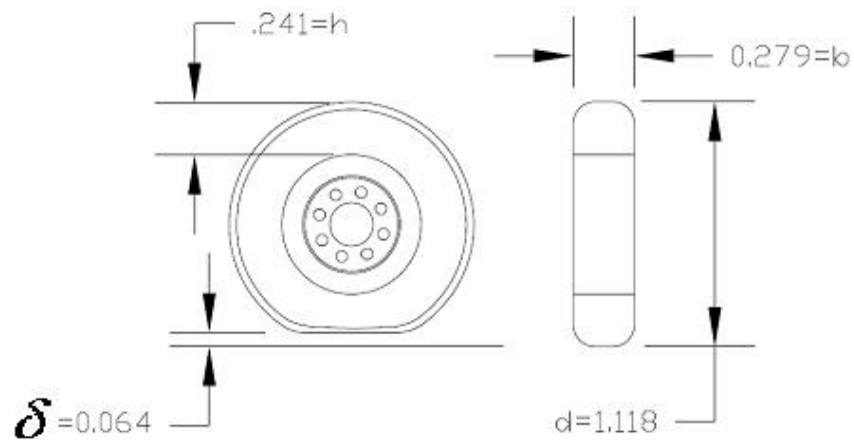
Figure 57: The geometry of the Michelin X tire on the Stryker vehicle (units: meters)

5.1.2 2002 U.S. Army Mission and Installation

Ayers et al (2005) detailed the maneuvers performed by Strykers from the U.S. Army's 3rd Infantry Regiment, 2nd Battalion, 3rd Brigade, 2nd Infantry Division. The Stryker vehicles conducted maneuvers at the Fort Lewis, Washington installation during a training mission that was performed 17 October 2005 through 25 October 2005. Live-fire, urban operations, and security training missions were performed by U.S. military personnel. A total of 19 Stryker vehicles were tracked with the VTS units. The mobility power duty cycle characteristics for three Stryker vehicles from "Charlie" company were estimated from the GPS tracking data. A map of the maneuvers performed by the three Stryker vehicles that were analyzed is given in Figure 58. The vehicle maneuvered primarily on-road while some off-road movements were performed. Approximately 97% of the Stryker maneuvers analyzed were on-road maneuvers (Ayers et al., 2005). Previous research by Richmond (2007) suggested that a *CI* value of 4137 kPa should be used for on-road terrains when using the Vehicle Terrain Interaction (VTI) model. The terrain where the vehicle maneuvered was assumed to have this *CI* value because nearly all of the maneuvers were conducted on-road. The *CI* of the terrain was assigned this value for the

same reasoning described in Section 4.3.7.1 (Richmond, 2006). The *CI* value was a necessary

input to Equation (2) described in Section 3.4.1.
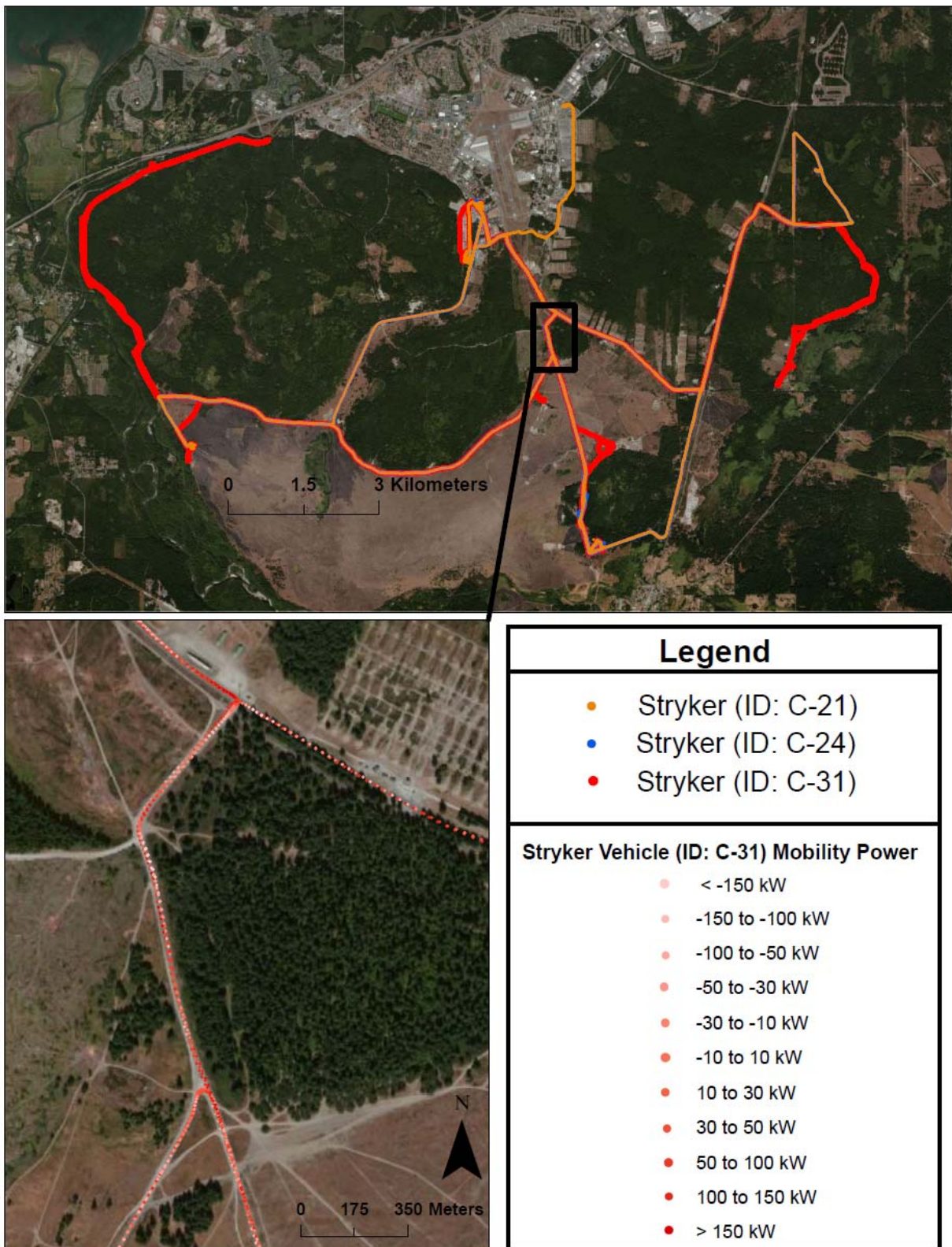
Figure 58: The maneuvers of the three Stryker vehicles at Fort Lewis, Washington along with a single vehicle's mobility power requirements

144

5.1.3 2009 U.S. Army Mission and Installation

According to Howard et al (2011), three Stryker vehicles from a reconnaissance platoon from the 2nd Brigade of the 25th Infantry Division conducted a single day proofing mission on 9 November 2009 at the U.S. Army's Pohakuloa Training Area (PTA) in Hawaii. Figure 59 details the maneuvers performed by the three Stryker vehicles analyzed. The objective of the proofing mission was to assess the trafficability of the region while identifying optimum access points and hazardous areas of the terrain. During the proofing mission, on-road and off-road maneuvers were performed. The off-road maneuvers were conducted at the Keamuku parcel of PTA. The soil type at the Keamuku parcel is classified as a coarse-grained Kilohana loamy fine sand. Off-road maneuvers were conducted in two areas of the Keamuku parcel, and the average measured *CI* was 1536 and 1970 kPa at each location respectively (Howard et al., 2011). The Vehicle Terrain Interaction (VTI) model's fine-grained equations were used even though the off-road maneuvers were conducted in a coarse-grained equation. The fine-grained equations were utilized because it was thought that they provide a better representation of the interaction between the tractive elements and the terrain compared to the coarse-grained equations. The on-road maneuvers were assigned to have a *CI* of 4137 kPa.
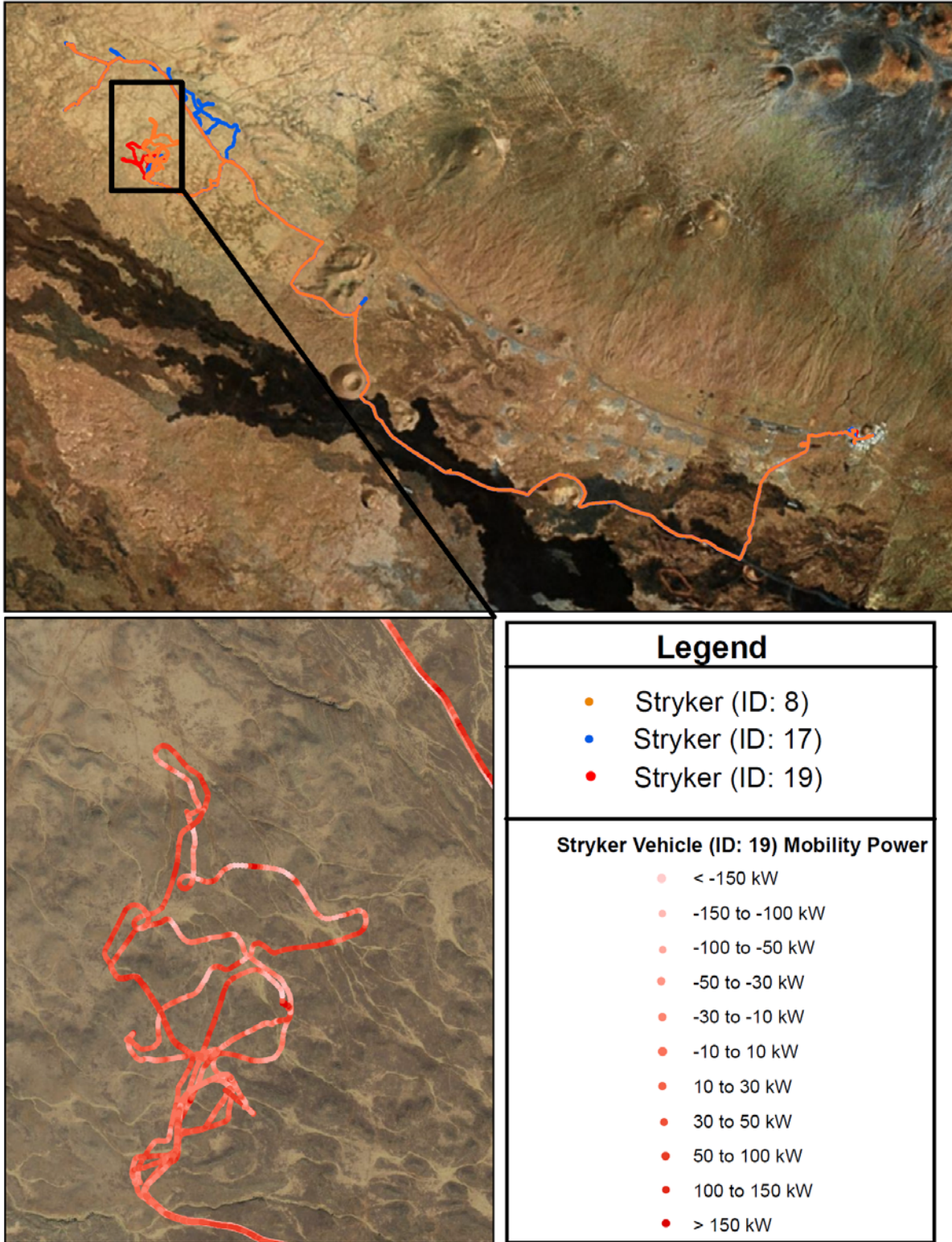
Figure 59: The maneuvers of the three Stryker vehicle at the Pohakuloa Training Area (PTA), Hawaii along with a single vehicle's mobility power requirements during off-road maneuvers at the Keamuku parcel

5.2 Methods

The controlled and uncontrolled tests performed validated the mobility power model's governing equation represented in Section 4.1. Equations (2 – 5) and (9 – 11), and (14 – 18) from Chapter 3 were used to estimate the motion resistance, grade, inertia, and aerodynamic forces of the Stryker vehicle and the subsequent power requirement. The Vehicle Terrain Interaction (VTI) model equations for estimating motion resistance of a wheeled vehicle operating in a fine-grained soil (Equations (2 – 5)) were used to quantify the motion resistance force of the wheels, as these equations were determined to be the best available. The mobility power estimates for the Stryker vehicle only include the linear inertia of the vehicle while the rotational inertia of the vehicle was not estimated. This mobility power estimate differs slightly compared to the mobility power estimate used in Chapter 4 for the validation test data. However, the predicted values for the Stryker are independent of vehicle drivetrain which is advantageous if a different drivetrain design is being considered for the vehicle.

The conclusions drawn in Section 4.3.9 indicated that a 2 s speed and acceleration GPS offset was necessary for the Garmin 18 GPS receiver. This 2 s speed and acceleration offset was used in the mobility power analysis of the Stryker maneuvers. Equation (11) from Section 3.6.1 was used to estimate the vehicle's acceleration from the discrete GPS speed data. The tests performed and summarized in Section 4.3.10 indicated the Garmin 18 GPS receiver's optimum elevation offset is 0 s. This 0 s elevation offset was used when applying the mobility power model to the Stryker maneuvers. A simple 5 s average was used to estimate the vehicle's rate of elevation change from the GPS elevation data (height above ellipsoid data). The proper offsets

147

allowed each discrete GPS point or spatial location where the vehicle maneuvered to have the correct discrete vehicle speed, acceleration, and elevation values.

5.3 Results

The power duty cycle characteristics for three Stryker vehicles operating at the Fort Lewis and the Pohakuloa Training Area (PTA) military installations were predicted by applying the mobility power model to the GPS tracking data. The mobility power duty cycle estimates are for the durations where a non-zero vehicle speed was estimated from the GPS tracking data. The GPS data and estimated average positive power requirements for the three Stryker vehicles operating at Fort Lewis are shown in Table 21. Figure 60 represents the mobility power duty cycle curves for the Stryker vehicles at Fort Lewis. Figure 58 details the estimated mobility power values for a portion of a Stryker vehicle's on-road maneuvers at Fort Lewis.

Table 21: A summary of the Garmin 18 GPS data and mobility power results for the three Stryker vehicles operating at Fort Lewis, Washington

Stryker ID:	Maneuver Time (hr)	Percent Moving	Avg. Daily Travel (km/day)	Avg. Travel Speed (m/s)	Avg. Absolute Acceleration (m/s^2)	Avg. Absolute Elevation Change (m/s)	Avg. Predicted Positive Power (kW)
C-21	2.50	3.5%	31.8	10.6	0.29	0.13	68.2
C-24	2.06	2.7%	26.9	10.9	0.27	0.15	71.2
C-31	4.01	5.4%	49.1	10.2	0.24	0.14	60.7
Average:	3.10	4.2%	38.7	10.5	0.26	0.14	65.4
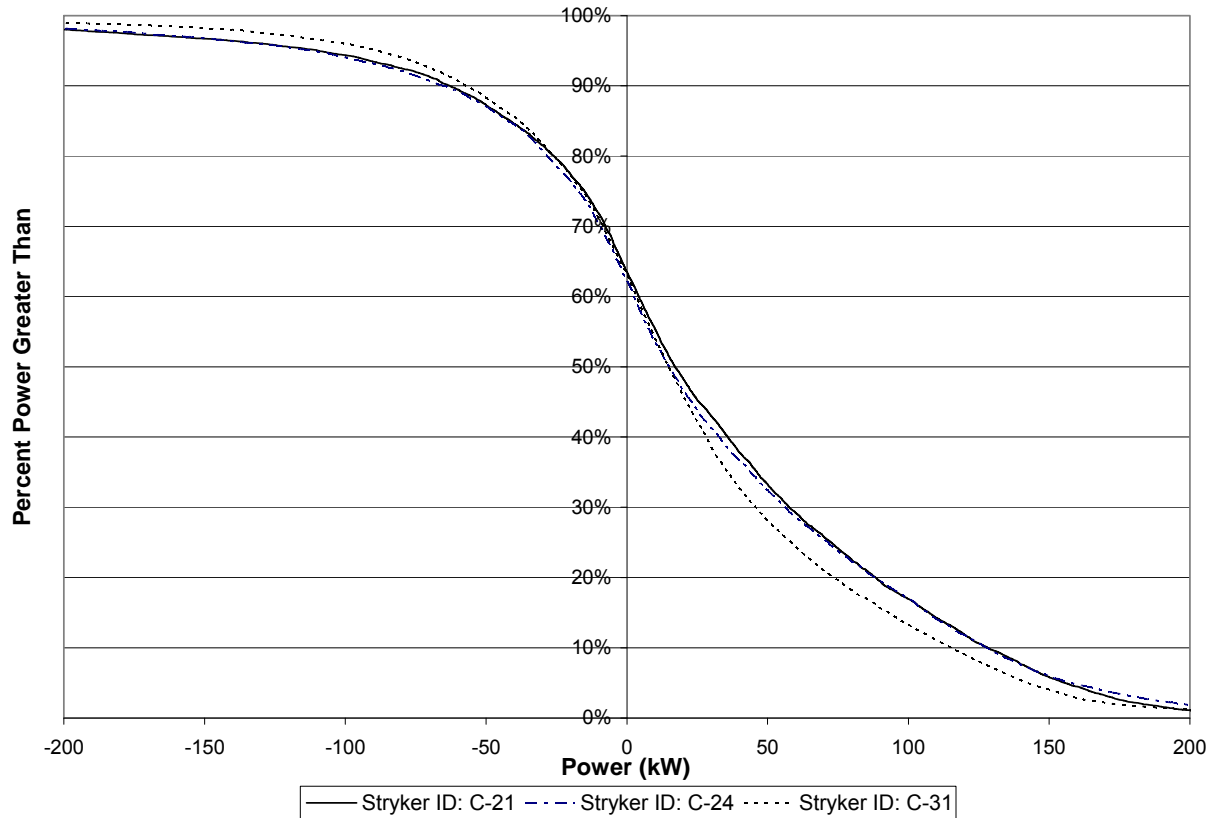
Figure 60: The mobility power duty cycle curves for the three Stryker vehicles performing live-fire, urban operations, and security training missions at Fort Lewis, Washington

On average, maneuvers were being conducted by the three Stryker vehicles for only 4.2% of the time during the nine day live-fire, urban operations, and security training missions conducted at Fort Lewis. The average travel speed of the vehicles was estimated to be approximately 10.5 m/s. The absolute average acceleration and rate of elevation change were 0.26 m/s^2 and 0.14 m/s respectively. The average positive power requirement was 65.4 kW, and the associated standard deviation of the average positive power requirements between the three vehicles was 5.4 kW. The estimated positive power requirement was approximately 25% of the rated engine power for the Stryker vehicle. Figure 60 indicated that the variability between the three mobility power duty cycle curves was small. All three vehicles had a positive power requirement for

approximately 62% of the time when the vehicles had a non-zero travel speed while conducting

maneuvers at Fort Lewis. The power duty cycle curve for the Stryker vehicle identified as "C-

31" differed the greatest compared to the other two vehicles' power duty cycle curves. The GPS

tracking data and estimated average positive power requirements are shown in Table 22 and the

mobility power duty cycle curves are represented in Figure 61 for the three Stryker vehicles

operating at Pohakuloa Training Area (PTA). Figure 59 details the estimated mobility power

values for a portion of a Stryker vehicle's off-road maneuvers at the Keamuku parcel of PTA.

Table 22: A summary of the Garmin 18 GPS data and mobility power results for the
three Stryker vehicles operating at the Pohakuloa Training Area, Hawaii

Stryker ID:	Maneuver Time (hr)	Percent Moving	Avg. Daily Travel (km/day)	Avg. Travel Speed (m/s)	Avg. Absolute Acceleration (m/s^2)	Avg. Absolute Elevation Change (m/s)	Avg. Predicted Positive Power (kW)
8	3.74	16.5%	64.6	4.8	0.17	0.22	42.4
17	6.55	20.7%	117.9	5.0	0.14	0.23	43.0
19	6.33	20.0%	116.2	5.1	0.15	0.24	44.9
Average:	5.83	19.5%	105.2	5.0	0.15	0.23	43.6
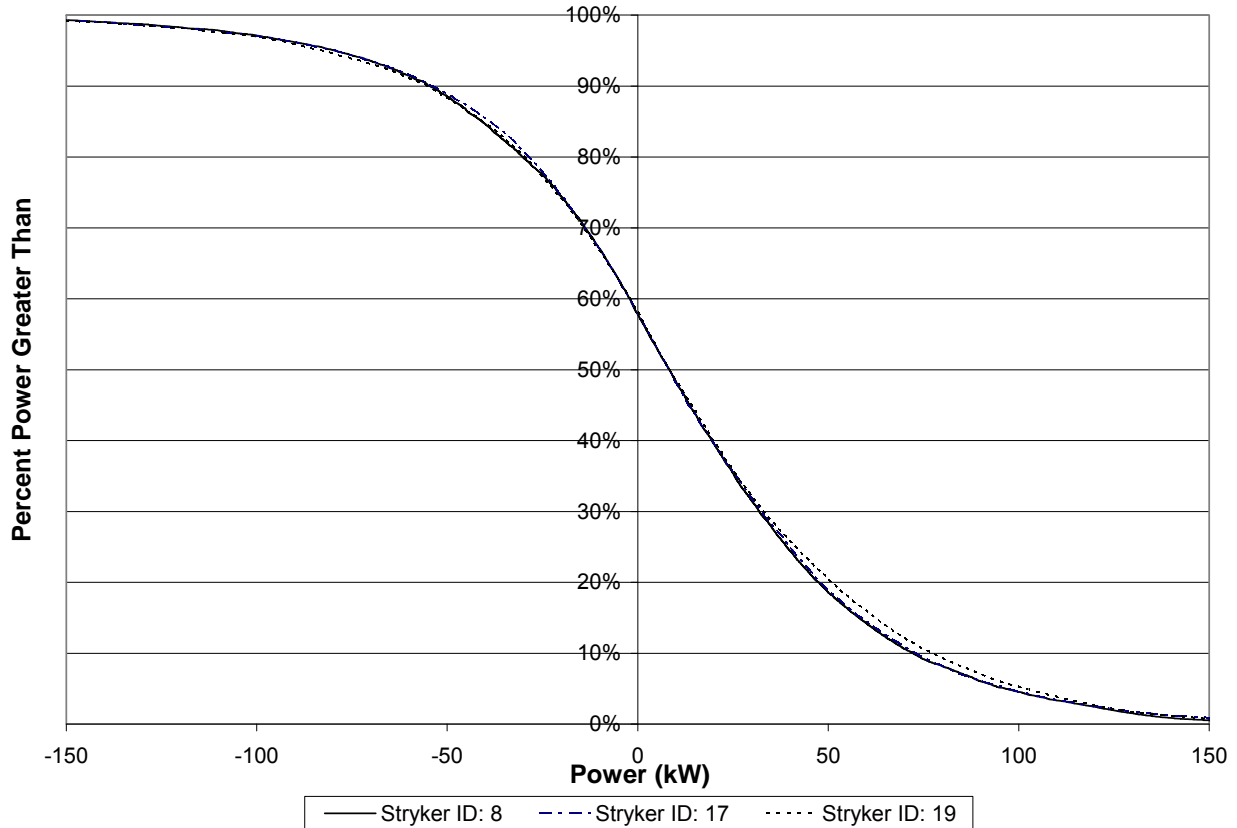
Figure 61: The mobility power duty cycle curves for the three Stryker vehicles performing a proofing mission at the Pohakuloa Training Area, Hawaii

The proofing mission conducted at PTA resulted in distinctly different power and duty cycle requirements compared to the power requirements for the Stryker vehicles operating at Fort Lewis. The vehicles conducted maneuvers for approximately 19.5% of the time during the single day proofing mission conducted at PTA. This percent moving value is significantly greater than the 4.2% value estimated for the mission performed at Fort Lewis. The estimated average travel speed and absolute average acceleration values for the three vehicles maneuvering at PTA were reduced by approximately 52 and 42% respectively. The absolute average rate of elevation change increased by 64% which indicated the grade component had a greater effect on the power requirement at PTA. The average positive power requirement decreased by 33% at

151

PTA compared to the positive power requirements at Fort Lewis while the standard deviation of the average positive power requirements between the three Stryker vehicles decreased by approximately 76%. The power duty cycle curves shown in Figure 61 for the Stryker vehicles operating at PTA also indicated that there was decreased variability in the power requirements. Each vehicle had very similar mobility power duty cycle curves while the power duty cycle curve for the Stryker identified as "19" had the greatest difference compared to the two other vehicles' curves. The Stryker vehicles had a positive power requirement for approximately 57% of the time when the vehicles were maneuvering compared to 62% when training at Fort Lewis. Figures 62 and 63 provide comparisons of the average mobility power duty cycle trends for the Stryker vehicles operating at Fort Lewis and PTA along with the associated one standard deviation bars between the three Stryker vehicles.
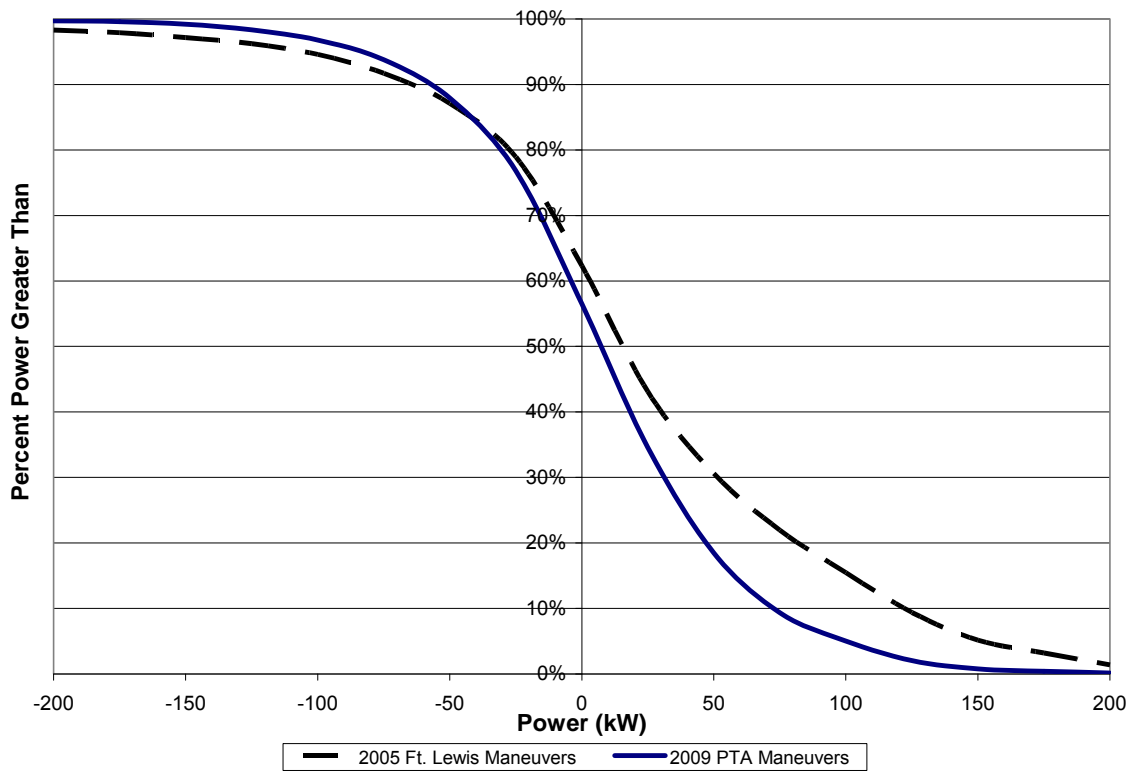
Figure 62: The average mobility power duty cycle curves for the Stryker vehicles operating at Fort Lewis, Washington and the Pohakuloa Training Area, Hawaii

152
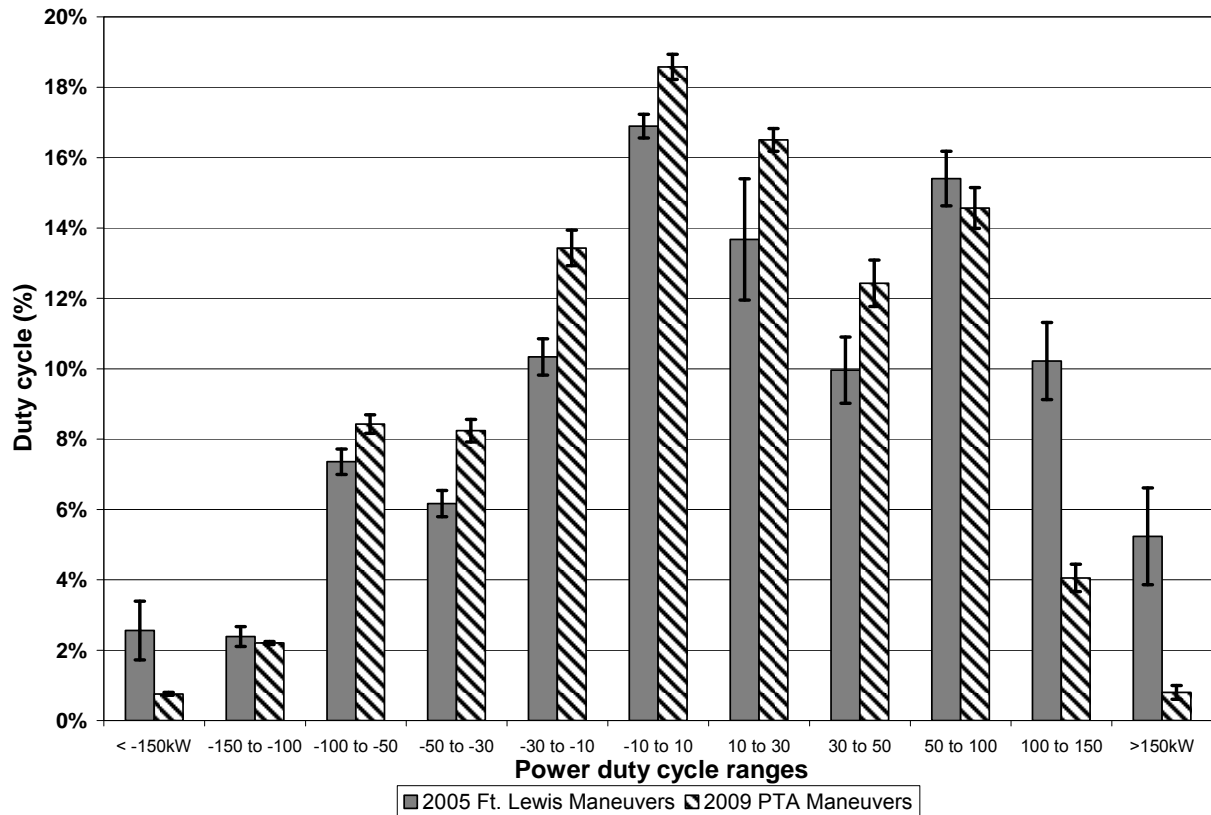
Figure 63: A comparison of the average mobility power duty cycles for three Stryker vehicles operating at Fort Lewis, Washington and the Pohakuloa Training Area, Hawaii along with the associated standard deviation between the vehicles

The 100 to 150 kW and greater than 150 kW power duty cycle ranges' values were approximately 152 and 555% greater in magnitude for the training missions conduced at Fort Lewis. The 10 to 30 kW and 30 to 50 kW power duty cycle ranges' values were approximately 21 and 25% greater in magnitude for the proofing missions conducted at PTA. These trends were another indicator that there was a greater positive power requirement for the maneuvers conducted at Fort Lewis.

In summary, the mobility power model was used to estimate the power duty cycle requirements from existing GPS tracking data for three Stryker vehicles operating at Fort Lewis and PTA. The results indicated that the GPS-based mobility power model can be used to identify differences in the power duty cycle requirements as a result of the specific training missions performed and the U.S. Army installation where the maneuvers were conducted.

Chapter 6: Conclusions

The principle objective of this study was to develop, validate, and apply a GPS-based mobility power model to characterize the power requirements of vehicles. Controlled tests were performed to validate the motion resistance, grade, and inertia components of the model. Uncontrolled tests were performed to validate the model in a scenario that simulated the maneuvers of military vehicles during reconnaissance missions executed by the U.S. Army. The predicted mobility power values were compared to "measured drivewheel power" values which were estimated from the engine speed and engine torque messages transmitted on certain 11 bit CAN signals. Finally, the model was applied to historical GPS tracking for the U.S. Army's Stryker vehicle conducting training missions at Fort Lewis, Washington and the Pohakuloa Training Area (PTA), Hawaii. The duty cycle characteristics of the Stryker vehicles maneuvering at each installation were characterized and compared.

6.1 Model Validation

Controlled and uncontrolled tests were conducted to validate the GPS-based mobility power model. The predicted values estimated from the Trimble 132 and Garmin 18 GPS receivers were compared to the drivewheel power values calculated from signals transmitted on the test vehicle's CAN network. Controlled motion resistance, grade, and inertia tests were performed to validate each component of the model. The uncontrolled test conducted simulated a typical reconnaissance mission performed by the U.S. Army. The uncontrolled test validated the model in a scenario that simulated the vehicle movement patterns typically performed by military vehicles during reconnaissance missions. The results from the uncontrolled test were considered

a combined validation of all components of the model. A 2 s GPS speed and acceleration offset was used during all validation tests while a 0 s elevation offset was used. The tests performed allowed for the accuracy of each component and the entire model to be characterized.

6.1.1 Controlled Tests

6.1.1.1 Motion Resistance Tests

Validation of the motion resistance component of the model was achieved by conducting 24 straight-line and five constant turning radius tests at several levels of constant travel speed. The predicted average mobility power values from the Trimble 132 GPS data showed reasonable agreement with the average predicted drivewheel power values. The discrete predicted values tended to concentrate around the 1:1 line slightly above the origin about a small positive value (Approximately 1 kW) for the straight-line tests. There was an increase in the average power requirement during the constant turning radius tests at a given average travel speed. The increased power requirement was due to the increase in motion resistance from the steered wheels. The results from the Garmin 18 data slightly increased the variability between the measured and predicted power values compared to the Trimble 132 GPS receiver. The Garmin 18 receiver's results had a greater amount of predicted average negative power values during the motion resistance tests. The negative average power values estimated from the Garmin 18 data were partially due to errors in the GPS elevation data. Fluctuations in the vehicle travel speed may have contributed to the power requirements that were greater than 5 kW and less than -2 kW during the straight-line and constant turning radius tests respectively. The constant turning

radius tests indicated that both GPS receivers can be used to estimate the turning radius of a vehicle.

6.1.1.2 Grade Tests

A total of nine grade tests were conducted at average travel speeds of approximately 3.3, 4.8, 7.1, 9.3, and 11.4 m/s while either the 1ˢᵗ or 2ⁿᵈ gear of the transmission was engaged. The elevation increase and average percent grade during each test was approximately 50 m and 7.3% respectively. A 5 s running average of the change in elevation value was needed to smooth the elevation data. The Trimble 132 and Garmin 18 GPS receivers were able to estimate with a reasonable level of accuracy the percent grade traversed by the test vehicle. The Garmin 18 receiver's elevation data (height above ellipsoid) had significantly greater variability than the Trimble 132's data, but a 5 s running average of the elevation data was used for the GPS elevation data from both receivers. The discrete predicted power values from both receivers had a moderate level of variability between the measured and predicted values. The receivers estimated with a high degree of accuracy the average power requirement during the nine grade tests. The Root Mean Square Error (RMSE) between the discrete measured and predicted power values increased as the average vehicle travel speed increased, but the CV RMSE decreased as the average travel speed increased for both GPS receivers. The CV RMSE statistic indicated that the model became more accurate as the average travel speed increased during the grade tests.

6.1.1.3 Inertia Tests

The model's greatest level of accuracy during the controlled tests was attained during the 15 inertia tests conducted at degrees of acceleration of slow, medium, and fast while the transmission was in either 1st or 2nd gear. The predicted discrete and average mobility power values had the lowest amount of variability compared to the controlled motion resistance and grade tests performed. The average acceleration during each test ranged from 0.6 to 2.2 m/s^2. The model tended to slightly overestimate the power requirement during each inertia test from the Trimble 132 and Garmin 18 receivers' data, despite slightly underestimating the test vehicle's acceleration during each inertia test. The average power requirement during the inertia tests ranged from approximately 9 to 65 kW for both receivers. The RMSE value between the predicted and measured power values tended to increase as the level of acceleration increased. The CV RMSE values for the Trimble 132 and Garmin 18 receivers during all 15 inertia tests were less than 0.44 and 0.42 respectively. The results from the Garmin 18 receiver's data had less variability than the Trimble 132 receiver's results, but this may have been due to the 2 s GPS speed and acceleration offset being biased to the Garmin 18 receiver. The gamma values (γ) used to estimate the vehicle's equivalent mass and subsequent inertia power requirement were calibrated by reducing the magnitude of the gamma values because the inertia test results indicated the model overestimated the average positive power requirement. The gamma values were reduced by 27 and 18% for the Trimble 132 data and Garmin 18 GPS data respectively, and this was deemed a combined calibration of the GPS receivers and the test vehicle. Decreasing the gamma values resulted in a 74 and 71% reduction in the magnitude of the RMSE values for the Trimble 132 and Garmin 18 GPS receivers respectively.

6.1.2 Uncontrolled Tests

The uncontrolled test simulated the vehicle movement patterns of U.S. Army vehicles during reconnaissance missions. Approximately 2400 s of test data was collected during the uncontrolled test while engine power was delivered to the drivewheels for only 2100 s of the test. The discrete mobility power values estimated for the durations when the clutch was not fully engaged while the transmission was in either 1st, 2nd, or 3rd gear were removed from the validation analysis. There was a moderate level of variability between the discrete measured and predicted power values from the Trimble 132 and Garmin 18 GPS data. The Trimble 132 receiver provided for accurate estimates of the average positive power requirements during the test, as indicated by an absolute average percent error value of 20%. The absolute average percent error values were calculated by dividing the magnitude of the difference between the predicted and measured average values by the magnitude of the average measured values. The Garmin 18 receiver had an absolute average percent error of 41% when estimating the average positive power requirement of the test vehicle. The peak power requirement during the uncontrolled test was estimated and compared to the measured peak power values. Approximately 20% of the maximum discrete power values were used in the analysis. The percent error of the predicted average positive mobility power value was approximately 37% from the Trimble 132 receiver data compared to 43% for the Garmin 18 receiver. The correlation coefficient was estimated between the discrete absolute error values from the model and the discrete Dilution of Precision (DOP) values from the GPS data. The correlation coefficient values for the Trimble 132 and Garmin 18 GPS receivers were 0.38 and -0.04 respectively. The correlation coefficient for the Trimble 132 receiver indicated that there was a moderate correlation between the GPS receiver's DOP values and the absolute error from the

159

model. Thus the Trimble 132 GPS receiver's DOP values could be used as indicator of the accuracy of the model.

The model provided for reasonable estimates of the positive power duty cycles between 2 – 12 kW in magnitude from the GPS data. The absolute average percent error for the duty cycles between 2 and 12 kW were estimated to be approximately 14% for both GPS receivers. The model tended to over predict the power duty cycle requirements greater than 12 kW or less than -9 kW while the magnitude of the variability tended to increase as the predicted power values increased. The accuracy of the model decreased slightly when estimating the power duty cycles that were between -9 and -2 kW. The variability of the power duty cycle values increased substantially when estimating the power duty cycle ranges that were greater than 12 kW or less than -9 kW. The model was able to accurately estimate the percent power greater than duty cycle curves while accurately estimating that approximately 55% of the required power during the uncontrolled test was greater than 0 kW. The Trimble 132 data was more accurate at estimating the characteristics of the percent greater than duty cycle curve in the positive power region, compared to the Garmin 18 receiver's estimate of the test vehicle's power duty cycle curve. The duty cycle curve estimated from the Garmin GPS 18 data was not as accurate as the curve estimated from the Trimble 132 data, and the trends of the curve in both the positive and negative power regions were similar. The results from the uncontrolled test indicated that the model's estimates of mobility power may be significantly affected by the quality of the GPS data. The accuracy of the model decreased when the Dilution of Precision (DOP) increased and the number of satellites transmitting data to the GPS receiver decreased. It is suggested that

160

future applications of this model should be applied to GPS data with good quality and DOP values less than 2.5.

6.2 Model Application

The mobility power model was used to estimate the power duty cycle requirements from existing GPS tracking data for three Stryker vehicles operating at Fort Lewis and the Pohakuloa Training Area (PTA). Live-fire, urban operations, and security training missions were performed at Fort Lewis in 2005 while a proofing mission was conducted at PTA in 2009. The results indicated that the GPS-based mobility power model can be used to identify differences in the vehicle's power duty cycle requirements due to the training mission being performed and the U.S. Army installation where the maneuvers were conducted. The average positive power requirement for the Stryker vehicles operating at Fort Lewis was 65.4 kW. The average positive power requirement at PTA was approximately 33% less than the power requirement at Fort Lewis. The Stryker vehicles had a positive power requirement for approximately 62% of the time while operating at Fort Lewis compared to only 57% of the time when the vehicles maneuvered at PTA. The three Stryker vehicles' power duty cycles at a given military installation were similar. The Stryker vehicles that conducted maneuvers at Fort Lewis had greater mobility power requirements in the extreme power duty cycle ranges (> 100 kW and < -150 kW).

The mobility power model represents a cost-effective approach for estimating the in-field power duty cycle requirements of military vehicles from GPS data. The model provides design engineers with a useful tool for quantifying the on-road and off-road power requirements of conventional or hybrid military vehicles. The duty cycles can be estimated for specific locations

where the effect of the terrain on the vehicle's mobility power requirement can be taken into account. Furthermore, the effect of the mission type being performed can be characterized, and the associated power requirements and operating characteristics can be quantified.

Chapter 7: Recommendations

The mobility power model that used GPS tracking data to estimate the required power to propel the vehicle was validated. The model utilizes the Vehicle Terrain Interaction (VTI) model to estimate the motion resistance force generated at the wheels. The mobility power duty cycle characteristics for the U.S. military's 8-wheeled Stryker vehicle were determined by applying the mobility power model to historical GPS tracking data when the vehicle conducted reconnaissance missions at Fort Lewis, Washington and the Pohakuloa Training Area (PTA), Hawaii. The application of this model demonstrated that the power duty cycles for a vehicle could be predicted from previously acquired GPS tracking data. There exists the potential to develop a substantial power duty cycle database by applying the mobility power model to historical GPS tracking data for many different types of military vehicles operating at numerous U.S. military installations.

The effect of the degree of acceleration of a vehicle has on the optimum GPS offset should be investigated further during any future validation efforts. Results from the controlled validation tests performed indicated that the ideal GPS offset increases in magnitude as the vehicle's level of acceleration increases. The effect of the quality of the GPS data on the mobility power estimates should be investigated further because the uncontrolled tests performed during validation of the model indicated that the model's accuracy may be dependent on the GPS data's Dilution of Precision (DOP) values. The results from the uncontrolled test indicated that the accuracy of the mobility power model decreased when the GPS quality was poor.

Validating the mobility power model with a tracked vehicle using the VTI model's tracked equations would vastly expand the potential application of the model for military vehicle design. Ideally, the torque and rotational speed at each driven sprocket would be measured directly. Any future validation testing should be conducted off-road in order to further characterize the VTI model's accuracy and the affect of varying soil strength conditions. Any validation effort should be completed using Real Time Kinetic (RTK) GPS along with the Garmin 18 GPS receiver that is typically used to track military vehicles. RTK GPS provides an accurate position within 2 cm, and represents the most accurate type of GPS currently available. This validation effort would be comparing the best possible mobility power estimates to the measured power delivered directly to the tractive elements. This approach would eliminate any errors introduced when estimating the power delivered to the tracks or wheels from measured engine power values. In the future, the application of the mobility power model to military vehicle design may increase as the accuracy of GPS improves while the associated costs decrease.

References

ASAE Standards. 2004. S313.3: Soil Cone Penetrometer. St. Joseph, Mich.: ASAE.

Ayers, P. D., M. Rice, C. Wu, H. Howard, and A. Anderson. 2005. Stryker tracking study performed at Fort Lewis military installation in October 2005. Internal final report, U.S. Army Corps of Engineers ERDC-CERL project.

Ayers, P. D., N. Potteti, A. Anderson, and H. Howard. 2009. Pre and post Stryker transformation maneuvers at Pohakuloa Training Area, Hawaii: tracking military vehicles and using GIS to quantify site-specific dust generation. *Proc. of 11th European Regional Conf.*, Bremen, *Germany*.

Bevly, D. M. and S. Cobb. 2010. *GNSS for Vehicle Control*. 1st Ed. Norwood, Mass.: Artech House.

Brixius, W. 1987. Traction prediction equations for bias ply tires. ASAE Paper No. 87-1622, St. Jospeph, Mich.: ASAE.

Bosch, R. 1993. *Automotive Handbook*. 3rd Ed. Mass.: Robert Bentley Publishers.

Brudnak, M., N. Pozolo, A. Meldrum, T. Mortsfield, A. Shvartsman, W. Smith, J. Goodell, and D. Holtz. 2008. Virtual combat vehicle experimentation for duty cycle measurement. *Proc. of SAE Conference Conf.*, Detroit, Mich.: SAE.

Department of the Army, Headquarters. 2000. The IBCT Infantry Battalion Reconnaissance Platoon. Field Manual No. 7-4. Draft.

Farsi, M., K. Ratcliff, and M. Barbosa. 1999. An overview of controller area network. *Computing & Control Engineering Journal*. 10(3): 113-120.

Garmin International, Inc., January 2008. GPS 18x Technical Specifications, Revision B.

Gillsepie, T. D. 1992. *Fundamentals of Ground Vehicles*. Warrendale, Pa.: SAE.

Gonder, J., T. Markel, A. Simpson, and M. Thornton. 2007. Using GPS travel data to assess the real world driving energy use of plug-in hybrid electric vehicles (PHEVs). NREL/CP Paper No. 540-40858. Oak Ridge, Tenn.: U.S. Dept. of Energy.

Haugen, L. B. 2002. Design and testing of a vehicle tracking system for monitoring environmental impact at U.S. Army training installations. MS thesis. Fort Collins, Colo.: Colorado State University, Chemical and Bioresource Engineering Department.

How, J., N. Pohlman and C. Park. 2002. GPS estimation algorithms for precise velocity, slip and race-track position measurements. SAE Paper No. 2002-01-3336, Warrendale, Pa.: SAE.

Howard, H., P. D. Ayers, D. Koch, A. Anderson, J. Kane, G. Bozdech, and N. Svendsen. Predicting soil erosion potential from military vehicle tracking and terrain impacts. 2011. *Proc. of the International Symposium on Erosion and Landscape Evolution.*, Anchorage, Alaska.

Jones, R. A., G. B. McKinley, P. W. Richmond, and D. C. Creighton. 2007. A vehicle terrain interface. *Proc. of the Joint North America, Asia-Pacific ISTVS.*, Fairbanks, Alaska.

Jun, J, J. Joonho, S. Yoon, and R. Guensler. 2006. Impacts of acceleration calculation methods on onroad vehicle engine power estimation. AWMA Paper No. 460. Philadelphia, Pa.: Taylor & Francis Group.

Millo, F, L. Rolando and M. Andreata. 2011. Numerical siumulation for vehicle powertrain development. *Numerical Analysis – Theory and Application* 1: 519-540.

NMEA Standards. 1995. 0183: Standard for Interfacing Marine Electronic Devices. New Bern, N.C.: SAE.

Potteti, N. S. 2009. Quantifying dust from pre and post transformation at Pohakuloa Training Area. MS thesis. Knoxville, Tenn.: University of Tennessee, Department of Biosystems Engineering and Soil Science.

Rutherford, C. 2004. Design and analysis of a low production cost hybrid electric high mobility multi-purpose wheeled vehicle for military use. MS thesis. Knoxville, Tenn.: University of Tennessee, Department of Mechanical Engineering.

Rakha, H., I. Lucic, S. Demarchi, J. Setti, and M. Van Aerde. 2001. Vehicle dynamics model for predicting maximum truck acceleration levels. *Journal of Transportation Engineering* 127(5): 1-34.

Rakha, H., M. Snare, and F. Dion. 2004. Vehicle dynamics model for estimating light-duty vehicle acceleration levels. *Journal of Transportation Research Board* 1883: 40-49.

Richmond, P. W., S. A. Shoop, A. A. Reid, and G. L. Mason. 2006. Terrain surface codes for an all-season, off-road ride motion simulator. *MSIAC M&S Journal.*

Ross, S. M. 2003. Peirce's criterion for the elimination of suspect experimental data. *Journal of Engineering Technology.*

SAE Standards. 1998. J1939-71: Surface Vehicle Recommended Practice. Warrendale, Pa.: SAE.

Stanford University. 2001. Road Grade and Vehicle Parameter Estimation for Longitudinal Control Using GPS. Stanford, Cal: Mechanical Engineering Department. Available at: http://gummo.stanford.edu/dynamic/PATH/Papers/bae_ieee_its2001.pdf.. Accessed 20 January 2011.

Suvinen, A., and M. Saarilahti. 2006. Measuring the mobility parameters of forwarders using GPS and CAN bus techniques. *Journal of Terramechanics* 43: 237-252.

Taylor, W. T. 2011. Fuel consumption test procedures for military wheeled hybrid vehicles. In *Proc. of the 2011 Ground Vehicle Systems Engineering Technology Symposium (GVSETS)*, CD-ROM. Dearborn, Mich.: NDIA.

Trimble Navigation Limited. January 2003. AgGPS 124/132 Operation Manual, Revision A.

Wismer, R. D. and H. J. Luth. 1973. Off-road traction prediction for wheeled vehicles. *Journal of Terramechanics*. 10(2): 49-61.

Wong, J. Y. 2008. *Theory of Ground Vehicles*. 4th Ed. Hoboken, N.J.: John Wiley & Sons, Inc.

Wong, J. Y. 2010. *Terramechanics and Off-road Vehicle Engineering*. 2nd Ed. N.Y.: Elsevier.

Yasin, T. P. 1978. The analytical basis of automobile coastdown testing. *Proc. of SAE Conf.*, Detroit, Mich.: SAE.

Appendices
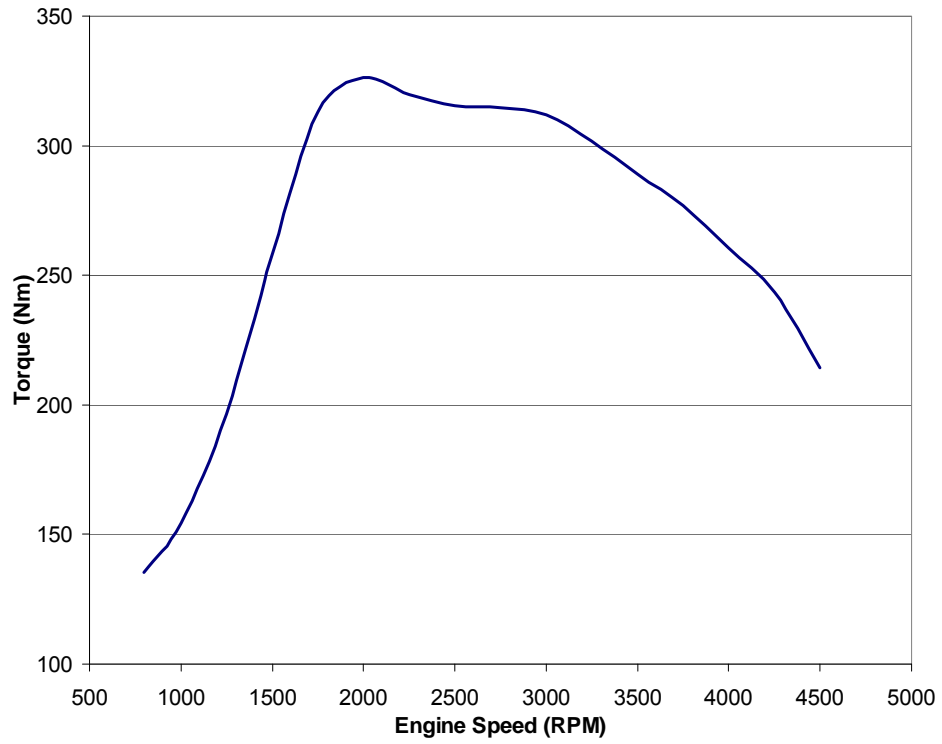
Appendix A

<u>*Engine and Test Vehicle Specifications*</u>
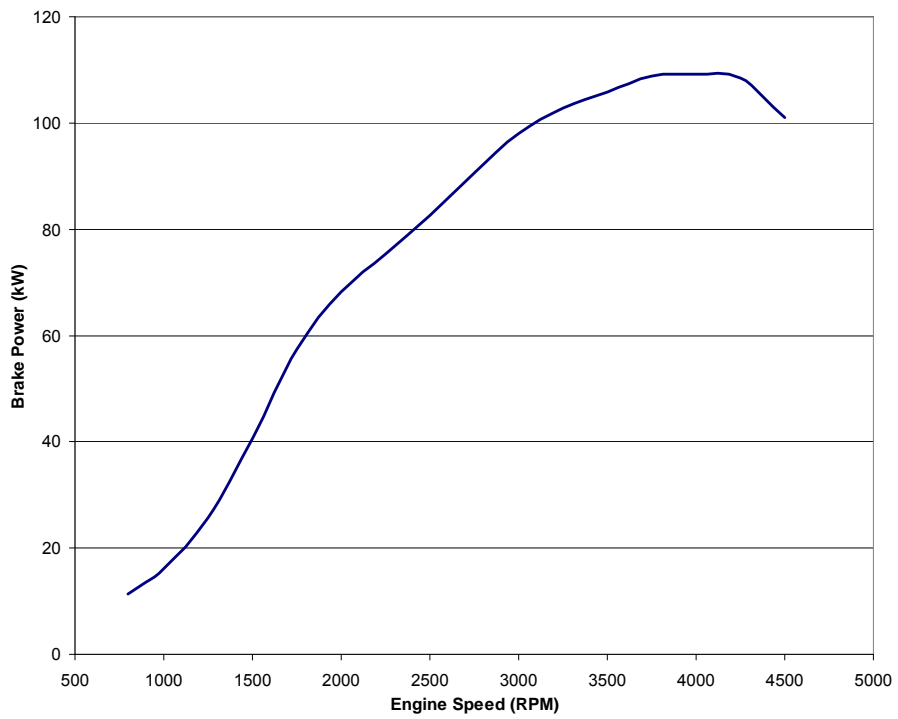
Figure 64: The 1.9L Fiat diesel engine's torque curve

Figure 65: The 1.9L Fiat diesel engine's brake power curve

171

Table 23: General specifications of the Chevrolet Equinox Test Vehicle

Vehicle Make: Chevrolet	
Vehicle Model: Equinox	
mass (kg):	1713
Frontal area (m^2):	2.686
C_d:	0.42
Tire Make/Model:	PAX Challenge X235-710 R460A
Tire radius (m):	0.355
Coeff. of rolling resistance:	0.00675
Front axle final drive ratio:	5.545

Table 24: Gear ratio, drivetrain efficiency, and gamma values for each gear of the transmisison

Transmission Specifications			
Gear	Gear Ratio	Drivetrain Effic.	Gamma
1	3.92	0.90	0.500
2	2.04	0.91	0.300
3	1.32	0.93	0.100
4	0.95	0.97	0.050
5	0.76	0.98	0.030
6	0.63	0.98	0.025

Appendix B

<u>MATLAB *.m file for CAN data conversion</u>

```
clear all
clc

%opens raw NEOVi CAN .csv file
fid =
fopen('F:\Equinox_Validation\NeoVI_Data\12_16_11\NeoVI_data_transform\Trans_12_16_11_
UTC202757.csv');
data = textscan(fid, '%f%f%f%f%f%f%f','delimiter',',');
fclose(fid);

%reads data into variable arrays
time_abs_in = data{1};
eng_speed_in = data{2};
eng_torque_in = data{3};
wheel_sp_fl_in = data{4};
wheel_sp_fr_in = data{5};
wheel_sp_rl_in = data{6};
wheel_sp_rr_in = data{7};

i = 1;
j = 0;                      %counter for each second being averaged
k = 1;
t_1 = 0;                    %keeps track of what second being averaged
sum_eng_speed = 0;         %Defines summation variables
sum_eng_torque = 0;
sum_sp_fl = 0;
sum_sp_fr = 0;
sum_sp_rl = 0;
sum_sp_rr = 0;
ratio_conv = 0.996994;     %conversion factor between 1 s NeoVI data and 1 s UTC GPS data

time_abs_in = time_abs_in / ratio_conv;
length = length(time_abs_in);
int_final_time = round(time_abs_in(length));

time_abs = zeros(1,round(time_abs_in(length)));
eng_speed = zeros(1,round(time_abs_in(length)));
eng_torque = zeros(1,round(time_abs_in(length)));
wheel_sp_fl = zeros(1,round(time_abs_in(length)));
wheel_sp_fr = zeros(1,round(time_abs_in(length)));
wheel_sp_rl = zeros(1,round(time_abs_in(length)));
wheel_sp_rr = zeros(1,round(time_abs_in(length)));


while i < length
```

```
if time_abs_in(i) > (t_1 - 0.5) && time_abs_in(i) <= (t_1 + 0.5)
    %sums all data points for a given UTC SECOND
        sum_eng_speed = sum_eng_speed + eng_speed_in(i);
        sum_eng_torque = sum_eng_torque + eng_torque_in(i);
        sum_sp_fl = sum_sp_fl + wheel_sp_fl_in(i);
        sum_sp_fr = sum_sp_fr + wheel_sp_fr_in(i);
        sum_sp_rl = sum_sp_rl + wheel_sp_rl_in(i);
        sum_sp_rr = sum_sp_rr + wheel_sp_rr_in(i);
        i = i + 1;
        j = j + 1;

elseif j ~= 0
    %divides all of the summed values for a given second and stores in
    %given array
        eng_speed(k) = sum_eng_speed / j;
        eng_torque(k) = sum_eng_torque / j;
        wheel_sp_fl(k) = sum_sp_fl / j;
        wheel_sp_fr(k) = sum_sp_fr / j;
        wheel_sp_rl(k) = sum_sp_rl / j;
        wheel_sp_rr(k) = sum_sp_rr / j;
        time_abs(k) = t_1;

        t_1 = t_1 + 1;
        j = 0;
        k = k + 1;
        sum_eng_speed = 0;
        sum_eng_torque = 0;
        sum_sp_fl = 0;
        sum_sp_fr = 0;
        sum_sp_rr = 0;
        sum_sp_rl = 0;
else
        eng_speed(k) = 0;
        eng_torque(k) = 0;
        wheel_sp_fl(k) = 0;
        wheel_sp_fr(k) = 0;
        wheel_sp_rl(k) = 0;
        wheel_sp_rr(k) = 0;
        time_abs(k) = t_1;

        t_1 = t_1 + 1;
        i = i + 1;
        j = 0;
        k = k + 1;
        sum_eng_speed = 0;
        sum_eng_torque = 0;
```

```matlab
        sum_sp_fl = 0;
        sum_sp_fr = 0;
        sum_sp_rr = 0;
        sum_sp_rl = 0;
    end


end

time_abs = time_abs';
eng_speed = eng_speed';
eng_torque = eng_torque';
wheel_sp_fl = wheel_sp_fl';
wheel_sp_fr = wheel_sp_fr';
wheel_sp_rl = wheel_sp_rl';
wheel_sp_rr = wheel_sp_rr';

%logs data to .txt file
fid = fopen('1_hz_avg_12_16_202757.txt','w');
data = [num2cell([time_abs.'; eng_speed.'; eng_torque.'; wheel_sp_fl.'; wheel_sp_fr.';
wheel_sp_rl.'; wheel_sp_rr.'])];
fprintf(fid, '%f,%f,%f,%f,%f,%f,%f\n', data{:})
fclose(fid)
```

Appendix C

<u>*GPS Speed and Acceleration Offset*</u>

Table 25: Optimum GPS offset for estimating vehicle speed and acceleration during ten inertia tests

Degree of Acceleration	Gear	Test Duration (s)	Garmin 18 Vehicle Speed Optimum GPS Offset (s)	Garmin 18 Vehicle Acceleration Optimum GPS Offset (s)	Trimble 114 Vehicle Speed Optimum GPS Offset (s)	Trimble 114 Vehicle Acceleration Optimum GPS Offset (s)
Slow	1	32	0	-1	-1	-1
Slow	1	21	0	0	0	0
Slow	1	37	0	0	-1	-1
Medium	1	29	0	0	-1	-1
Medium	1	32	0	0	-1	-1
Medium	2	23	1	2	1	1
Fast	1	25	2	2	1	2
Fast	1	23	2	2	1	2
Fast	2	20	2	2	1	1
Fast	2	23	2	2	1	1
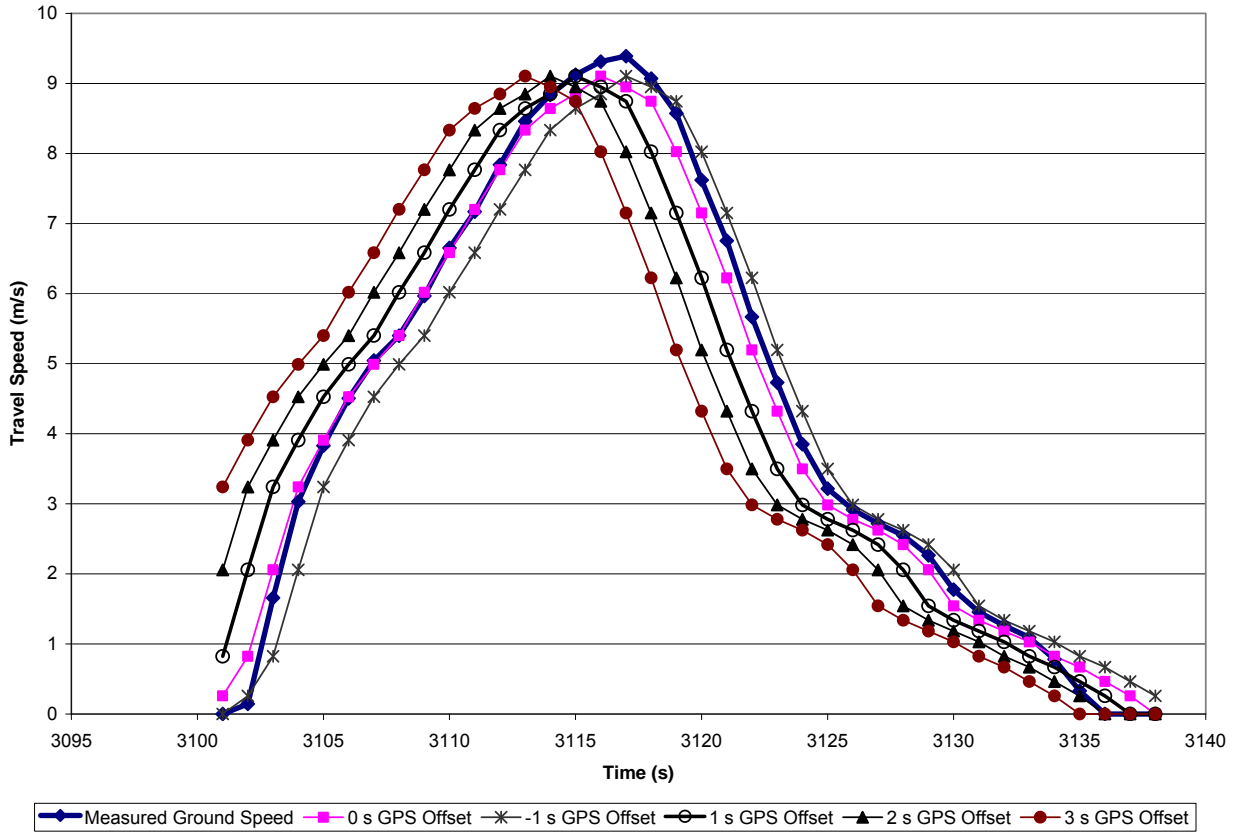
Figure 66: Vehicle travel speed at various Garmin 18 GPS offsets during a slow inertia test
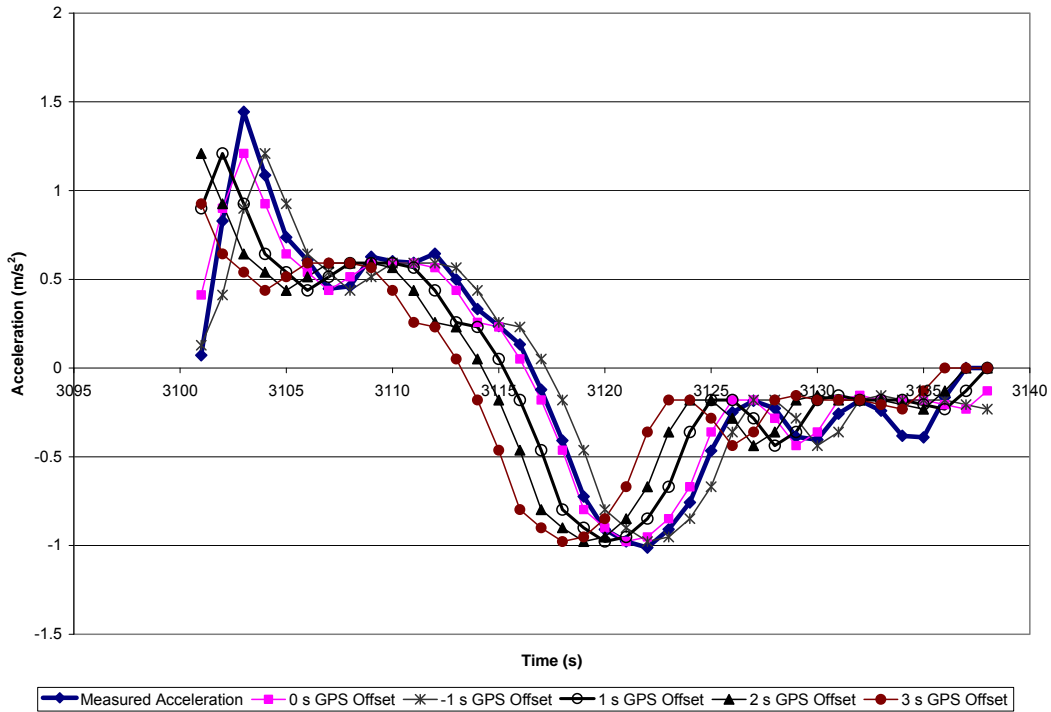
Figure 67: Vehicle acceleration at various Garmin 18 GPS offsets during a slow inertia test
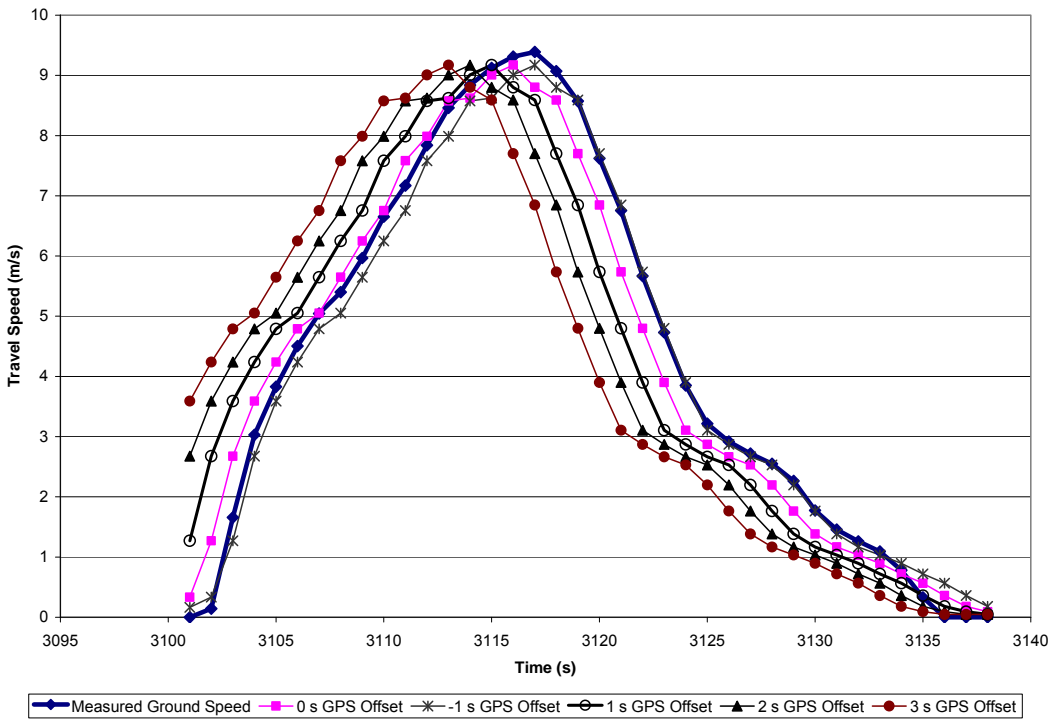
Figure 68: Vehicle travel speed at various Trimble 132 GPS offsets during a medium inertia test
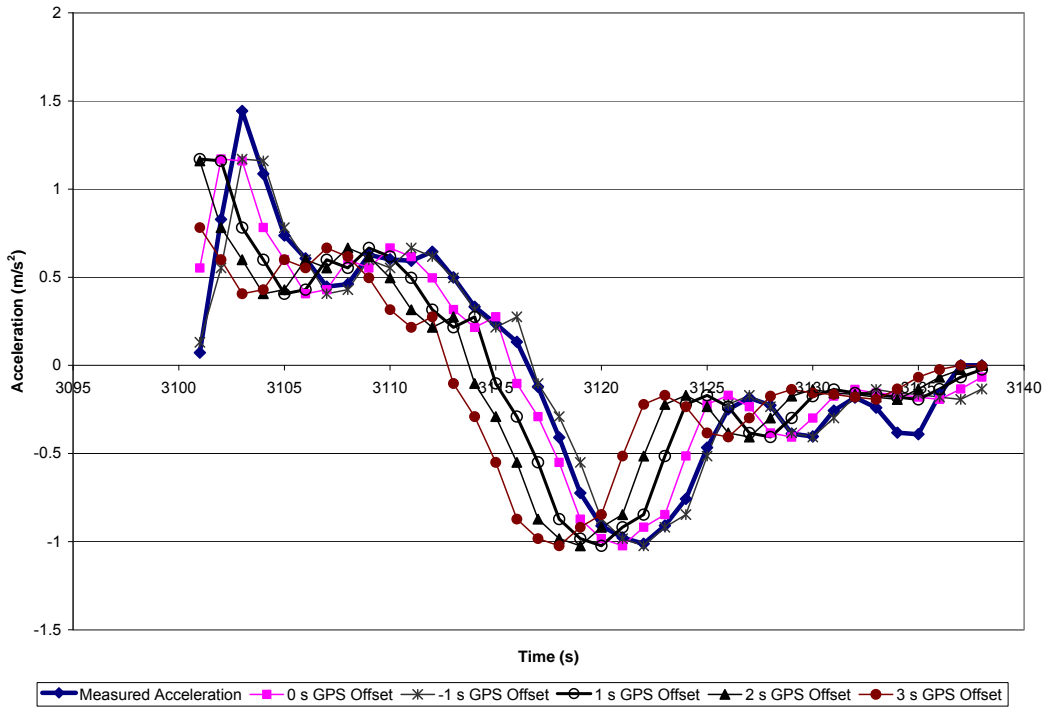
179

Figure 69: Vehicle acceleration at various Trimble 132 GPS offsets during a medium inertia test
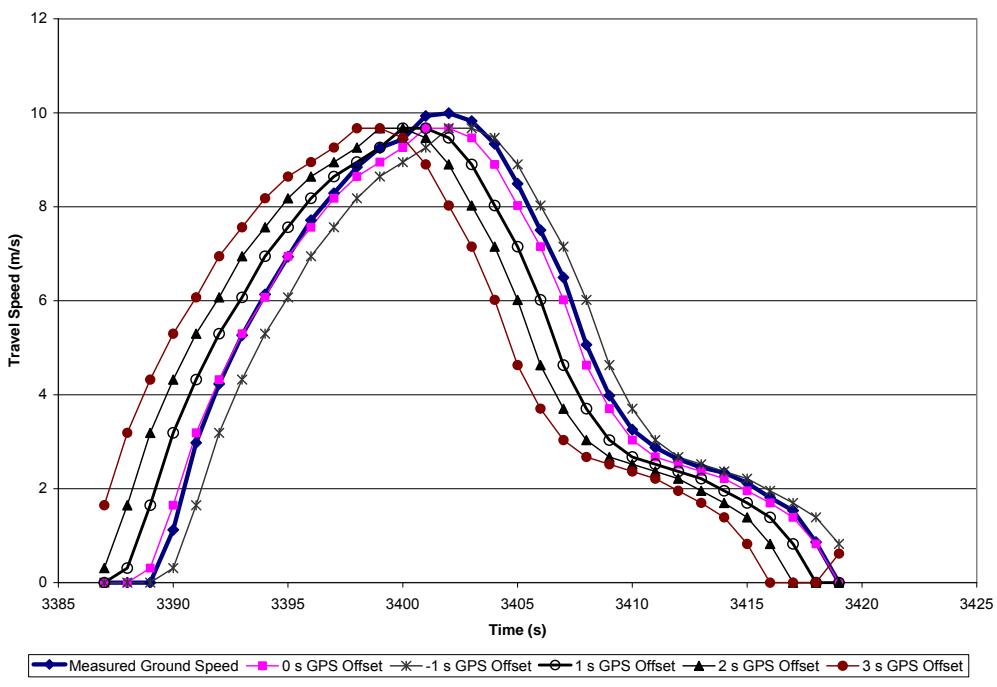

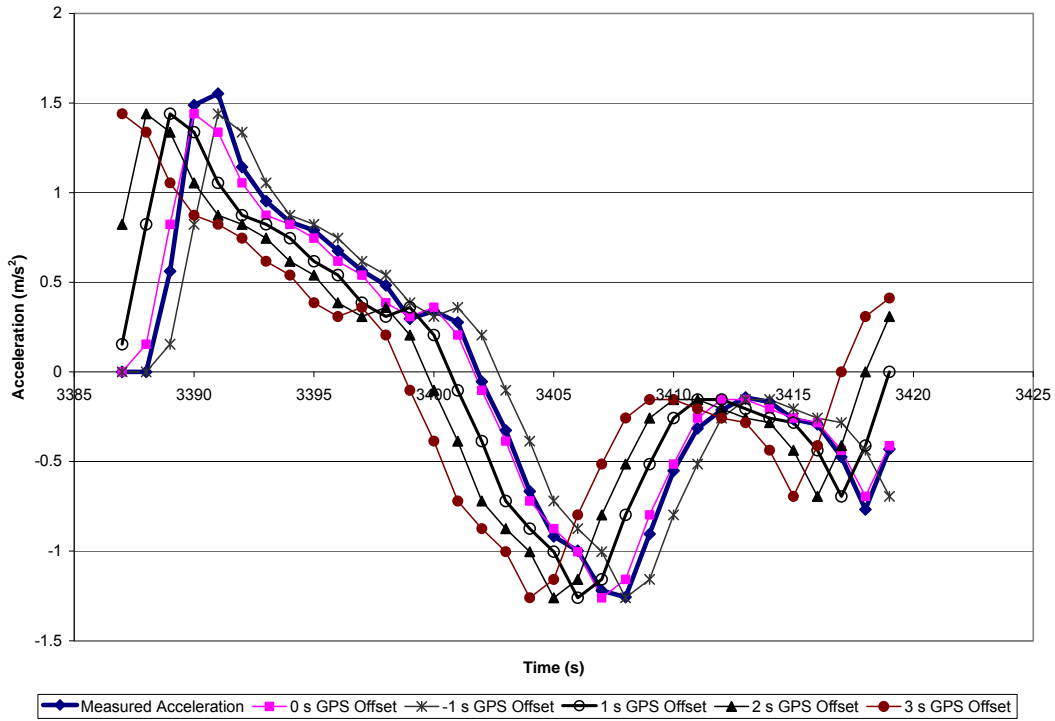Figure 70: Vehicle travel speed at various Garmin 18 GPS offsets during a medium inertia test

Figure 71: Vehicle acceleration at various Garmin 18 GPS offsets during a medium inertia test
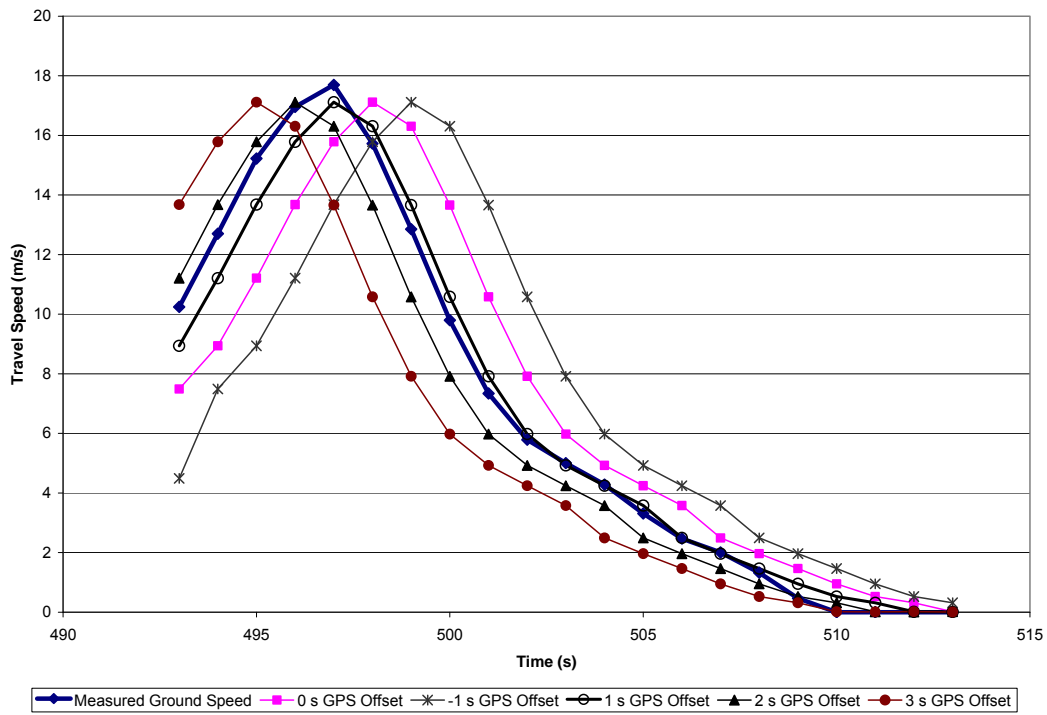

Figure 72: Vehicle travel speed at various Trimble 132 GPS offsets during a fast inertia test
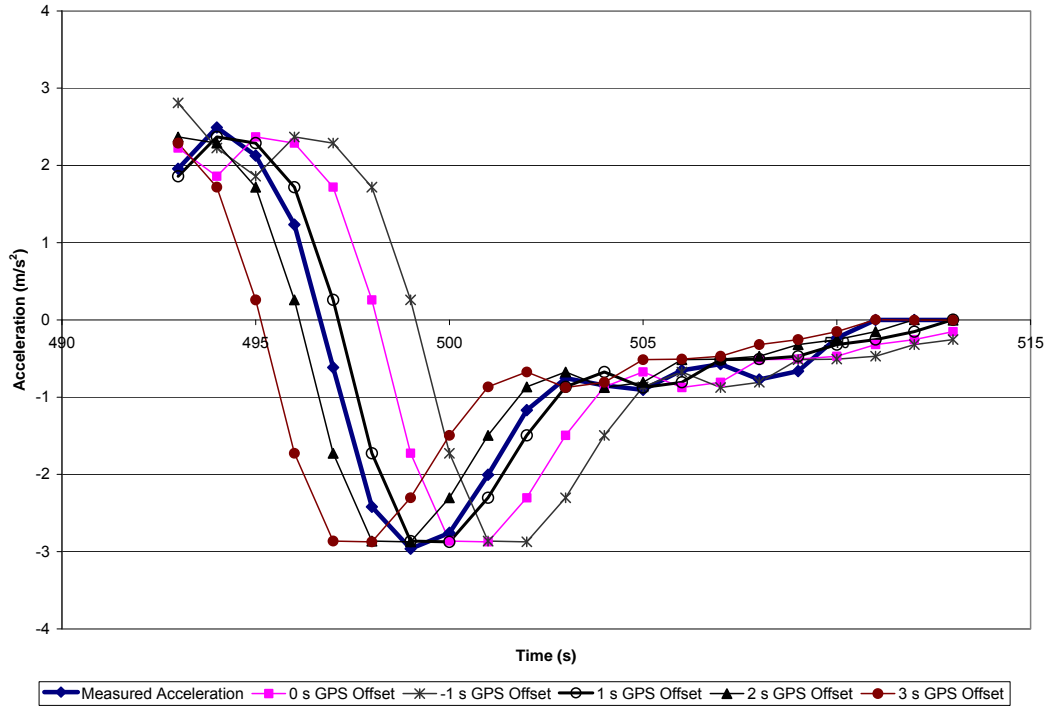
181

Figure 73: Vehicle acceleration at various Trimble 132 GPS offsets during a fast inertia test
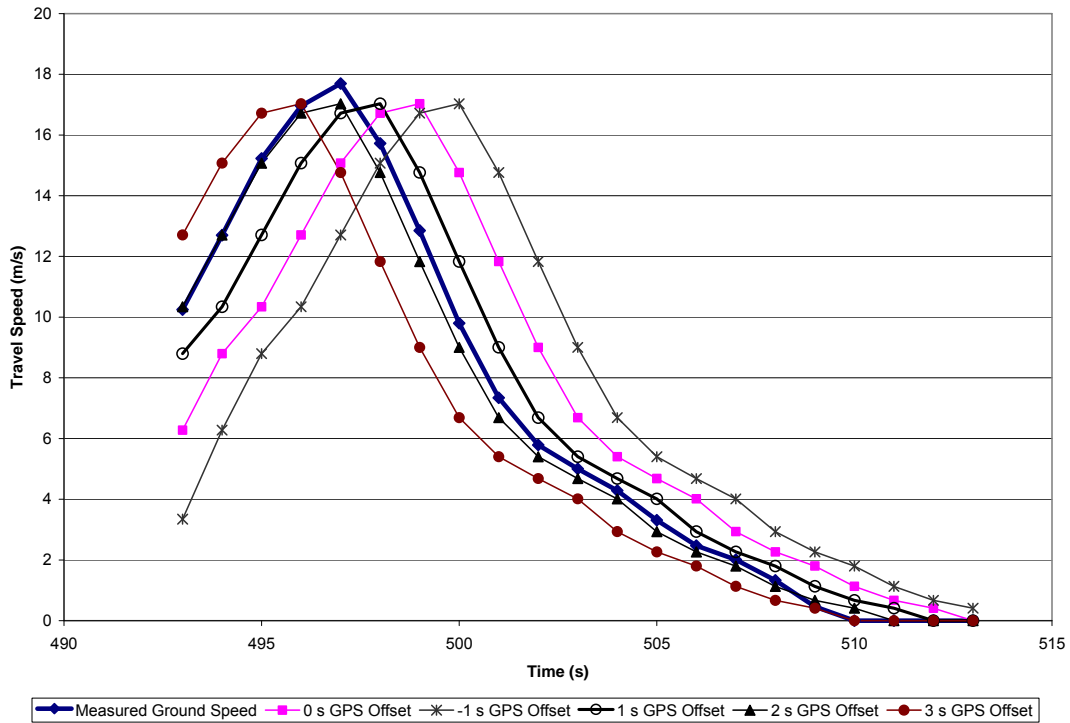

Figure 74: Vehicle travel speed at various Garmin 18 GPS offsets during a fast inertia test
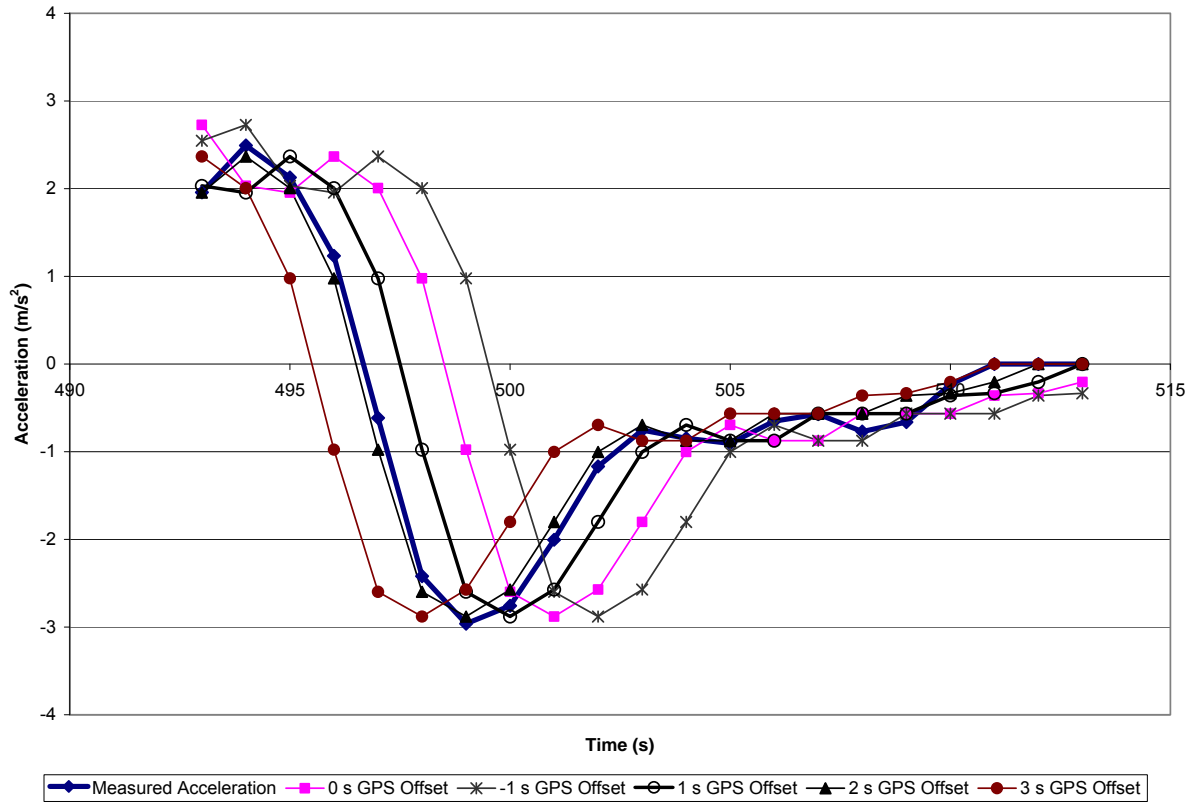
Figure 75: Vehicle acceleration at various Garmin 18 GPS offsets during a fast inertia test

Table 26: The variability between the predicted and measured mobility power values at 0, 1, 2, and 3 s GPS speed and acceleration offsets

| GPS Offset	Receiver	Degree of Acceleration	Gear	R-Squared
0	Garmin 18	Slow	1	0.0584
0	Garmin 18	Fast	1	0.0781
0	Garmin 18	Fast	2	0.1915
1	Garmin 18	Slow	1	0.1048
1	Garmin 18	Fast	1	0.4029
1	Garmin 18	Fast	2	0.0182
2	Garmin 18	Slow	1	0.4400
2	Garmin 18	Fast	1	0.9024
2	Garmin 18	Fast	2	0.9654
3	Garmin 18	Slow	1	0.5927
3	Garmin 18	Fast	1	0.2452
3	Garmin 18	Fast	2	0.3218
0	Trimble 132	Slow	1	0.0070
0	Trimble 132	Fast	1	0.1764
0	Trimble 132	Fast	2	0.1092
1	Trimble 132	Slow	1	0.1148
1	Trimble 132	Fast	1	0.6402
1	Trimble 132	Fast	2	0.3895
2	Trimble 132	Slow	1	0.6694
2	Trimble 132	Fast	1	0.7408
2	Trimble 132	Fast	2	0.6507
3	Trimble 132	Slow	1	0.5296
3	Trimble 132	Fast	1	0.0450
3	Trimble 132	Fast	2	0.1539
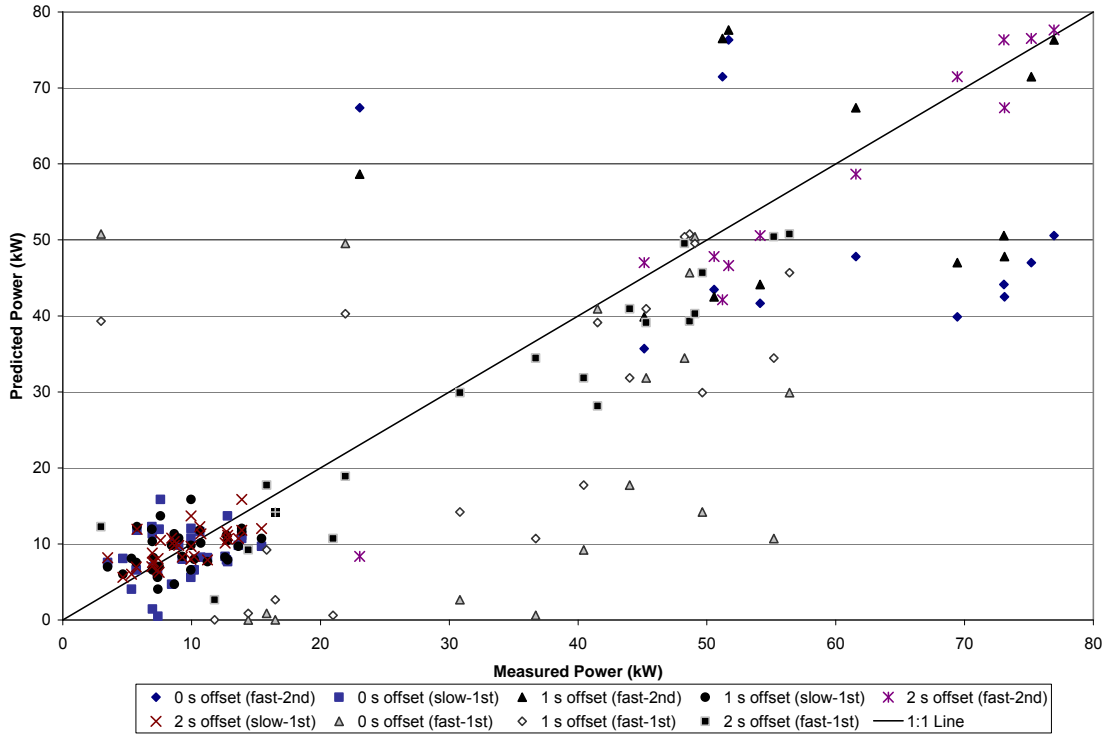
Figure 76: A comparison of predicted and measured mobility power at various GPS speed and acceleration offsets during nine inertia tests for the Garmin 18 GPS receiver
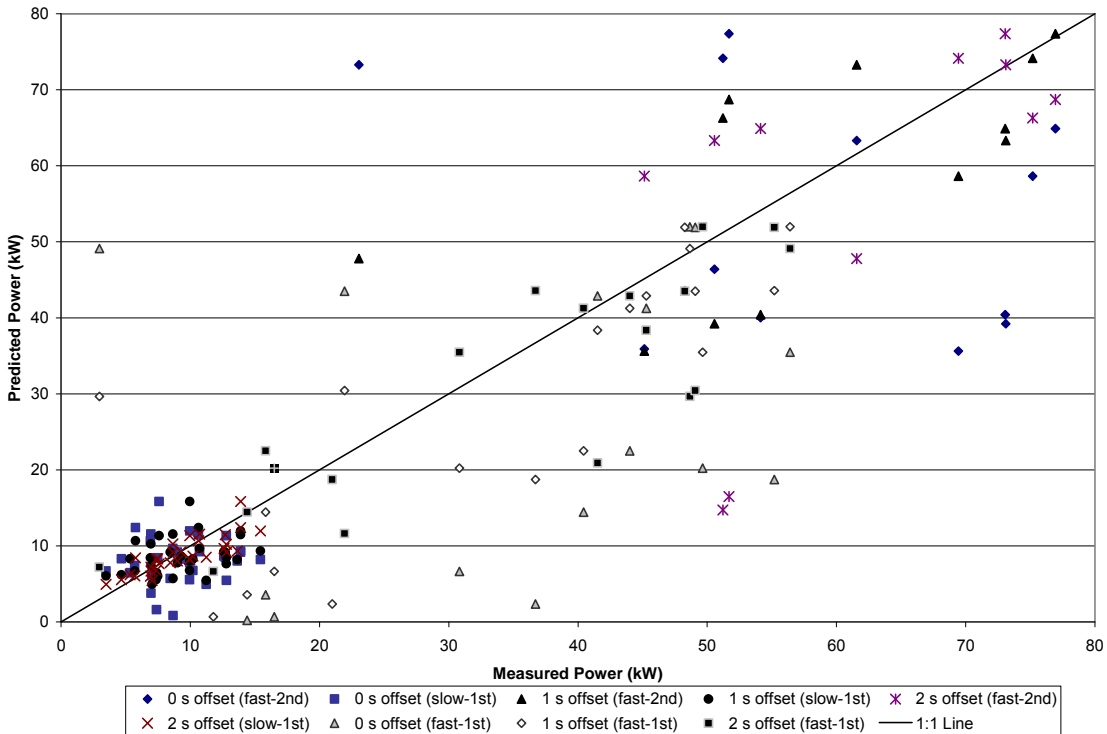

Figure 77: A comparison of predicted and measured mobility power at various GPS speed and acceleration offsets during nine inertia tests for the Garmin 18 GPS receiver

185

Vita

George William Bozdech was born on 20 June 1988 in Peoria, Illinois and graduated from Mahomet-Seymour High School in 2006. He earned a Bachelor of Science degree in Agricultural and Biological Engineering with a specialization in off-road machinery from the University of Illinois in May 2010. He was an intern at the U.S. Army Corps of Engineers' Construction Engineering Research Laboratory (CERL) from 2008 to 2009, and interned with John Deere at the Product Engineering Center (PEC) in Waterloo, Iowa in 2009. George began pursuing his Master of Science degree in Biosystems Engineering at the University of Tennessee in June 2010.